# A STUDY OF A DYNAMICAL FINITE ELEMENT ANALYSIS FOR APPLICATION TO AXIAL WAVE PROPAGATION PROBLEMS IN SEMI-INFINITE AND FINITE MEMBRANES AND SHELLS OF REVOLUTION

by

Joel Gray Bennett

Thesis submitted to the Graduate Faculty of the
Virginia Polytechnic Institute and State University
in partial fulfillment of the requirements for the degree of

DOCTOR OF PHILOSOPHY

in

Engineering Mechanics

APPROVED:

John Counts

Frederick H. Lutze, Jr.

Francis J. Maher

Dean T. Mook

Charles W. Smith

August 1970

Blacksburg, Virginia

## ACKNOWLEDGMENTS

The author wishes to express his sincere appreciation to his advisor, Dr. J. Counts, who suggested the topic and to thank him for the guidance and encouragement he gave during the course of the investigation. The author also wishes to express his thanks to the other members of his committee for their criticisms, advice, and for their excellent classroom instruction. The U.S. Steel Corporation made this thesis possible by giving the author financial aid in the form of a fellowship for which the author is grateful.

TABLE OF CONTENTS


| Chapter | Page |
|---|---|
| ACKNOWLEDGMENTS | ii |
| LIST OF FIGURES | v |
| NOMENCLATURE | x |
| INTRODUCTION | 1 |
| General | 1 |
| Specific Objective | 2 |
| LITERATURE REVIEW | 4 |
| FORMULATION OF THE MEMBRANE PROBLEM | 7 |
| General Principles | 7 |
| The Membrane of Revolution | 7 |
| Ordering of the Computations | 15 |
| Boundary Conditions at the Excitation End | 19 |
| Boundary Conditions for Finite Membranes | 23 |
| Membrane Geometries | 25 |
| THE THIN CYLINDRICAL SHELL | 27 |
| Formulation for Solution by the Dynamical Finite Element Method | 30 |
| Boundary Conditions for the Finite Cylindrical Shell | 37 |
| Energy Balance | 38 |
| DISCUSSION | 41 |
| General | 41 |
| Discussion of Results | 43 |
| Step Sizes Used and Computational Time | 88 |

Chapter Page

Concluding Remarks . . . . . 89

REFERENCES . . . . . 91

VITA . . . . . 93

LIST OF FIGURES


| Figure | | Page |
|---|---|---|
| 1. | Membrane Coordinates and Finite Element Representation. . . . | 8 |
| 2. | Momentum and Velocity Elements. . . . . | 10 |
| 3. | Schematic of Spatial Distribution of Nondimensionalized Dependent Variables at T = 4dT for Velocity Excitation (Wave Front Positions Indicated by Arrows). . . . . | 18 |
| 4. | Schematic of Spatial Distribution of Nondimensionalized Dependent Variables at T = 4dT for Stress Excitation (Wave Front Positions Indicated by Arrows). . . . . | 20 |
| 5. | Geometry of Input Velocity. . . . . | 22 |
| 6. | Membrane Geometries . . . . . | 26 |
| 7. | Thin Shell Coordinate System and Positive Stress Resultants . | 28 |
| 8. | Finite Element Representation of Thin Cylindrical Shell with Momentum and Velocity Elements. . . . . | 31 |
| 9. | Spatial Distribution of the Nondimensionalized Radial Velocity in a Finite Cylindrical Membrane at T = 15 (free-end at L = 10) for dT = 0.1, 0.05, 0.025, 0.0125. $V_o$ = 1, $\nu$ = 1/3 . . . . . | 44 |
| 10. | Spatial Distribution of the Nondimensionalized Meridional Stress in a Semi-infinite Cylindrical Membrane at T = 50. $V_o$ = 1, $\nu$ = 1/3, dT = 0.025 . . . . . | 45 |
| 11. | Spatial Distribution of the Nondimensionalized Meridional Stress in a Semi-infinite Cylindrical Membrane at T = 5, 10, Resulting from a Rectangular Stress Pulse Excitation at X = 0, $\nu$ = 1/3, dT = 0.025. . . . . | 47 |
| 12. | Spatial Distribution of the Nondimensionalized Meridional Stress at T = 5, 10, 15, 20, 25 in a Finite Cylindrical Membrane (free-end at L = 10). $V_o$ = 1, $\nu$ = 1/3, dT = 0.025 . | 49 |
| 13. | Spatial Distribution of the Nondimensionalized Circumferential Stress at T = 5, 10, 15, 20, 25 in a Finite Cylindrical Membrane (free end at L = 10). $V_o$ = 1, $\nu$ = 1/3, dT = 0.025 . | 50 |

Figure Page

14. Spatial Distribution of the Nondimensionalized Meridional Velocity at T = 5, 10, 15, 20, 25 in a Finite Cylindrical Membrane (free end at L = 10). $V_o$ = 1, $\nu$ = 1/3, dT = 0.025. . 51

15. Spatial Distribution of the Nondimensionalized Radial Velocity at T = 5, 10, 15, 20, 25 in a Finite Cylindrical Membrane (free end at L = 10). $V_o$ = 1, $\nu$ = 1/3, dT = 0.025. . 52

16. Temporal History of the Nondimensionalized Meridional and Circumferential Stresses at the end, x = 0, in a Finite Cylindrical Membrane (free end at L = 10). $V_o$ = 1, $\nu$ = 1/3, dT = 0.025 . . . . . 54

17. Comparison of Spatial Distribution of the Nondimensionalized Meridional Stresses in a Semi-infinite 15° Conical Membrane at T = 3.8625, 10, 15 resulting from Flat and Tangential Velocity Inputs at x = 0, $V_o$ = 1, $\nu$ = 0.3, dT = 0.0125 . . . . 55

18. Spatial Distribution of the Nondimensionalized Circumferential Stress in a Semi-infinite 15° Conical Membrane at T = 3.8625, 10, 15. Velocity Input Tangent to Meridian, $V_o$ = 1, $\nu$ = 0.3, dT = 0.0125. . . . . 57

19. Spatial Distribution of the Nondimensionalized Meridional Stress at T = 15, 20, 25 in a Finite 15° Conical Membrane (free end at L = 10). $V_o$ = 1, $\nu$ = 0.3, dT = 0.0125. . . . . 58

20. Spatial Distribution of the Nondimensionalized Circumferential Stress at T = 5, 10, 15, 20, 25 in a Finite 15° Conical Membrane (free-end at L = 10). $V_o$ = 1, $\nu$ = 0.3, dT = 0.0125. . 59

21. Temporal History of the Nondimensionalized Meridional Stress at the End, x = 0, in a Finite 15° Conical Membrane (free end at L = 10). $V_o$ = 1, $\nu$ = 0.3, dT = 0.0125. . . . . 60

22. Temporal History of the Nondimensionalized Circumferential Stress at the end, x = L in a Finite 15° Conical Membrane (free end at L = 10). $V_o$ = 1, $\nu$ = 0.3, dT = 0.0125. . . . . 61

23. Spatial Distribution of the Nondimensionalized Meridional Stress at T = 5.175, 10.3875, 15.6, 20.8125, 26.025 in a Parabolic Membrane (free end at L = 10). $V_o$ = 1, $\nu$ = 1/3, dT = 0.0125. . . . . 62

24. Spatial Distribution of the Nondimensionalized Circumferential Stress at T = 5.175, 10.3875, 15.6, 20.8125, 26.025 in a Parabolic Membrane (free-end at L = 10). $V_o$ = 1, $\nu$ = 1/3, dT = 0.0125. . . . . 63

Figure Page

25. Temporal History of the Nondimensional Meridional Stress at the End, L = 0, of a Parabolic Membrane (free end at L = 10). $V_o$ = 1, $\nu$ = 1/3, dT = 0.0125. . . . . 64

26. Spatial Distribution of the Nondimensionalized Meridional Stress Resultant in a Semi-infinite Thin Cylindrical Shell at T = 1, 2, resulting from Frictionless Axial Impact. h/R = 0.1, $V_o$ = 1, $\nu$ = 1/3, $k^2$ = 0.87, dT = 0.005 . . . . . 66

27. Spatial Distribution of the Nondimensionalized Moment Resultant in a Semi-infinite Thin Cylindrical Shell at T = 1, 2 resulting from Frictionless Axial Impact. h/R = 0.1, $V_o$ = 1, $\nu$ = 1/3, $k^2$ = 0.87, dT = 0.005. . . . . 67

28. Spatial Distribution of the Nondimensionalized Shear Stress Resultant in a Semi-infinite Thin Cylindrical Shell at T = 1, 2, resulting from Frictionless Axial Impact. h/R = 0.1, $V_o$ = 1, $\nu$ = 1/3, $k^2$ = 0.87, dT = 0.005. . . . . 68

29. Spatial Distribution of the Nondimensionalized Meridional Stress Resultant in a Finite Thin Cylindrical Shell at T = 5, 10, and 15, resulting from Frictionless Axial Impact, (free end at L = 10). h/R = 0.1, $V_o$ = 1, $\nu$ = 1/3, $k^2$ = 0.87, dT = 0.005 . . . . . 70

30. Spatial Distribution of the Nondimensionalized Circumferential Stress Resultant in a Finite Thin Cylindrical Shell at T = 5, 10, and 15, resulting from Frictionless Axial Impact, (free end at L = 10). h/R = 0.1, $V_o$ = 1, $\nu$ = 1/3, $k^2$ = 0.87, dT = 0.005. . . . . 71

31. Spatial Distribution of the Rotation of the Centroidal Surface in a Finite Thin Cylindrical Shell at T = 5, 10, and 15, resulting from Frictionless Axial Impact, (free end at L = 10). h/R = 0.1, $V_o$ = 1, $\nu$ = 1/3, $k^2$ = 0.87, dT = 0.005 . . . . . 72

32. Spatial Distribution at T = 5 of the Nondimensionalized Moment Resultant in a Finite Thin Cylindrical Shell resulting from Frictionless Axial Impact, (free end at L = 10). h/R = 0.1, $V_o$ = 1, $\nu$ = 1/3, $k^2$ = 0.87, dT = 0.005 . . . . . 74

33. Spatial Distribution at T = 10 of the Nondimensionalized Moment Resultant in a Finite Thin Cylindrical Shell resulting from Frictionless Axial Impact, (free end at L = 10). h/R = 0.1, $V_o$ = 1, $\nu$ = 1/3, $k^2$ = 0.87, dT = 0.005 . . . . . 75

Figure Page

34. Spatial Distribution at T = 15 of the Nondimensionalized Moment Resultant in a Finite Thin Cylindrical Shell resulting from Frictionless Axial Impact, (free end at L = 10). $h/R = 0.1$, $V_o = 1$, $\nu = 1/3$, $k^2 = 0.87$, $dT = 0.005$. . 76

35. Spatial Distribution at T = 5 of the Nondimensionalized Shear Stress Resultant in a Finite Thin Cylindrical Shell resulting from Frictionless Axial Impact, (free end at L = 10). $h/R = 0.1$, $V_o = 1$, $\nu = 1/3$, $k^2 = 0.87$, $dT = 0.005$. . 77

36. Spatial Distribution at T = 10 of the Nondimensionalized Shear Stress Resultant in a Finite Thin Cylindrical Shell resulting from Frictionless Axial Impact, (free end at L = 10). $h/R = 0.1$, $V_o = 1$, $\nu = 1/3$, $k^2 = 0.87$, $dT = 0.005$. . 78

37. Spatial Distribution at T = 15 of the Nondimensionalized Shear Stress Resultant in a Finite Thin Cylindrical Shell resulting from Frictionless Axial Impact, (free end at L = 10). $h/R = 0.1$, $V_o = 1$, $\nu = 1/3$, $k^2 = 0.87$, $dT = 0.005$. . 79

38. Temporal History of the Energy Balance Check for the Thin Cylindrical Shell . . . . . 80

39. Spatial Distribution of the Nondimensionalized Meridional Velocity in a Finite Thin Cylindrical Shell at T = 5, 10, and 15, resulting from Frictionless Axial Impact, (free end at L = 10). $h/R = 0.1$, $V_o = 1$, $\nu = 1/3$, $k^2 = 0.87$, $dT = 0.005$ 82

40. Spatial Distribution of the Nondimensionalized Meridional Displacement in a Finite Thin Cylindrical Shell at T = 5, 10, and 15, resulting from Frictionless Axial Impact, (free end at L = 10). $h/R = 0.1$, $V_o = 1$, $\nu = 1/3$, $k^2 = 0.87$, $dT = 0.005$ . . . . . 83

41. Spatial Distribution of the Nondimensionalized Radial Velocity in a Finite Thin Cylindrical Shell at T = 5, 10 and 15, resulting from Frictionless Axial Impact, free end at L = 10, $h/R = 0.1$, $V_o = 0$, $\nu = 1/3$, $k^2 = 0.87$, $dT = 0.005$ . 84

42. Spatial Distribution of the Nondimensionalized Radial Displacement in a Finite Thin Cylindrical Shell at T = 5, 10, and 15, resulting from Frictionless Axial Impact, (free end at L = 10). $h/R = 0.1$, $V_o = 1$, $\nu = 1/3$, $k^2 = 0.87$, $dT = 0.005$ . . . . . 85

Figure Page

43. Temporal History of the Nondimensionalized Radial Displacement at the end, L = 0, in a Finite Thin Cylindrical Shell resulting from Frictionless Axial Impact, (free end at L = 10). h/R = 0.1, $V_o$ = 1, = 1/3, $k^2$ = 0.87, dT = 0.005 . . . . . 86

44. Temporal Histories of the Nondimensionalized Moment Resultant at L = 0 and L = 2.5, in a Finite Thin Cylindrical Shell resulting from Frictionless Axial Impact, (free end at L = 10). h/R = 0.1, $V_o$ = 1, = 1/3, $k^2$ = 0.87, dT = 0.005 . . . . . 87

## NOMENCLATURE

$C_p$ plate velocity $= \sqrt{\frac{E}{\rho(1 - \nu^2)}}$

$C_s$ shear velocity $= k\sqrt{\frac{G}{\rho}}$

$E$ Young's modulus of Elasticity

ES, ET meridional and circumferential strain

FX dimensionless meridional stress resultant $= \frac{n_x}{\rho C_p^2 h}$

FT dimensionless circumferential stress resultant $= \frac{n_\theta}{\rho C_p^2 h}$

$G$ shear modulus of Elasticity

$h$ shell thickness

$I$ mass moment of inertia

$k^2$ shear correction factor

$L$ dimensionless meridional coordinate $= \frac{s}{r_o}$

$M$ dimensionless moment resultant $= \frac{m_x}{\rho C_p^2 h R}$

$m_x$ moment resultant

$n_x$, $n_\theta$ meridional and circumferential stress resultants

$q_x$ shear stress resultant

$Q$ dimensionless shear stress resultant $= \frac{q_x}{\rho C_p^2 h}$

$r$ radial coordinate, radius of a parallel circle

$r_o$ initial radius at the end $x = 0$ of the shell

$R$ dimensionless radial coordinate $= \frac{r}{r_o}$, radius of middle surface

$s$ meridional coordinate

$\dot{SI}$ dimensionless angular velocity of the centroidal surface $= \frac{C_p}{r_o} \frac{d\psi}{dT}$

$SI$ rotation about the centroidal surface

$SS$ dimensionless meridional stress $= \frac{\sigma_s}{\rho C_p^2}$

$ST$ dimensionless circumferential stress $= \frac{\sigma_\theta}{\rho C_p^2}$

$t$ time

$T$ dimensionless time $= \frac{C_p}{r_o} t$

$u$ meridional displacement

$U$ dimensionless meridional displacement $= \frac{u}{r_o}$

$\dot{u}$ meridional velocity

$\dot{U}$ dimensionless meridional velocity $= \frac{\dot{u}}{C_p}$

$v_o$ initial or excitation velocity

$V_o$ dimensionless initial or excitation velocity $= \frac{v_o}{C_p}$

$w$ radial or normal displacement

$W$ dimensionless radial or normal displacement $= \frac{w}{r_o}$

$\dot{w}$ radial or normal velocity

$\dot{W}$ dimensionless radial or normal velocity $= \frac{\dot{w}}{C_p}$

$x$ axial coordinate

$X$ dimensionless axial coordinate $= \frac{x}{r_o}$

$z$ radial coordinate

$\alpha$ tangent angle between the meridional curve and the axis of revolution

$\varepsilon_s$, $\varepsilon_\theta$ meridional and circumferential strains

$\nu$ Poisson's ratio

$\eta$ centroidal distance ratio

$\rho$ mass density

$\sigma_s$, $\sigma_\theta$ meridional and circumferential stresses

$\psi$ rotation about the centroidal surface

$\dot{\psi}$ angular velocity of the centroidal surface

$\theta$ circumferential coordinate

# INTRODUCTION

## General

Although the theory of elastic wave propagation was developed in the previous century as an extension of the theory of elasticity to vibrating elastic bodies and as a tool to aid in the understanding of the transmission of light (which was considered to be vibrations of an elastic ether [1]*), the necessity of studying such problems is of current importance. Clearly, with an increasing number of structural shapes being subjected to dynamic transient loadings in environments where strength to weight ratios are considered critical, it becomes increasingly important to have the ability to design efficiently for such loadings. While as early as 1872, when experiments carried out by John Hopkinson on the impact loading of iron wire showed that material behavior under such conditions could be quite different [2], it is only in the last several decades that the science of instrumentation has developed enough to allow more sophisticated experimental studies to be conducted for such loadings. Similarly, while the governing equations for these problems could be formulated both exactly and approximately, it is only recently that through the use of approximate and numerical techniques in combination with the modern high speed computer that the practical solution to more sophisticated problems has become

*Numbers in brackets refer to appended references.

feasible. Even with such techniques available, the solution of exact equations is difficult and the usual approach is to work with the more feasible so called engineering or approximate theories. However, as more solutions to these problems become available, the practicing engineer can design and test accordingly with more confidence.

## Specific Objective

Some of the more common structural shapes which are used in applications involving sudden dynamic loadings are the shells of revolution. For this reason, these shapes have been chosen for study. Also, a common type of loading on such structures is the axial type which generally results from impact. These loadings may be adequately represented by discontinuities in stress and particle velocities on the boundaries. Since most structural applications for the above mentioned shapes do not really involve enough length to be considered semi-infinite, the finite problems are also considered.

This investigation, then, concerns the application of a dynamical finite element analysis to wave propagation in semi-infinite and finite thin shells of revolution using both membrane theory and thin shell theory. The thin shell theory is included in order to ascertain some idea of the influence of shear effects and rotary inertia.

The contribution here is to have available in the engineering literature the solution to some original problems and to illustrate the use of a technique which to date has received very little attention in

the literature. The specific problems considered in this investigation are as follows:

1. Axial velocity excitation of semi-infinite and finite cylindrical membranes,
2. Stress pulse input to a semi-infinite cylindrical membrane,
3. Velocity excitation of semi-infinite and finite conical membranes,
4. Meridional velocity excitation of a finite parabolic membrane of revolution,
5. Transient solution for impacting semi-infinite and finite cylindrical thin shells including rotary inertia and shear effects.

## LITERATURE REVIEW

Since the appearance of survey articles such as that of R. M. Davies [3] and Miklowitz [4], several papers related to the problems considered here have been published.

Berkowitz [5] obtained a long time solution to the problem of a semi-infinite impacting cylindrical membrane shell by an asymptotic expansion of the Laplace transform of the dependent variables and inversion by contour integration in the complex plane.

Using a similar technique, Testa and Bleich [6] obtained the response of a semi-infinite cylindrical viscoelastic shell subjected to longitudinal impact. Berkowitz and Bleich [7] extended the technique to the impact of an elastic right conical membrane shell.

Spillers [8] proposed a largely numerical technique for use with the method of characteristics and presented small-time solutions for the semi-infinite cylindrical membrane shell and the semi-infinite thin cylindrical shell using the equations derived by Herrmann and Mirsky [9]. The results for the thin shell are highly suspect and it was pointed out by Chou [10] that, apparently, numerical instability had occurred in the integration scheme.

Chou [10] derived a set of thin cylindrical shell equations which he solved by the method of characteristics. The difference between Chou's equations and the Herrmann-Mirsky equations is that the centroidal surface rather than the middle surface is used as a reference surface for the moment and rotation in Chou's equations. This allows an un-

coupling effect such that second derivatives of only one dependent variable appear in each equation of motion which simplifies the numerical scheme.

King [11] complemented Berkowitz and Bleich's solution to the conical membrane shell by using the method of characteristics to obtain a small-time solution. Counts and Akin [12] and Akin and Counts [13] solved wave propagation problems in a viscoelastic rod and a semi-infinite cylindrical membrane. They were able to obtain both small and long time solutions by isolating the discontinuity in the Laplace transform space and expanding the remaining smooth function in a power series of the reciprocal of the transform parameter. Continued fractions were then used to generate rational approximations in the form of the ratio of two polynomials which allows inversion by standard techniques.

Spillers and Chapman [14] showed that what appears to be numerical instability in the method of characteristics solution to the semi-infinite cylindrical membrane can be eliminated by decreasing the mesh size. The results they give are for a cylindrical membrane shell for the wavefront out to 50 radii.

Spillers and Callegari [15] point out in a later paper that some numerical schemes such as those used with the method of characteristics in problems of this type, sometimes create distortion of the wave fronts, but they conjecture that if a starting point is known from, say, short-time analytical solutions, much of this distortion may be avoided.

Davids and Mehta [16] proposed a technique referred to by them as "computer analysis" which they demonstrated by solving impacting elastic

and plastic rods using elementary theory. Recently Keonig and Davids [17] have applied the technique to wave propagation problems in beams and plates.

Very recently Raney and Howlett [18] used modal superposition on a finite cylindrical membrane shell to solve wave propagation problems. A finite element analysis was used to obtain the required modes. It was found that for transient problems, as many as 100 or more modes are necessary for rapid numerical convergence. The excitation cases considered are polynomial type initial conditions. The method is compared with the method of characteristics and with a finite difference scheme.

## FORMULATION OF THE MEMBRANE PROBLEM

### General Principles

The approach to be presented in what follows is generally the same as the one taken by Davids, et al [16,17]. The method consists of formulating the equations of motion in impulse-momentum form directly from a finite element representation of the problem geometry. Repetitive operations follow directly without reduction to the differential equations governing only one type of dependent variable; that is, velocities are cumulated from the differential changes given by the impulse-momentum law, strains and displacements from velocities, stresses from strains or displacements, and the solution is marched out along the geometry by proper arrangement of the order of the computations. Since propagation by this procedure is achieved automatically, reflections produced by boundaries are relatively easy to handle in that no special formulation is required other than the proper specification of the boundary condition. In general, the principles are elementary but the specific application of the method requires considerable care if numerical stability is to be achieved.

### The Membrane of Revolution

The upper portion of figure 1 represents the meridional curve for a general membrane of revolution with the radius of a parallel circle

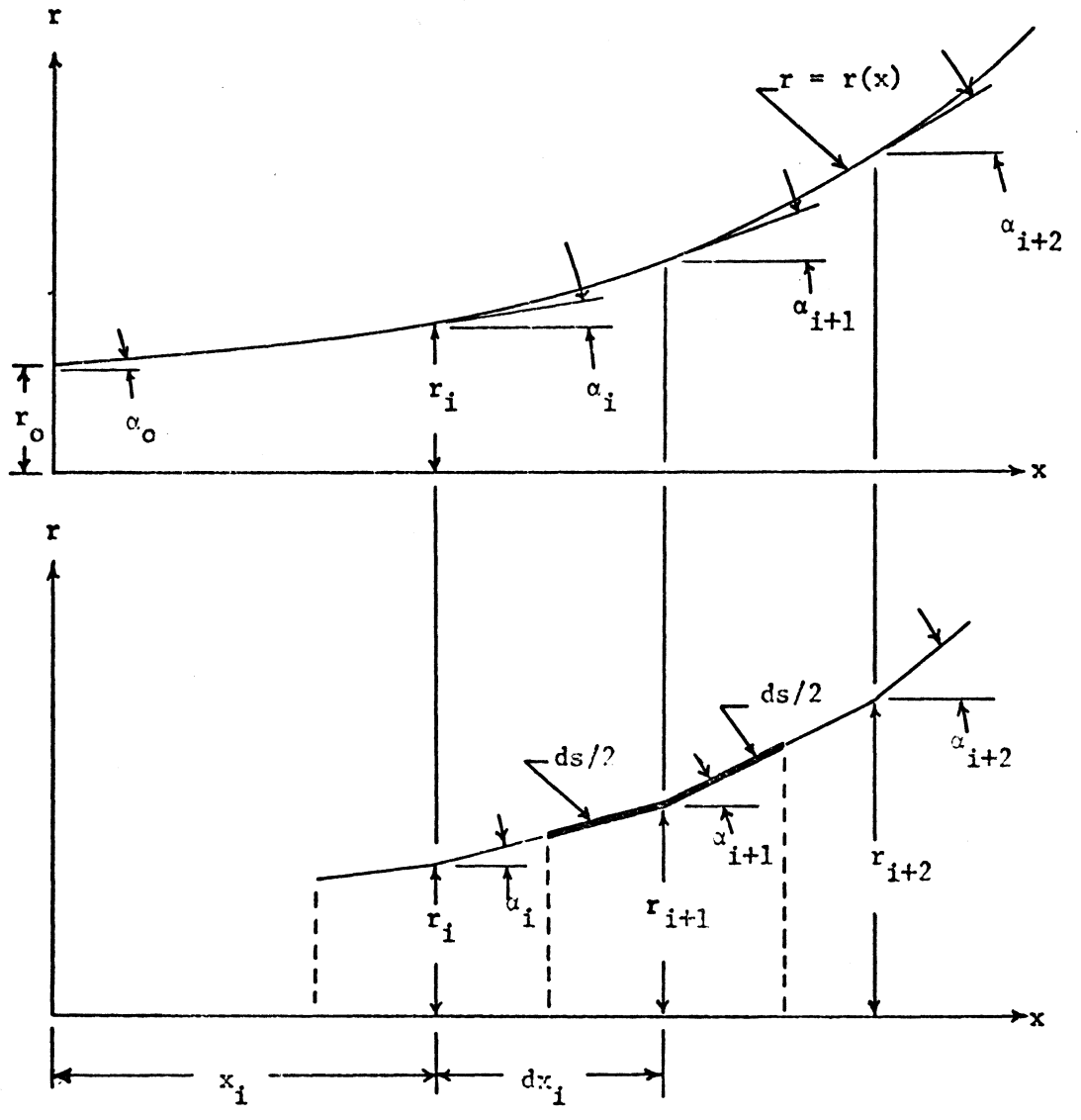


Figure 1. Membrane Coordinates and Finite Element Representation.

given by $r = r(x)$. This geometry is shown approximated in the lower part of this figure by a series of conical elements with $\alpha_i$ being the tangent angle between the meridional curve and the longitudinal x axis. The meridional curve is divided into equal arc lengths of ds units and beginning with $r = r_o$, $\alpha = \alpha_o$, $dx_1$ will be given by ds cos $\alpha_o$. The next radius is then $r_1 = r(x_1)$ where $x_i = x_{i-1} + dx_i$ and the corresponding tangent angle $\alpha_1 = \arctan \left[ \frac{dr(x_1)}{dx_1} \right]$. This computation, which is carried out over the arc length of the membrane, only approximately defines the meridional curve of a chosen membrane since it is a straight line approximation, but as ds becomes smaller, the error in making this approximation vanishes. Note that in approximating this geometry with conical frustra, discontinuities in slope and curvature are inherent. However, since this is a membrane, only membrane stresses will arise, and no fictitious moments or shears will be generated by this approximation.

The upper part of figure 2 shows a free body diagram of the portion of the finite element representation of the meridional curve indicated in figure 1 by the heavy lines of length ds/2. The meridional stresses are indicated at the ends of the element by $\sigma_s^i$ and $\sigma_s^{i+1}$, with the resultant radial projections of the circumferential stresses indicated as $\sigma_\theta^i d\theta$ and $\sigma_\theta^{i+1} d\theta$ as shown. The $\sigma_\theta^i$ projections normal to the r-x plane do not enter the momentum relations. Also note that $\sigma_\theta^i$ and $\sigma_\theta^{i+1}$ have been assumed uniform over the lengths ds/2. Such a free-body diagram will hereafter be referred to as a momentum element.

Assuming that the stresses indicated exist at time t, application

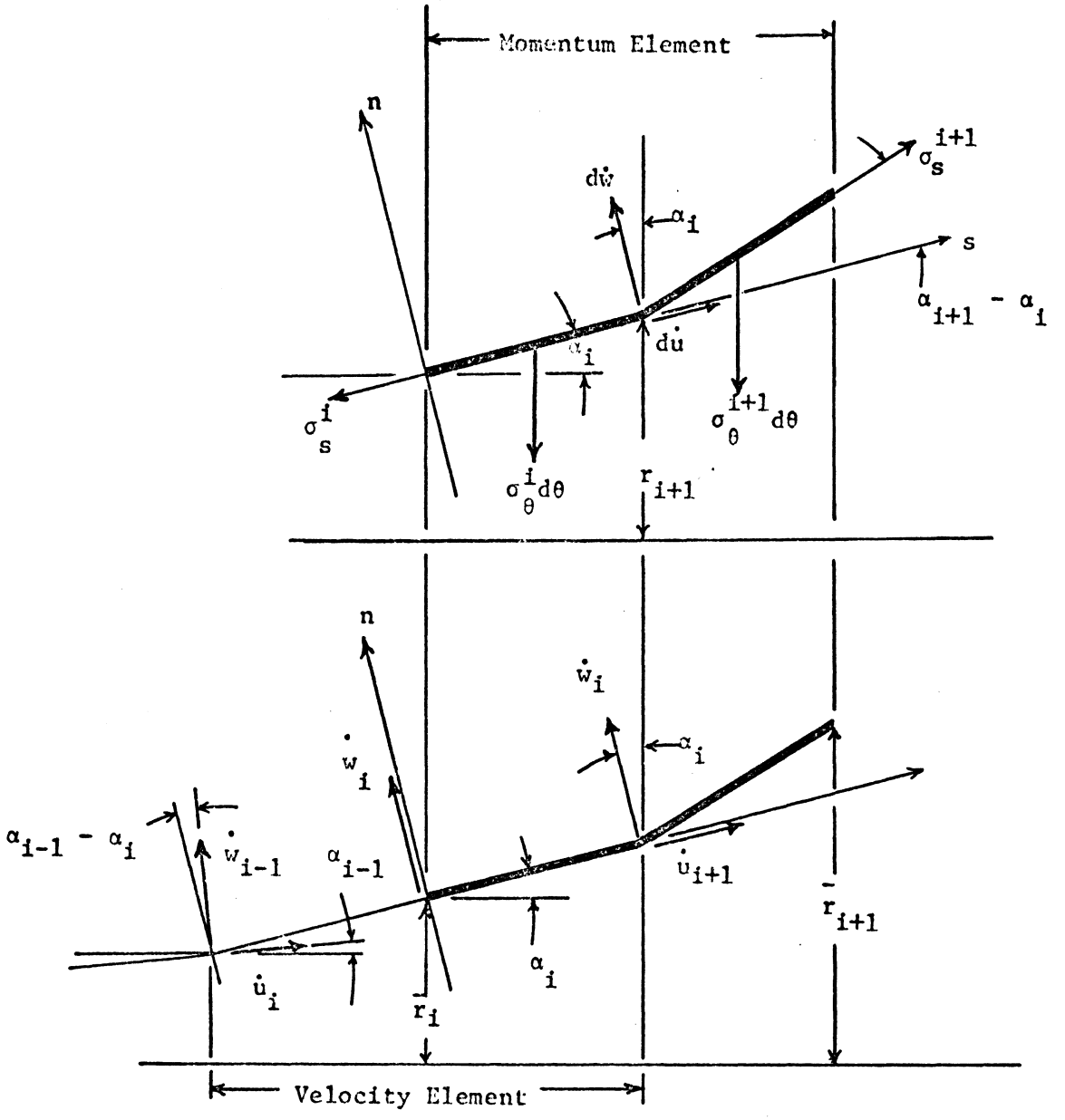


Figure 2. Momentum and Velocity Elements.

of the impulse-momentum law in the meridional (s) and normal (n) directions yield the following velocity changes for the mass-center which will occur in the next dt increment of time:

$$d\dot{u}_{i+1} = \frac{dt}{dm_i} \{\sigma_s^{i+1}\bar{r}_{i+1} \cos(\alpha_{i+1} - \alpha_i) - \sigma_s^i \bar{r}_i - ds \sin\alpha_i \left[\frac{\sigma_\theta^{i+1} + \sigma_\theta^i}{2}\right]\} \qquad 3.1$$

and

$$d\dot{w}_i = \frac{dt}{dm_i} \{\sigma_s^{i+1}\bar{r}_{i+1} \sin(\alpha_{i+1} - \alpha_i) - ds \cos\alpha_i \left[\frac{\sigma_\theta^{i+1} + \sigma_\theta^i}{2}\right]\} \qquad 3.2$$

where

$$\bar{r}_i = \frac{1}{2}(r_{i+1} + r_i)$$

and

$$dm_i = \frac{\rho ds}{8}(r_i + 6r_{i+1} + r_{i+2}).$$

These velocity changes are given to the center of the element as indicated in figure 2, and will be cumulated at these points along the membrane. Note that while the center of the element is not the mass-

center, it will be a close approximation, and will approach it as ds becomes smaller.

The lower portion of figure 2 shows the normal velocities, $\dot{w}$, and the meridional velocities, $\dot{u}$. An element removed from this portion of the finite element representation will be referred to as a velocity or strain element indicating that strains are computed from and cumulated on this element.

Assuming that the velocities shown exist at time t, the incremental strains that will occur in the next dt increment of time will be

$$d\varepsilon_s^i = \frac{dt}{ds} \{ \dot{u}_{i+1} - \dot{u}_i \cos (\alpha_i - \alpha_{i-1}) + \dot{w}_{i-1} \sin (\alpha_{i-1} - \alpha_i) \} \quad 3.3$$

and

$$d\varepsilon_\theta^i = \frac{dt}{\bar{r}_i} \{ [ \dot{w}_i + d\dot{w}/2] \cos \alpha_i + \sin \alpha_i \cdot$$

$$[ \frac{\dot{u}_{i+1} + \dot{u}_i \cos (\alpha_i - \alpha_{i-1})}{2} ] \}. \quad 3.4$$

Note that $\dot{w}$ has been assumed uniform over the element ds having the tangent angle $\alpha_i$, and the average of $\dot{u}_{i+1}$ and $\dot{u}_i \cos (\alpha_i - \alpha_{i-1})$ has been used in these strain increment calculations. The strains which now exist at the center of the velocity element are given by

$$\varepsilon_s^i = \varepsilon_s'^i + d\varepsilon_s \quad 3.5$$

$$\varepsilon_\theta^i = \varepsilon_\theta'^i + d\varepsilon_\theta \qquad 3.6$$

where the primes indicate that these strains existed before the dt occurred and new strains are being cumulated at this position.

While any physically admissible constitutive equation can be used, linearly elastic equations have been chosen for this study. At the center of the strain element, application of Hooke's laws for plane stress gives

$$\sigma_s^i = \frac{E}{1-\nu^2}\left[\varepsilon_s^i + \nu\varepsilon_\theta^i\right] \qquad 3.7$$

and

$$\sigma_\theta^i = \frac{E}{1-\nu^2}\left[\varepsilon_\theta^i + \nu\varepsilon_s^i\right] \qquad 3.8$$

where E is Young's modulus and $\nu$ is Poisson's ratio. With new stresses now known, the time may be incremented and the impulse-momentum law again applied to this element to obtain relations at a later time.

Equations 3.1-3.8 can be nondimensionalized by making the following substitutions:

$$r = Rr_o, \quad x = Xr_o, \quad s = Lr_o, \quad \sigma_s = \rho C_p^2(SS), \quad \sigma_\theta = \rho C_p^2(ST),$$

$$t = T\left(\frac{r_o}{C_p}\right), \quad d\varepsilon_s = dES, \quad d\varepsilon_\theta = dET, \quad \dot{u} = \dot{U}C_p, \quad \dot{w} = \dot{W}C_p \qquad 3.9$$

with $C_p^2 = \frac{E}{\rho(1 - \nu^2)}$, where $C_p$ can be shown to be the speed of propagation of the discontinuities in $\sigma_s$, $\sigma_\theta$, $\varepsilon_s$, $\varepsilon_\theta$, $\dot{u}$, and their derivatives along the meridional curve, and the upper-case symbols on the right-hand side of the above equations are the nondimensional counterparts of the lower-case symbols on the left-hand sides.

In nondimensional form with dL = dT, equations 3.1 through 3.9 become the following:

$$d\dot{U} = \frac{1}{dM_i} \{ SS_{i+1} \bar{R}_{i+1} \cos(\alpha_{i+1} - \alpha_i) - SS_i \bar{R}_i - dT \sin \alpha_i \left[ \frac{ST_{i+1} + ST_i}{2} \right] \} \quad 3.1a$$

$$d\dot{W} = \frac{1}{dM_i} \{ SS_{i+1} \bar{R}_{i+1} \sin(\alpha_{i+1} - \alpha_i) - dT \cos \alpha_i \left[ \frac{ST_{i+1} + ST_i}{2} \right] \} \quad 3.2a$$

$$dES = \dot{U}_{i+1} - \dot{U}_i \cos(\alpha_i - \alpha_{i-1}) + \dot{W}_{i-1} \sin(\alpha_{i-1} - \alpha_i) \quad 3.3a$$

$$dET = \frac{dT}{\bar{R}_i} \{ (\dot{W}_i + d\dot{W}/2) \cos \alpha_i + \sin \alpha_i \left[ \frac{\dot{U}_{i+1} + \dot{U}_i \cos(\alpha_i - \alpha_{i-1})}{2} \right] \} \quad 3.4a$$

$$ES_i = ES'_i + dES \quad 3.5a$$

$$ET_i = ET'_i + dET \quad 3.6a$$

$$SS_i = ES_i + \nu ET_i \qquad 3.7a$$

$$ST_i = ET_i + \nu ES_i \qquad 3.8a$$

with $dM_i = \frac{1}{8}(R_i + 6R_{i+1} + R_{i+2})$.

## Ordering of the Computations

The order of the computations must now be arranged so that beginning at the excitation end of the membrane, the solution can be "marched out" along the arc-length. If the problem were formulated by the usual finite element technique, the order in which the calculations are performed would not matter. The present technique, however, does not involve the solution of simultaneous algebraic equations; instead, the solution is marched forward so that diffusion is prohibited while maintaining the total energy in balance by the order in which the calculations are performed.

Consideration of the excitation boundary conditions (velocity or stress type), allows a velocity or stress division of elements to be constructed. In other words, if the boundary condition is to prescribe the velocity, the first element will be a strain or velocity element, with the first momentum element being isolated from the middle of the first two strain elements. If stress boundary conditions are prescribed, the first element is a momentum element. This construction gives the allowable subscripts in the equations.

Since the one dimensional subscripts have temporal as well as spatial implications, an identification of the meaning of the subscripts temporally in the x-t plane is combined with the next two rules to order the equations.

The two criteria which must be met are that the discontinuities in the dependent variables must be maintained at the wavefront, and that quiescent or initial conditions must be maintained beyond the wavefront; that is, if the computations are carried out beyond the wavefront, the order should prohibit diffusion of the solution.

Velocity Excitation - Application of the above principles to the problem for velocity excitation leads to the following order for the membrane of revolution:

1. $d\dot{U}$ = ---(Equation 3.1a)
2. $\dot{U}_{i+1} = \dot{U}'_{i+1} + d\dot{U}$
3. $d\dot{W}$ = ---(Equation 3.2a)
4. $\dot{W}_i = \dot{W}'_i + d\dot{W}$
5. Specification of the boundary condition on the velocity
6. dES = ---(Equation 3.3a) 3.10
7. dET = ---(Equation 3.4a)
8. $ES_i = ES'_i + dES$
9. $ET_i = ET'_i + dET$
10. $SS_i = ES_i + \nu ET_i$
11. $ST_i = ET_i + \nu ES_i$

Step 5 represents the input boundary condition on the velocity which is discussed in the next section. Steps 2, 4, 8, and 9 represent cumulation statements in that the dependent variable at the $i^{th}$ position is a sum of the incremental changes which occur there.

The procedure is executed by choosing a dT (= dL) and performing the operations indicated by steps 1-11 along the membrane arc length. This establishes a set of dependent variables which exist after the first dT has occurred. The time is then incremented by dT and steps 1-11 are repeated to or beyond the new wavefront. The new wavefront appears because the propagation is automatically carried out by step 2 which continually moves the wavefront to a new position each time it is executed with i having the value of the wavefront subscript. This statement is encompassed by saying that propagation is carried forward by the meridional velocity. A schematic representation of the spatial distribution of the dependent variables which exist after 4dT is indicated in figure 3.

Stress Excitation - With the meridional stress specified as the excitation boundary condition, the first element is a momentum element as explained previously. The application of the rules of order to this problem leads to the following order for the computations:

1. dES = ---(Equation 3.3a)
2. $ES_{i+1} = ES'_{i+1} + dES$
3. $SS_{i+1} = ES_{i+1} + \nu ET_{i+1}$
4. $ST_{i+1} = ET_{i+1} + \nu ES_{i+1}$

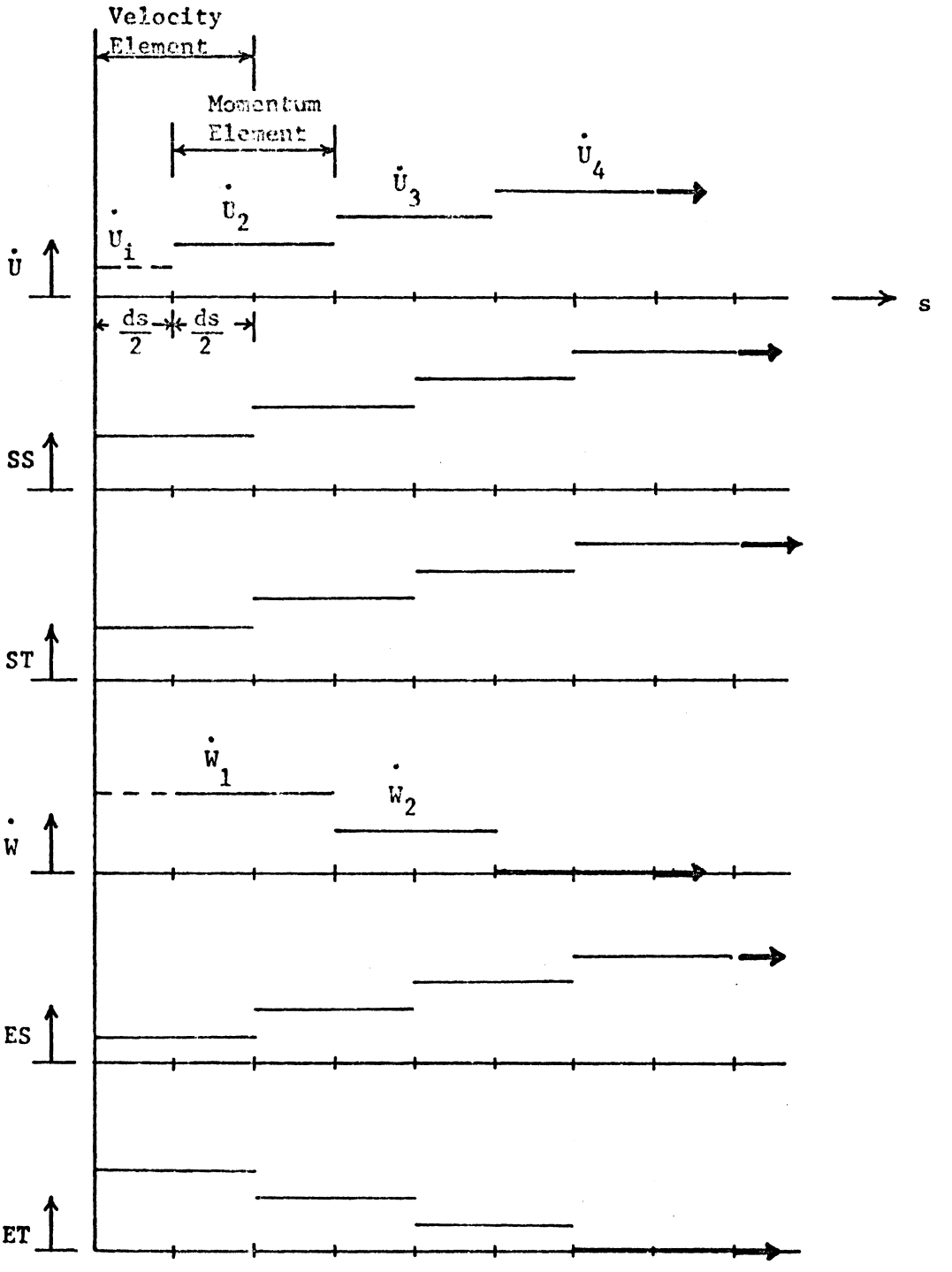


Figure 3. Schematic of Spatial Distribution of Nondimensionalized Dependent Variables at T = 4dT for Velocity Excitation (Wave Front Positions Indicated by Arrows).

5. $ST_o = ST_1$

6. dET = ---(Equation 3.4a)

7. $ET_{i+1} = ET'_{i+1} + dET$

8. Specification of the boundary condition on the stress

9. $d\dot{U}$ = ---(Equation 3.1a)

10. $\dot{U}_i = \dot{U}'_i + d\dot{U}$

11. $d\dot{W}$ = ---(Equation 3.2a)

12. $\dot{W}_i = \dot{W}'_i + d\dot{W}$

3.11

The fifth step assumes that the circumferential stress is uniform over the first momentum element and is necessitated by the fact that there is no other way to compute $ST_o$. As dT (= dL) becomes smaller this assumption of uniformity will tend to be correct. The eighth step is the position chosen to specify the input boundary condition which must appear before the momentum calculation in step 9 to start the procedure correctly.

The propagation procedure for stress excitation produces discontinuities in meridional velocity ($\dot{U}$), and the circumferential stress (ST) due to an input jump in meridional stress (SS). A schematic representation of the dependent variables which exist after 4dT for the stress excitation boundary condition is indicated in figure 4.

## Boundary Conditions at the Excitation End

While the only boundary condition a membrane of revolution can accept without necessitating transverse shear forces and moments is

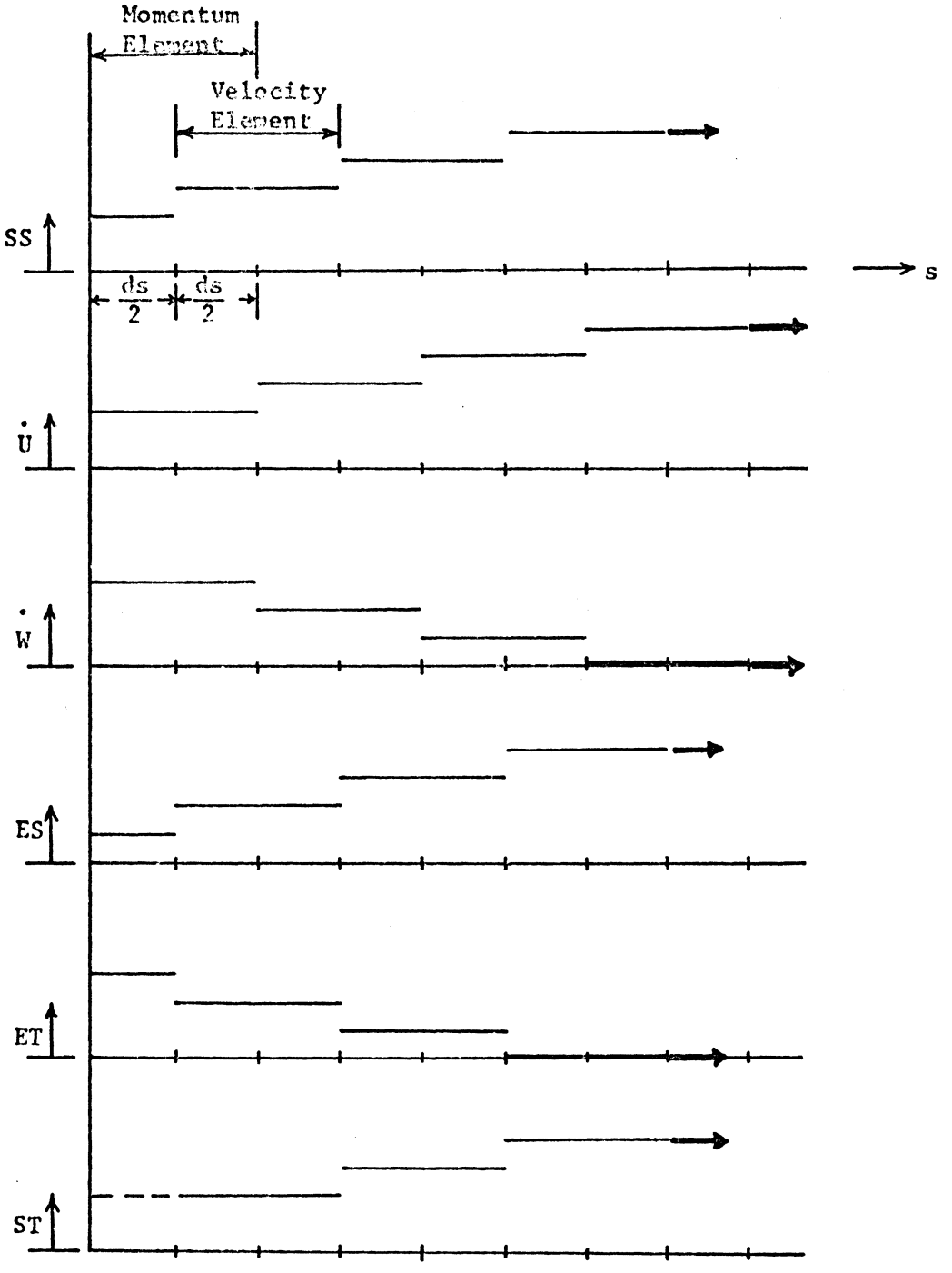


Figure 4. Schematic of Spatial Distribution of Nondimensionalized Dependent Variables at T = 4dT for Stress Excitation (Wave Front Positions Indicated by Arrows).

the specification of the meridional stress or meridional velocity, two boundary conditions may be considered for the velocity excitation of the end of the membrane. The first is the specification of the longitudinal velocity, $v_o$, of a smooth, plane, rigid wall at the end, $x = 0$ of the membrane. If the velocity of the wall is constant, the stresses in the membrane will be the same as those resulting from the membrane impacting the wall with an initial velocity $v_o$. This boundary condition is expressed as

$$v_o = \dot{u}_o \cos \alpha_o - \dot{w}_o \sin \alpha_o,$$

or in nondimensional form as

$$V_o = \dot{U}_o \cos \alpha_o - \dot{W}_o \sin \alpha_o,$$

where $V_o = v_o/C_p$.

Since this boundary condition seems inconsistent with the inability of the membrane to support a transverse shear force, a more realistic condition is the specification of the meridional velocity, $\dot{u}_o$. The difference between these two cases is examined in the discussion for a conical membrane. The specification of the meridional velocity is equivalent to the wall being normal to the meridian at the end $x = 0$. These two cases are illustrated in figure 5.

Note that for both velocity and stress excitation, the boundary condition is included in the propagation procedure in such a way that

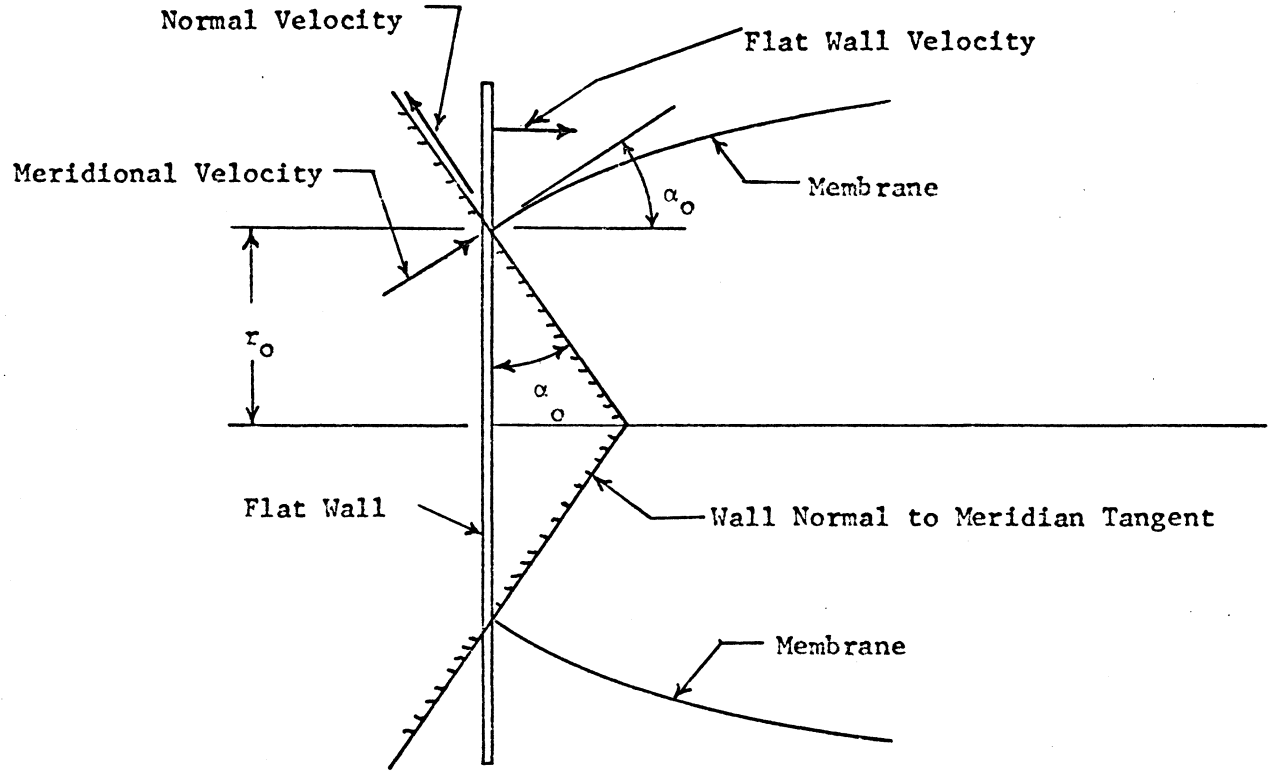


Figure 5. Geometry of Input Velocity.

either constant velocity or stress, or a time-dependent velocity or stress pulse may be specified since it is only a matter of reading in the necessary condition at the proper time.

## Boundary Conditions for Finite Membranes

Since the propagation procedure is automatically carried out, this method of analysis has the property that upon proper specification of the boundary condition for the element making up the membrane end, reflection of the wave is achieved automatically. Davids, et al [16, 17] imply in their work that it is only necessary to specify the boundary condition on the dependent variable involved to achieve reflection; that is, for a fixed-end boundary, set $\dot{u}_{j+1} = 0$, where j is the subscript of the end element. Investigation has shown that this principle is not true in general. The boundary condition must be stated through the dependent variables which carry the propagation forward.

The finite membranes studied here are assumed to be free of meridional stress at the right-hand boundary. Referring to the calculation procedure for velocity excitation (Equations 3.10), the free-end boundary condition cannot be satisfied by setting $SS_j = 0$ after step 10 in the procedure. Instead, setting $SS_j = 0$ implies that $ES_j = -\nu ET_j$. Beginning with this relation and substituting up through the equations, the value of the meridional velocity which must be specified to obtain $SS_j = 0$ is as follows:

$$\dot{U}_{i+1} = \frac{1}{1 + \frac{\nu dT}{2\bar{R}_i} \cdot \sin \alpha_i} \{ - SS_i + \dot{U}_i \cos (\alpha_i - \alpha_{i-1})(1 - \frac{\nu dT}{2\bar{R}_i} \sin \alpha_i)$$

$$- \cos \alpha_i \frac{\nu dT}{\bar{R}_i} \dot{W}_i - \cos \alpha_i \frac{\nu dT}{2\bar{R} dM_i} [ SS_{i+1} \bar{R}_{i+1} \sin (\alpha_{i+1} - \alpha_i)$$

$$- \frac{dL}{2} \cos \alpha_i (ST_{i+1} + ST_i)] - \frac{1}{dM_i} (1 + \frac{\nu dT}{2\bar{R}_i} \sin \alpha_i) \cdot \qquad 3.12$$

$$[SS_{i+1} \bar{R}_{i+1} \cos (\alpha_{i+1} - \alpha_i) - SS_i \bar{R}_i - \frac{dL}{2} \sin \alpha_i \cdot$$

$$(ST_{i+1} + ST_i)] - \dot{W}_{i-1} \sin (\alpha_{i-1} - \alpha_i)\} .$$

This statement would appear after step 2 in the procedure and would be executed when i = j where j is the subscript for the element making up the membrane end as before. As with all of the equations presented thus far, equation 3.12 will reduce to the conical membrane when all the α's are equal, and to the cylindrical membrane when all the α's are zero and the R's are unity.

The fixed-end boundary condition can be satisfied by executing the statement $\dot{U}_{i+1} = 0$ when i = j. The reason that the free-end condition cannot be handled this way is that the variables which are present due to a nonzero Poisson's ratio cannot be specified at the boundary, but must be computed as a consequence of the meridional variables. If ν is set equal to zero, the procedure gives the solution for the velocity input to an axial rod, and the free-end boundary condition can be satisfied by setting $\dot{U}_{j+1} = \dot{U}_j$ (which follows from equation 3.12), or

$ES_j = 0$, or $SS_j = 0$ because ST, ET and $\dot{W}$ do not appear.

Although finite membranes subjected to stress excitation have not been treated here, the above principles presented for velocity excitation can be used to specify the proper boundary conditions. The case of a stress free boundary at i = j can be satisfied by executing the statement $SS_{i+1} = 0$ after step 3 in equations 3.11. The case of a fixed-end boundary can be accommodated by setting $\dot{U}_j = 0$ and substituting up through step 3 to obtain the necessary expression for $SS_{j+1}$.

## Membrane Geometries

The geometries of the membranes studied in this investigation are shown in figure 6. The arc lengths of the cylindrical and conical membranes are both $10r_o$. The computations for the arc length of the parabolic membrane were carried out until the axial length was equivalent to $10r_o$ so that the arc length itself is slightly longer.

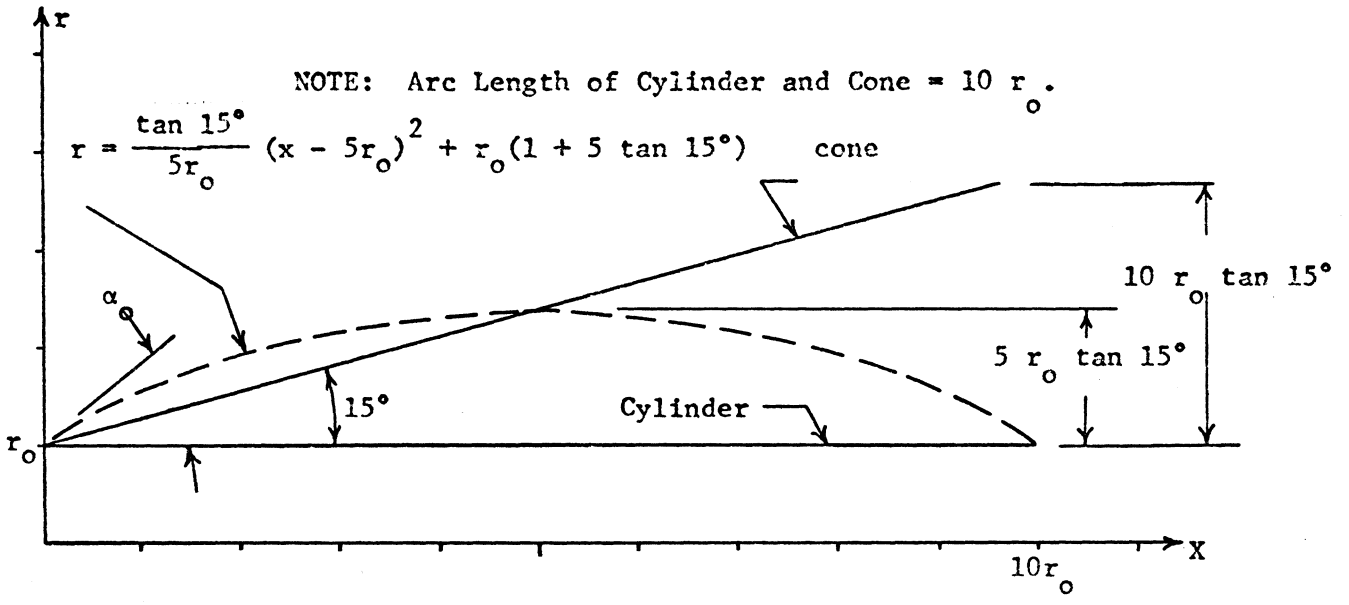


Figure 6. Membrane Geometries.

## THE THIN CYLINDRICAL SHELL

The formulation of the problem of axial wave propagation in a thin cylindrical shell by the dynamical finite element approach which follows is based upon the equations and theory derived by Chou [10]. This theory uses the centroidal surface rather than the middle surface as a reference surface for the moment and rotation. Figure 7 shows the coordinates used with the centroidal surface being located at $R + \eta R$ where $\eta = \frac{1}{12}(\frac{h}{R})^2$. The positive sense of the stresses and stress resultants is shown in the lower part of this figure. With lines normal to the centroidal surface before displacement remaining normal, the displacement of some point z on such a line is approximately $u_x(x, t) = u(x, t) + (z - \eta R)\psi$, and $u_z(x, t) = w(x, t)$. If the stresses are integrated over the shell thickness in this coordinate system, the following definitions are obtained for the shell stress resultants:

$$
\begin{aligned}
n_x &= \int_{-h/2}^{h/2} \sigma_x (1 + \tfrac{z}{R}) dz \\
n_\theta &= \int_{-h/2}^{h/2} \sigma_\theta dz \\
q_x &= \int_{-h/2}^{h/2} \sigma_{xz} (1 + \tfrac{z}{R}) dz \\
m_x &= \int_{-h/2}^{h/2} \sigma_x (1 + \tfrac{z}{R})(z - \eta R) dz
\end{aligned}
\qquad 4.1
$$

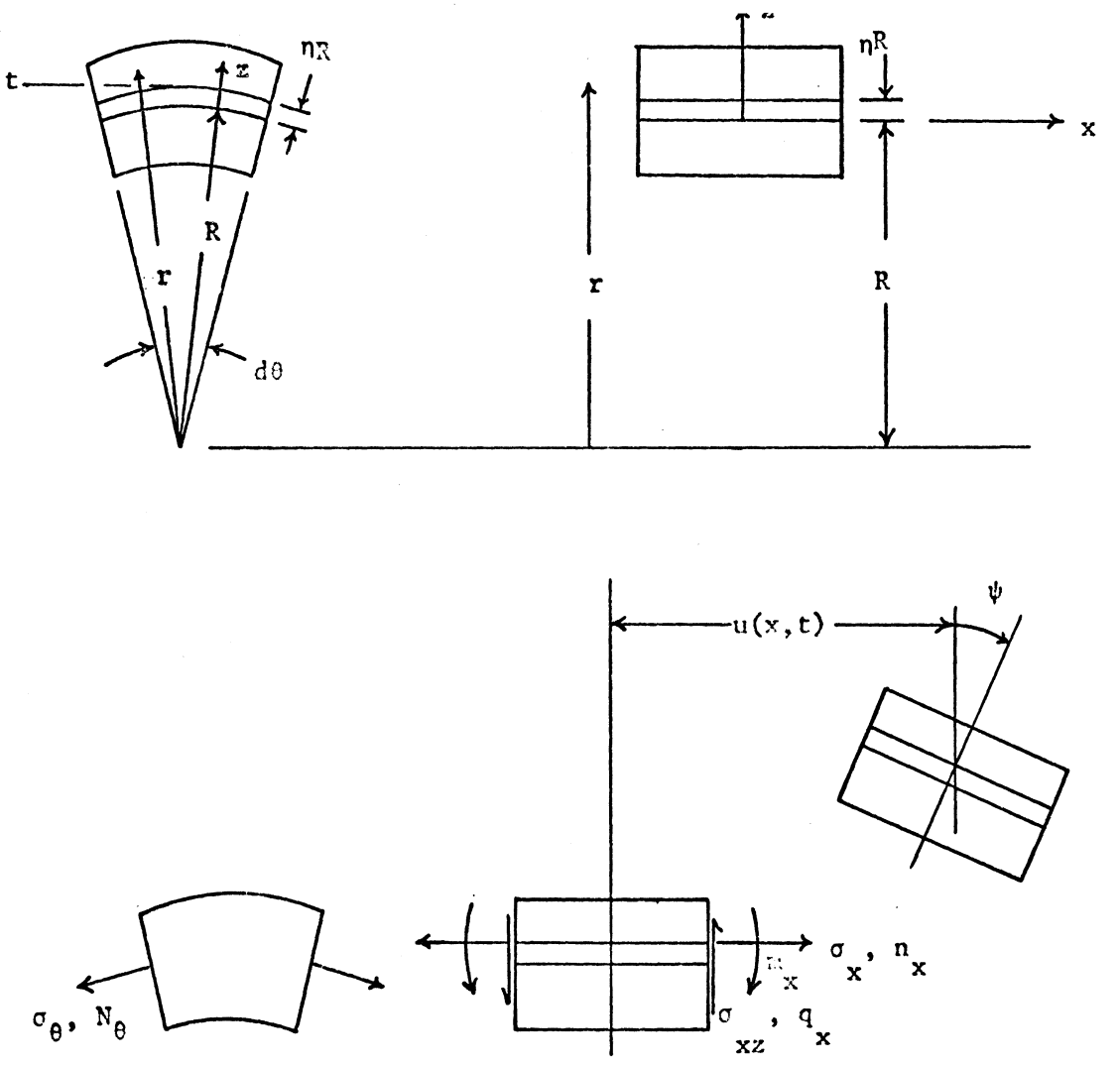


Figure 7. Thin Shell Coordinate System and Positive Stress Resultants.

The stress resultant displacement relations are obtained in the usual manner. The strain displacement relations in terms of u and $\psi$ are substituted into the Hooke's law equations and the resulting equations into the definitions of the stress resultants. The integration is carried out with the integrals containing $\sigma_z$ being neglected and the integral containing $\sigma_{xz}$ being multiplied by a constant, $k^2$, a shear correction factor in the Timoshenko beam theory sense. The determination of the value of $k^2$ has been discussed in reference [9]. Carrying out the above steps, the following stress resultant displacement relations are obtained [10]:

$$
\begin{aligned}
n_x &= \frac{hE}{(1-\nu^2)}\left[u' + \frac{\nu}{R}w\right] \\
n_\theta &= \frac{hE}{(1-\nu^2)}\left[\nu u' - \nu\eta R\psi' + \frac{w}{R}\log\left(\frac{1+\frac{h}{2R}}{1-\frac{h}{2R}}\right)\right] \\
q_x &= k^2 Gh\left[w' + \psi\right] \\
m_x &= \frac{Eh^3}{12(1-\nu^2)}\left[(1-\eta)\psi' - \frac{\nu}{R^2}w\right]
\end{aligned}
\qquad 4.2
$$

where G is the shear modulus of Elasticity and the primes denote differentiation with respect to x.

The problem to be considered here is the frictionless axial impact of the shell moving initially with a dimensionless rigid body velocity of $V_o = \frac{v_o}{C_p}$ into a flat rigid wall. It can be shown by using Hamilton's

Principle that the natural boundary conditions for this problem are the specification of three of the following: (1) either $m_x(o, t)$ or $\psi(o, t)$; (2) either $n_x(o, t)$ or $u(o, t)$; (3) either $q_x(o, t)$ or $w(o, t)$ [10]. While in any physical problem it may not be possible to realize a completely frictionless impact, the specification of $u(o, t) = 0$ and $q_x(o, t) = 0$ is not an unreasonable requirement from an intuitive point of view. The problem arises with the first boundary condition, in that in a physical situation, neither $m_x(o, t)$ or $\psi(o, t)$ can be specified from an intuitive viewpoint. Experimental evidence would be required about one or the other to be assured of a realistic physical model. Nevertheless, in the absence of experimental evidence, an additional requirement will be that the end of the shell is not free to rotate, but is allowed only to expand in the radial direction, that is $\psi(o, t) = 0$. The moment required to maintain this condition will be generated in the solution.

While the equations allow discontinuities in shear and radial velocity to be propagated at a slower wavespeed, $C_s$, axial impact subject to the above boundary conditions does not generate such discontinuities. $C_s$ is known as the speed with which discontinuities in shear, radial velocity, and the spatial derivative of the radial displacement propagate and can be shown to be numerically equal to $k\sqrt{\frac{G}{\rho}}$.

## Formulation for Solution by the Dynamical Finite Element Method

Figure 8 shows the division of the shell into a series of finite

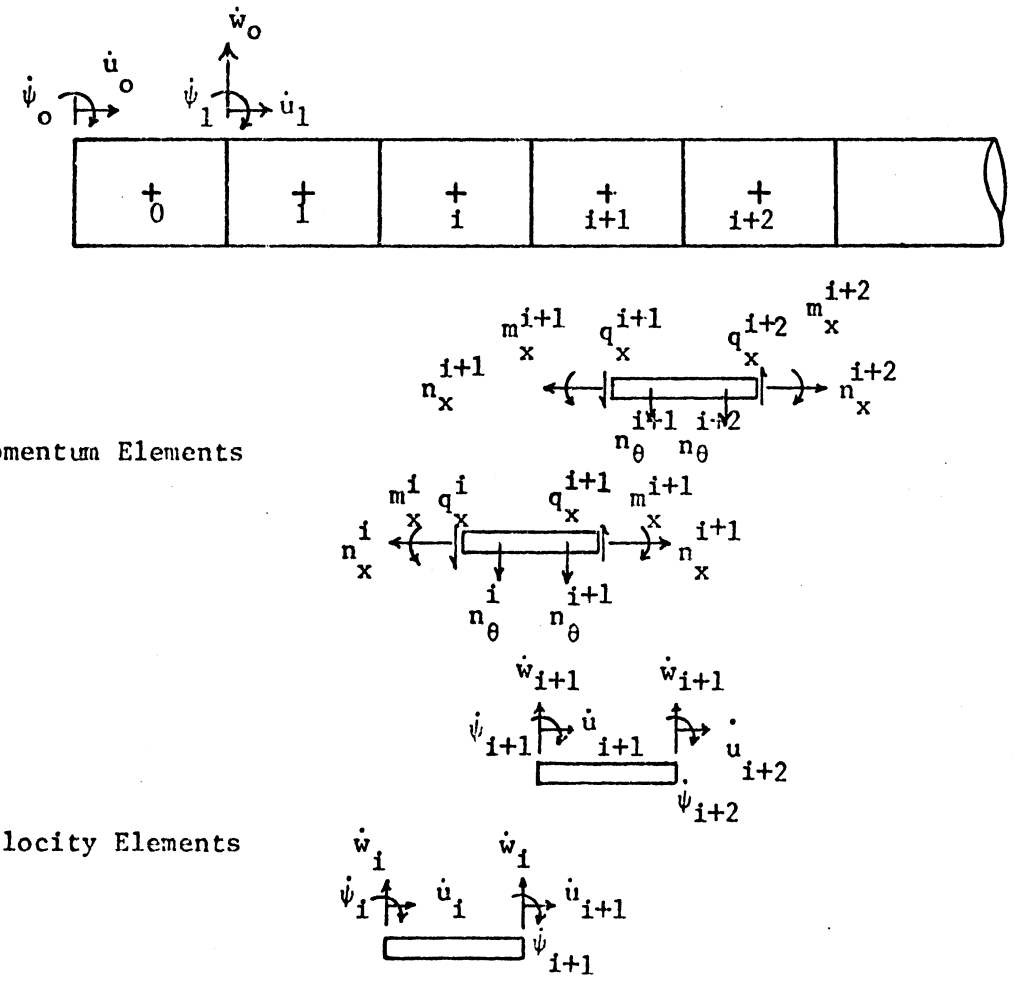


Figure 8. Finite Element Representation of Thin Cylindrical Shell with Momentum and Velocity Elements.

elements with the location of the momentum and velocity elements illustrated in the lower portion. The stress resultant displacement relations are rewritten with the derivatives in a finite difference form and the subscripts and superscripts being determined by reference to the division of elements given in figure 8.

$$n_x^i = \frac{hE}{(1-\nu^2)}\left[\left(\frac{u_{i+1}-u_i}{dx}\right)+\frac{\nu}{R}w_i\right]$$

$$n_\theta^i = \frac{hE}{(1-\nu^2)}\left[\nu\left(\frac{u_{i+1}-u_i}{dx}\right)-\nu\eta R\left(\frac{\psi_{i+1}-\psi_i}{dx}\right)+\frac{w_i}{R}\log\left(\frac{1+\frac{h}{2R}}{1-\frac{h}{2R}}\right)\right] \qquad 4.3$$

$$q_x^{i+1} = k^2Gh\left[\left(\frac{w_{i+1}-w_i}{dx}\right)+\psi_{i+1}\right]$$

$$m_x^i = \frac{Eh^3}{12(1-\nu^2)}\left[(1+\eta)\left(\frac{\psi_{i+1}-\psi_i}{dx}\right)-\frac{\nu}{R^2}w_i\right]$$

Note that the superscript i+1 is required for the shear since $q_x^o$ will be specified and $q_x^1$ will be the first shear calculated.

Application of the impulse-momentum law to the momentum element in figure 8 in the axial and radial directions yields the following changes in axial and radial velocity which will occur in the next dt increment of time:

$$d\dot{u} = \frac{(n_x^{i+1}-n_x^i)dt}{\rho h dx} \qquad 4.4$$

and

$$\dot{dw} = \frac{(n_\theta^i + n_\theta^{i+1})dt}{2\rho hR} + \frac{(q_x^{i+1} - q_x^i)dt}{\rho h dx} \qquad 4.5$$

As in the membrane, the distribution of the circumferential stress resultant has been assumed uniform over the length $\frac{dx}{2}$.

From the angular impulse-angular momentum law, the following relation is obtained:

$$I_t \dot{d\psi} = (m_x^{i+1} - m_x^i)Rd\theta dt - q_x^i Rd\theta dx dt \qquad 4.6$$

where

$$I_t = \rho hR^3 \eta(1 - \eta)dx d\theta.$$

Equations 4.3 through 4.8 may be nondimensionalized by the introduction of the following dimensionless variables in addition to those given by equations 3.9:

$$n_x = \rho C_p^2 h(FX),\ n_\theta = \rho C_p^2 h(FT),\ m_x = \rho C_p^2 hRM$$

$$q_x = \rho C_p^2 hQ,\ \psi = SI,\ u = RU,\ w = RW$$

with $G = \frac{E}{2(1 + \nu)}$, where the capitalized variables on the right hand sides are the nondimensional counterparts of the lower case variables on the left hand sides. With the introduction of these variables and with $dX = dT$, equations 4.1 through 4.6 become

$$\dot{dU} = FX_{i+1} - FX_i \qquad 4.4$$

$$\dot{dW} = Q_{i+1} - Q_i - \left(\frac{FT_{i+1} + FT_i}{2}\right) dT \qquad 4.5$$

$$\dot{dSI} = \frac{1}{\eta(1 - \eta)} [M_{i+1} - M_i - Q_i dT] \qquad 4.6$$

$$FX_i = \left(\frac{U_{i+1} - U_i}{dX}\right) + \nu W_i$$

$$FT_i = \nu\left(\frac{U_{i+1} - U_i}{dX}\right) - \nu\eta \left(\frac{SI_{i+1} - SI_i}{dX}\right) + W_i \frac{R}{h} \log \left(\frac{1 + \frac{h}{2R}}{1 - \frac{h}{2R}}\right) \qquad 4.3$$

$$Q_{i+1} = \frac{k^2(1 - \nu)}{2} \left\{\frac{W_{i+1} - W_i}{dX} + SI_{i+1}\right\}$$

$$M_i = \eta\left\{(1 - \eta)\left(\frac{SI_{i+1} - SI_i}{dX}\right) - \nu W_i\right\}$$

The equations must now be ordered for the computational procedure in accordance with the principles given in "Ordering of the Computations" in the preceding chapter. If these principles are applied, and the usual cumulation statements are introduced, the following ordered equations are obtained:

(1) $\dot{dU} = FX_{i+1} - FX_i$

(2) $\dot{U}_{i+1} = \dot{U}'_{i+1} + \dot{dU}$

(3) $dU = \dot{U}_{i+1} dT$

(4) $U_{i+1} = U'_{i+1} + dU$

$$(5)\quad d\dot{S}I = \frac{1}{(\eta - \eta^2)}\,[M_{i+1} - M_i - Q_i\,dT]$$

$$(6)\quad \dot{SI}_{i+1} = \dot{SI}'_{i+1} + d\dot{S}I$$

$$(7)\quad dSI = \dot{SI}_{i+1}\,dT$$

$$(8)\quad SI_{i+1} = SI'_{i+1} + dSI$$

$$(9)\quad Q_{i+1} = \frac{k^2(1 - \nu)}{2}\,[(\frac{W_{i+1} - W_i}{dX}) + SI_{i+1}]$$

$$(10)\quad d\dot{W} = Q_{i+1} - Q_i - (\frac{FT_{i+1} + FT_i}{2})\,dT$$

4.7

$$(11)\quad \dot{W}_i = \dot{W}'_i + d\dot{W}$$

$$(12)\quad dW = (\dot{W}_i + \frac{d\dot{W}}{2})\,dT$$

$$(13)\quad W_i = W'_i + dW$$

$$(14)\quad M_i = \eta[(1 - \eta)(\frac{SI_{i+1} - SI_i}{dX}) - \nu W_i]$$

$$(15)\quad FX_i = (\frac{U_{i+1} - U_i}{dX}) + \nu W_i$$

$$(16)\quad FT_i = \nu(\frac{U_{i+1} - U_i}{dX}) - \nu\eta(\frac{SI_{i+1} - SI_i}{dX}) + W_i\,\frac{R}{h}\log\,(\frac{1 + \frac{h}{2R}}{1 - \frac{h}{2R}})$$

where the primes indicate that this value of the dependent variable existed before the dT occurred.

Since this problem requires the specification of mixed boundary conditions, that is, both stress-type and displacement or velocity-type, some difficulty was experienced in arriving at the proper order. Observation reveals that it may be possible to establish an additional rule concerning the ordering based on the experience with the three separate problems encountered thus far. Note that in all three cases (equations 3.10, 3.11, and 4.7), the dependent variable having the i+1 subscripts on the left-hand sides of the equations are computed first. Behind the wavefront, this insures that they are available for use in the equations following their computation, whereas at the wavefront, the execution of these steps gives back initial values thus insuring that diffusion is prohibited.

The procedure is executed by initializing the dependent variables of all elements to zero with the exception of the axial velocities $\dot{U}_i$ which are set equal to $V_o$. $\dot{U}_o$ and $U_o$ are then set equal to zero and steps 1 through 16 are carried out across the shell for the first dT with i taking on all values from zero to j. The time is incremented and steps 1 through 16 are repeated beginning again with i = 0 and working through j. Note that for the initial value problem, it is necessary to carry out the computation to the end of the shell, $x = \ell$, in order to compute the axial displacements which the elements beyond the wavefront have relative to the end x = 0, due to their initial velocities $V_o$.

## Boundary Conditions for the Finite Cylindrical Shell

The free end of the shell must be stress free which requires that three boundary conditions be specified as follows:

(1) $Q_{j+1} = 0$

(2) $FX_j = 0$

(3) $M_j = 0$

where j is the subscript of the last element. In accordance with "Boundary Conditions for Finite Membranes" in the last chapter, the first boundary condition can be satisfied by executing the statement $Q_{i+1} = 0$ when $i = j$ after step 9 of equations 4.7. The remaining two boundary conditions must be satisfied by setting $M_j = 0$ and $FX_j = 0$ in steps 14 and 15, respectively, of equations 4.7 and working up through the steps to obtain expressions for $\dot{SI}_{j+1}$ and $\dot{U}_{j+1}$. Carrying out the algebra results in the following expressions for these quantities:

$$\dot{U}_{i+1} = \frac{1}{dT}\{U_i - U'_{i+1} - \nu dX[W'_i + \dot{W}'_i dT - \frac{3dT^2}{4} FT'_i]\} \qquad 4.8$$

and

$$\dot{SI}_{i+1} = \frac{1}{dT}\{SI_i - SI'_{i+1} + \frac{\nu dX}{(1 - \nu)}[W'_i + \dot{W}'_i dT - \frac{3dT^2}{4} FT'_i]\} \qquad 4.9$$

where the primes refer to the values which existed before the dT occurred. These steps are executed when i = j with equation 4.8 appearing after step 1 of equations 4.7 and equation 4.9 appearing after step 5 of the same equations.

## Energy Balance

One of the strongest criticisms expressed by Chou [10] about the Method of Characteristics solution to the impacting semi-infinite cylindrical shell in reference [8] is that the resulting kinetic energy stored in the shell at a given time is several orders of magnitude larger than the total energy input. The conjecture is that numerical instability occurred in the integration scheme. Since all dependent variables necessary for the calculation of the various energies are available for computational use at any time t, in the scheme used here, a check can be maintained on the solution by evaluating numerically the expressions for the energy balance over the length of the shell.

At any time t for the initial value problem posed, conservation of energy requires that the sum of the strain and kinetic energies stored in the shell be equal to the initial kinetic energy which the shell had before impact. Expressions for the kinetic and strain energies can be obtained in the usual manner leading to the following energy balance:

$$\frac{1}{2}mv_o^2 = \pi\rho hR\int_{x=0}^{x=\ell}[\dot{u}^2 + \eta R^2(1-\eta)\dot{\psi}^2 + \dot{w}^2]dx$$

$$+ \pi R\int_{x=0}^{x=\ell}\{\frac{hE}{1-\nu^2}[u' + \frac{\nu}{R}w]^2 + \frac{E}{R(1-\nu^2)}[\log(\frac{1+\frac{h}{2R}}{1-\frac{h}{2R}}) - \frac{\nu^2 h}{R}(1 + \frac{\eta}{1-\eta})]w^2$$

$$+ \frac{Eh^3(1-\eta)}{12(1-\nu^2)}[\psi' - \frac{\nu w}{R^2(1-\eta)}]^2 + k^2Gh(w' + \psi)^2\}dx \qquad 4.10$$

where m is the total mass of the shell, $\ell$ is the length, and the dot and prime refer to differentiation with respect to t and x, respectively. The expressions on the right-hand side of equation 4.10 for the kinetic and strain energies respectively are the same as those used by Chou [10] in connection with Hamiltons Principle with the exception of the logarithmic term which he approximated by $\log(\frac{1+\frac{h}{2R}}{1-\frac{h}{2R}}) \approx \frac{h}{R}(1 + \eta + \ldots)$.

In nondimensional form equation 4.10 becomes:

$$LV_o^2 = \int_{X=0}^{X=L}[\dot{U}^2 + \eta(1-\eta)\dot{SI}^2 + \dot{W}^2]dX$$

$$+ \int_{X=0}^{X=L}\{[U' + \nu W]^2 + \eta(1-\eta)[SI' - \frac{\nu}{1-\eta}W]^2$$

$$+ \frac{R}{h}[\ln(\frac{1+\frac{h}{2R}}{1-\frac{h}{2R}}) - \frac{\nu^2 h}{R}(1 + \frac{\eta}{1-\eta})]W^2 \qquad 4.11$$

$$+ \frac{k^2}{2}[W' + SI]^2\}dX$$

where $\ell = LR$, L being the nondimensional length of the shell and the dot and prime referring to differentiation with respect to T and X, respectively.

The check is carried out by visualizing the results of equations 4.7 as values from which curves can be plotted under which the areas must be found to evaluate the integrals on the right-hand side of equation 4.11. Any of the standard numerical integration rules can be used for the evaluation of these integrals. Care must be taken, however, to account for any discontinuities in the dependent variables that arise at the wavefront or some small avoidable error will occur. Since the position of the wavefront is known at all times, the necessary integration can be carried out in two parts:

$$\int_{X=0}^{X=L} = \int_{X=0}^{X=WF} + \int_{X=WF}^{X=L}$$

where WF represents the wavefront coordinate.

# DISCUSSION

## General

While no formal proofs can be given at this time, it is appropriate to discuss the conditions used in determining that the computational procedure yields the unique solution for the problems under consideration. The conditions to be discussed are as follows:

(1) In the limit as dt and ds approach zero simultaneously, the equations derived from the finite element representation of the problem geometry reduce to the differential equations which govern the problem.

(2) The boundary and initial conditions are satisfied.

(3) The conditions at the wavefront are satisfied without artificiality.

(4) The various energies computed from the results are properly in balance.

(5) Numerical convergence of the results is observed.

Conditions (1) and (2) are clearly necessary to obtain the correct solution and warrant little discussion. Condition (3) is not so obvious, however. Satisfaction of the wavefront conditions implies several considerations. First, the discontinuities which appear at the wavefront do so without any artificial manipulation in that they arise naturally through the equations from the initial and boundary conditions. Secondly, these discontinuities are seen to vary properly in magnitude. For example, the jump in meridional stress, $\{\sigma_s\}$, for the conical membrane

impacting with an axial velocity $v_o$ can be shown to be [11],

$$\{\sigma_s\} = -\frac{v_o}{\sqrt{s}} \sec \alpha$$

where $\alpha$ is the cone angle and s is the meridional coordinate. The results from equations 3.10 for the conical membrane give a jump in meridional stress which does vary in exactly this fashion. Finally, the jumps are seen to propagate without diffusion and furthermore diffusion is not prohibited artificially. A computational order is found so that if the calculations are carried out beyond the wavefront, initial conditions are obtained. That such a computational order should exist seems reasonable on the basis of the hyperbolic nature of the equations governing these problems.

Condition (4) is not only a check on the correctness of the results, but also provides a check on the stability of the calculations. The nature of the method is to cumulate new values of dependent variables which are calculated from values computed before the new dT occurs. This means that any per-step numerical error is also cumulative. The numerical computations necessary to perform the energy balance check do not involve such open-ended error cumulation since the energy depends only on the values that exist at a given time. When the solution becomes seriously unstable through numerical error accumulation, the energy is no longer balanced.

The first four conditions are considered necessary with the fifth condition providing sufficiency. Decreasing the step size and observing

convergence is the numerical equivalent of the limiting process and it is on this basis, along with the satisfaction of the first four conditions, that the solutions given here were determined. Successive decreases in step size yield results which for practical purposes agree as illustrated in figure 9. This figure shows the spatial distribution of the nondimensional radial velocity ($\dot{W}$) for the finite cylindrical membrane at T = 15 for dT = 0.1, 0.05, 0.025, and 0.0125. The radial velocity appeared to be the dependent variable which was most sensitive to the magnitude of dT for the cylindrical membrane. For all practical purposes the results for dT = 0.0125 changed a negligible amount from the values found at dT = 0.025 and hence the results at dT = 0.025 were considered to be the solution. Although a step size of dT = 0.0125 and dT = 0.005 is necessary for convergence of the parabolic membrane of revolution and the thin cylindrical shell, respectively, figure 9 is typical of the nature of the convergence for all cases studied.

The rapid variations observed at the end, L = 10, are also characteristic of the membranes studied and appear to be due to some form of truncation error since as dT is decreased, these oscillations also decrease to zero. These oscillations only appear in the radial variables and never encompass more than a few elements. The meridional variables are quite smooth for all values of dT.

## Discussion of Results

Semi-infinite Cylindrical Membrane - Figure 10 shows a portion of

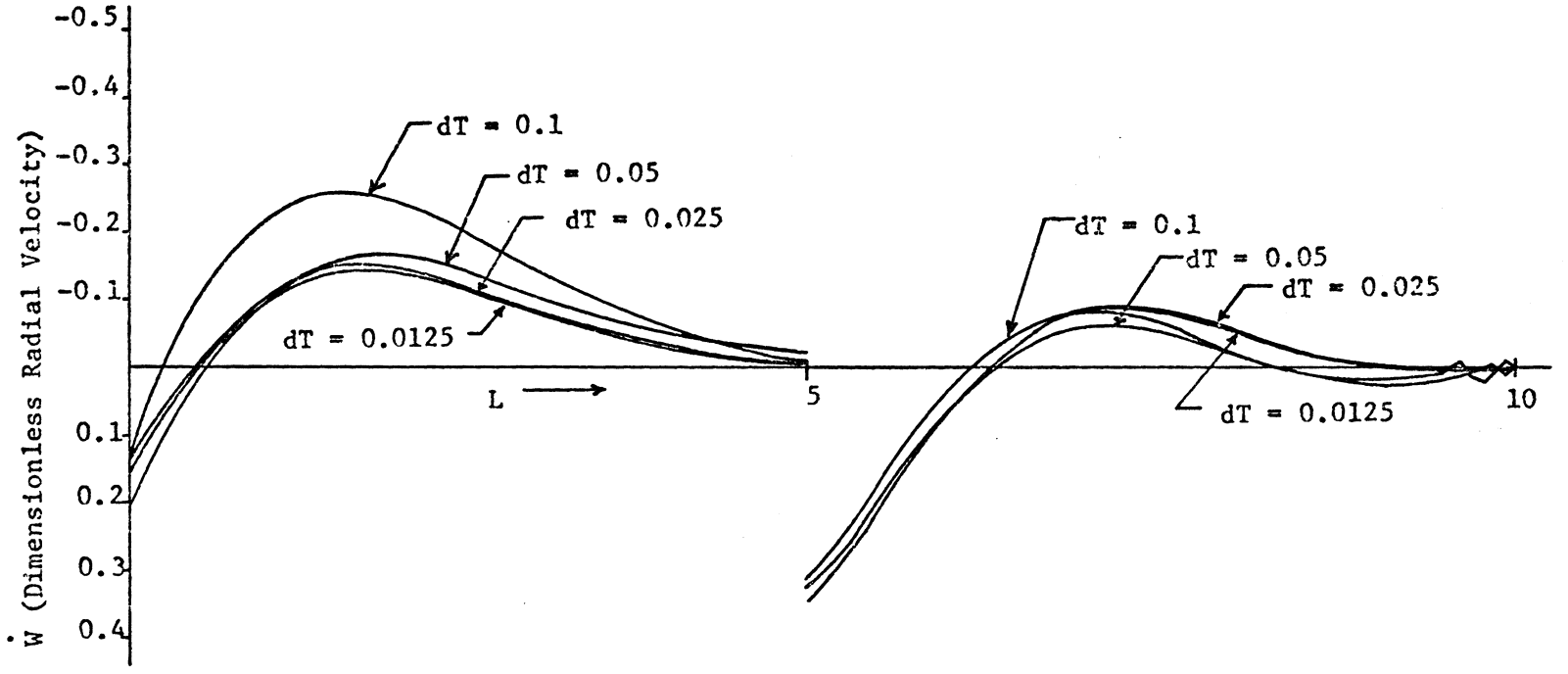


Figure 9. Spatial Distribution of the Nondimensionalized Radial Velocity in a Finite Cylindrical Membrane at T = 15 (free-end at L = 10) for dT = 0.1, 0.05, 0.025, 0.0125. $V_o = 1$, $\nu = 1/3$.

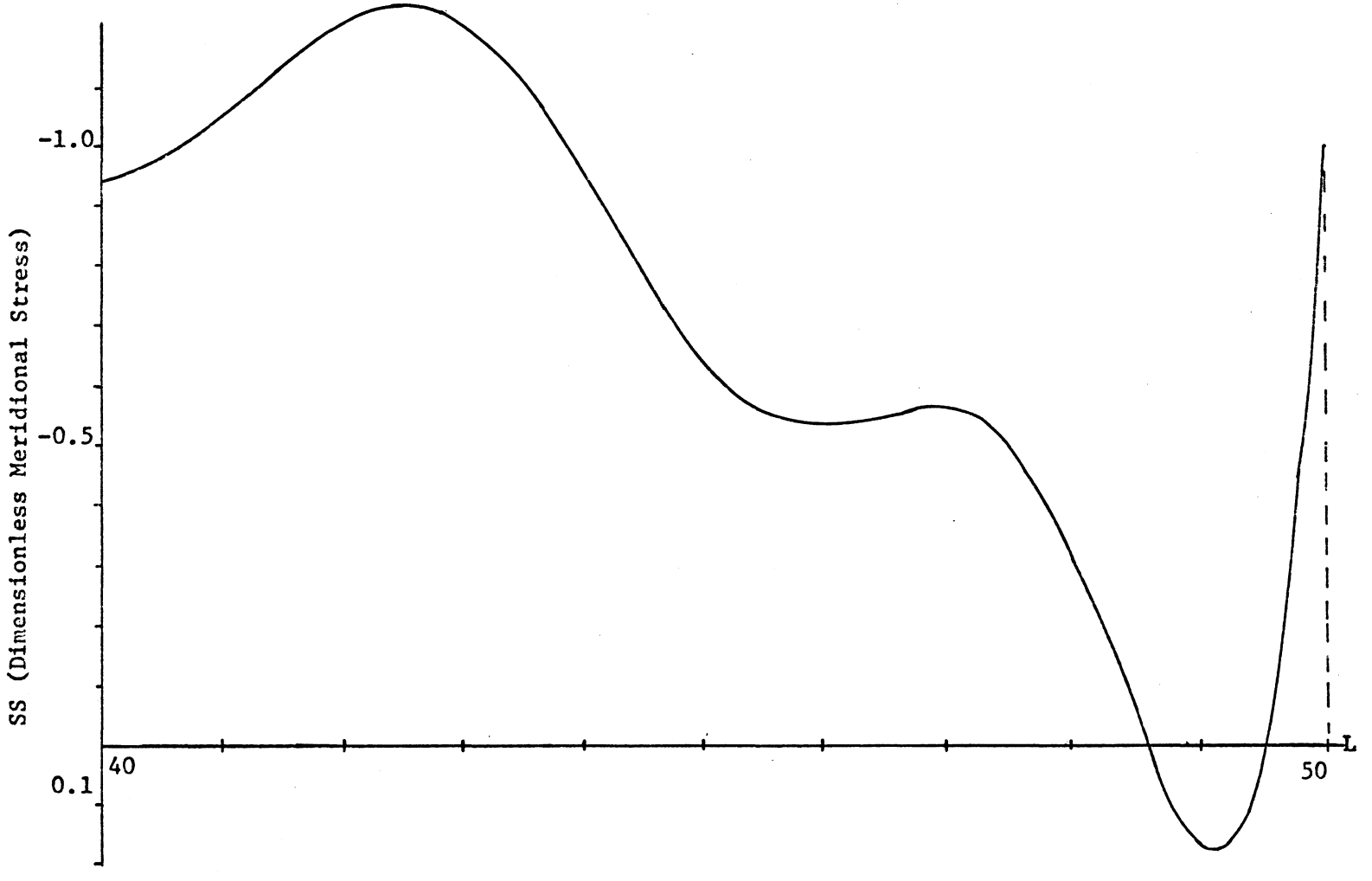


Figure 10. Spatial Distribution of the Nondimensionalized Meridional Stress in a Semi-infinite Cylindrical Membrane at T = 50. $V_o$ = 1, $\nu$ = 1/3, dT = 0.025.

the spatial distribution of the nondimensional meridional stress, (SS), in a semi-infinite cylindrical membrane which exists when the wavefront has reached 50 radii away from the excited end of the membrane. The excitation in this case is the specification of a sudden jump in meridional velocity with quiescent conditions elsewhere. The spatial distribution, which is plotted for 10 radii behind the wavefront, clearly shows the precursor which decays rapidly into a tensile region before beginning to increase in compression. These results are in good agreement with results published by Spillers and Chapman [14], Akin and Counts [13], and Berkowitz [5] at and behind the wavefront. Immediately behind the tensile region, however, the better agreement seems to be with the continued fraction analysis in reference [13] rather than with the asymptotic solution given in [5].

Figure 11 shows the spatial distribution of the nondimensional meridional stress, (SS), at T = 5 and 10 in a semi-infinite cylindrical membrane resulting from a rectangular stress pulse excitation at X = 0. The input stress pulse lasts for a time equivalent to one nondimensional radius and has a magnitude of unity. The stress pulse involves two discontinuities in meridional stress, the first resulting from sudden application and the second from sudden removal. Both jumps are computed by the procedural equations with no inputs other than a description of the stress pulse, and both jumps are seen to propagate down the membrane with constant magnitudes. It is interesting to note that a tensile "precursor" appears to be developing behind the second jump while the stress between the two jumps is compressive.

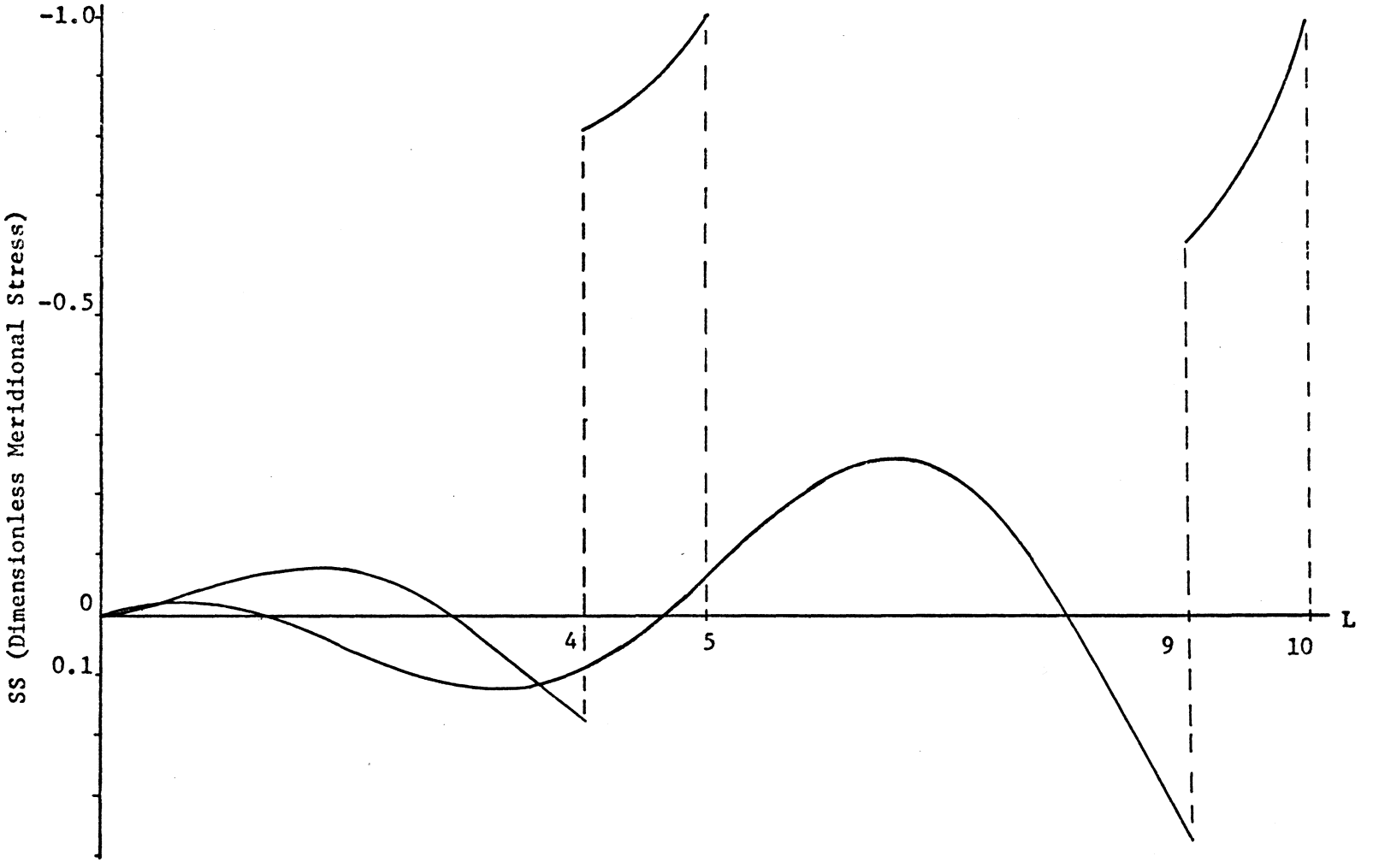


Figure 11. Spatial Distribution of the Nondimensionalized Meridional Stress in a Semi-infinite Cylindrical Membrane at T = 5, 10, resulting from a Rectangular Stress Pulse Excitation at X = 0. $\nu = 1/3$, dT = 0.025.

Finite Cylindrical Membrane - Figures 12 and 13 show the spatial distribution at T = 5, 10, 15, 20 and 25 of the nondimensional meridional, (SS), and circumferential stress, (ST), respectively in a finite, (L = 10), cylindrical membrane. The input is the specification of a discontinuity in the meridional velocity of magnitude unity at the excited end, L = 0, with the end, L = 10, assumed to be free. The jumps are seen to propagate with constant magnitude and to bear the relationship that {ST} = $\nu${SS}, (where the braces, {}, mean "the jump in"), which is consistent with analysis by other means. Note that the region immediately behind the wavefront is beginning to show the "rapid decay" at T = 10 observed in figure 10 at T = 50. This region is "flipped over" at T = 15 and 20 with the slope behind the wavefront becoming progressively steeper.

With the return of the reflected wave to the excited end of the membrane at T = 20, much of the stress that exists at T = 10 has been relieved, and consequently, from energy consideration it is expected that the velocities should correspondingly increase. Examination of figures 14 and 15 which show the spatial distribution of the nondimensional meridional ,$\dot{U}$, and normal velocities, $\dot{W}$, at the corresponding times illustrate the consequent increase in kinetic energy. Note that figure 15 is consistent with the requirement that no jump in the normal velocity should appear, but that a very definite jump in the spatial derivative of this velocity is seen at T = 5, 15, and 25 at which time the jump should be at L = 5. It is also noted that all dependent variables vanish at the free end, as might be expected for the cylindrical

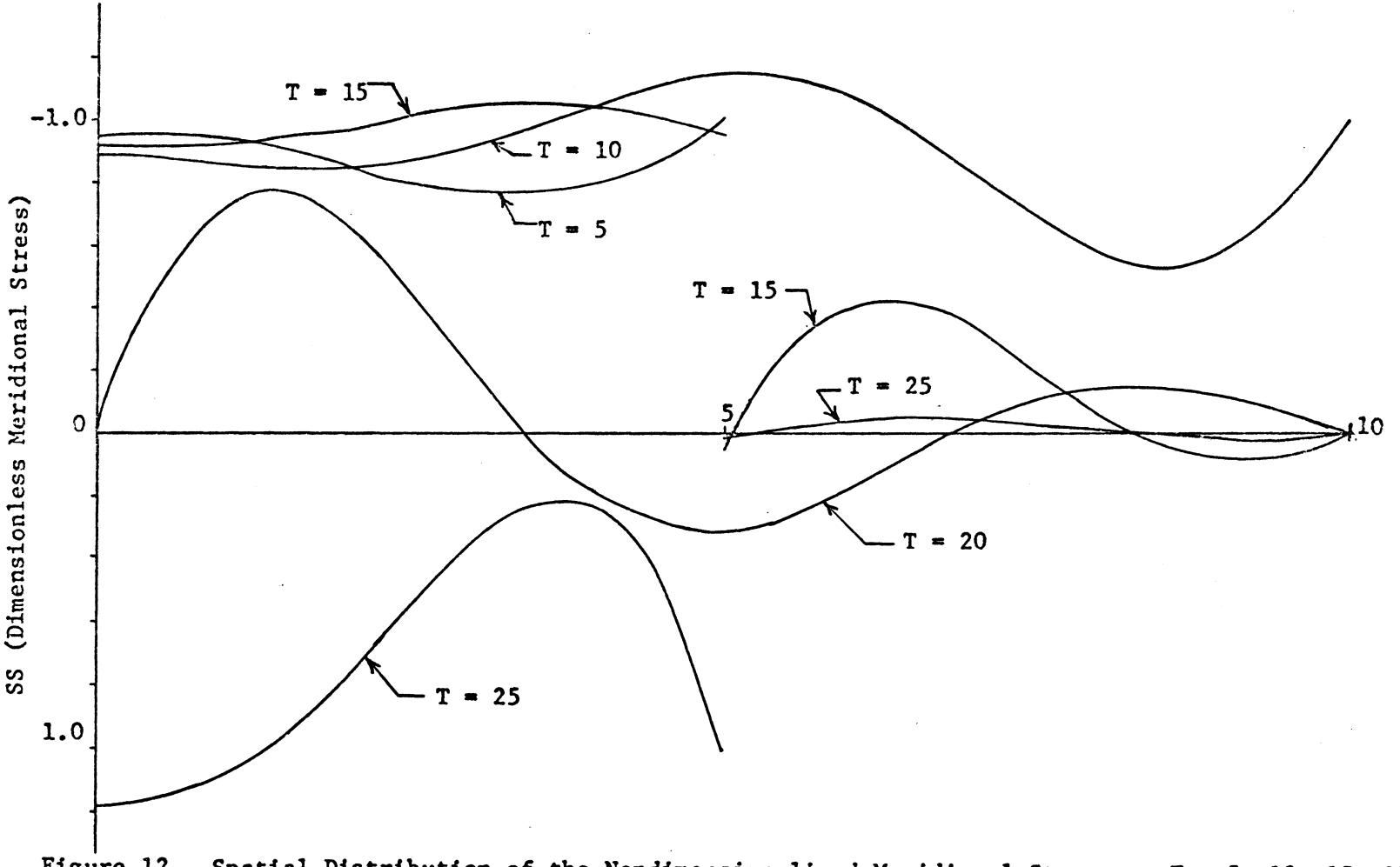


Figure 12. Spatial Distribution of the Nondimensionalized Meridional Stress at T = 5, 10, 15, 20, 25 in a Finite Cylindrical Membrane (free-end at L = 10). $V_o = 1$, $\nu = 1/3$, $dT = 0.025$.

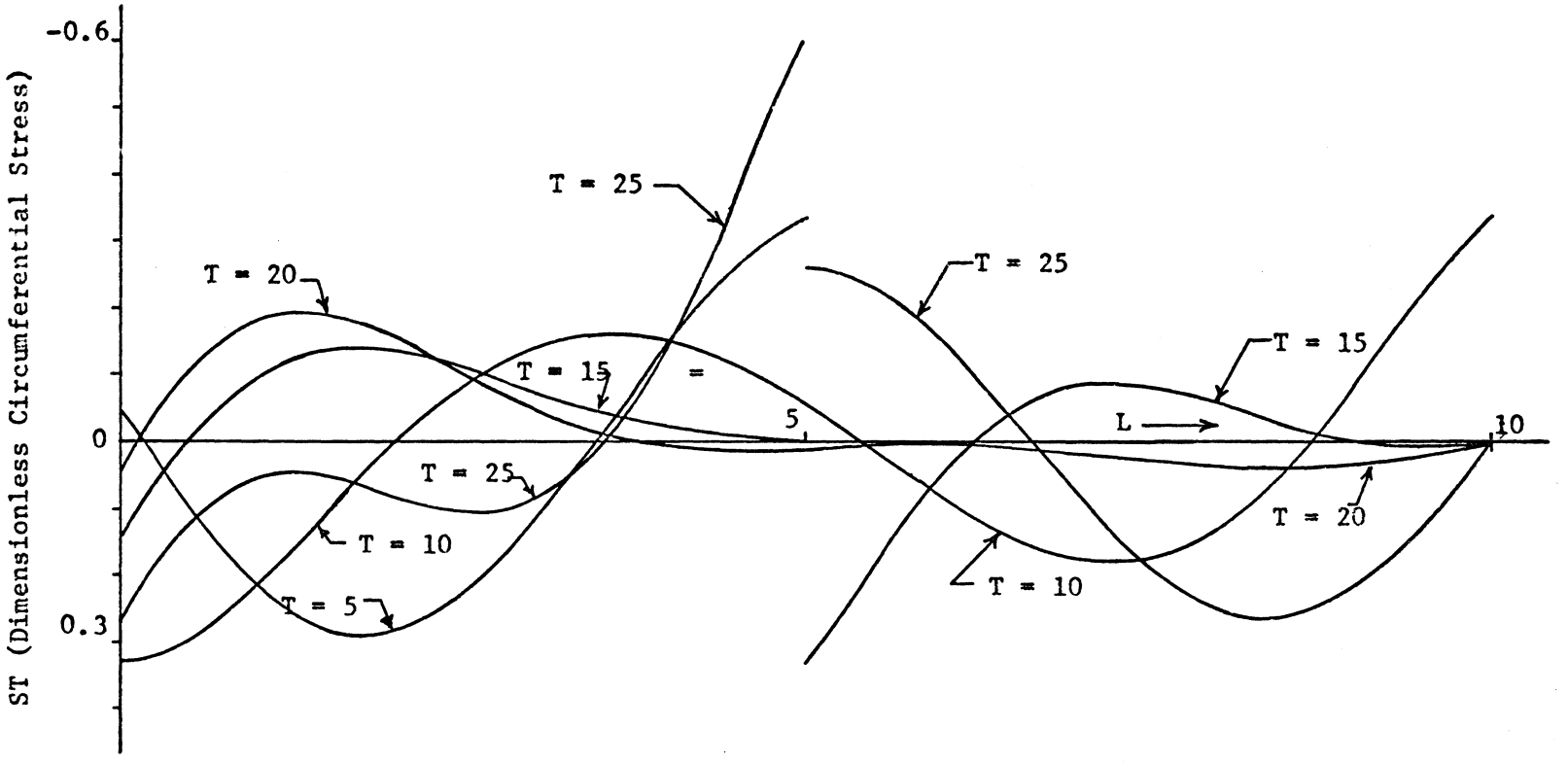


Figure 13. Spatial Distribution of the Nondimensionalized Circumferential Stress at T = 5, 10, 15, 20, 25 in a Finite Cylindrical Membrane (free end at L = 10). $V_o = 1$, $\nu = 1/3$, dT = 0.025.

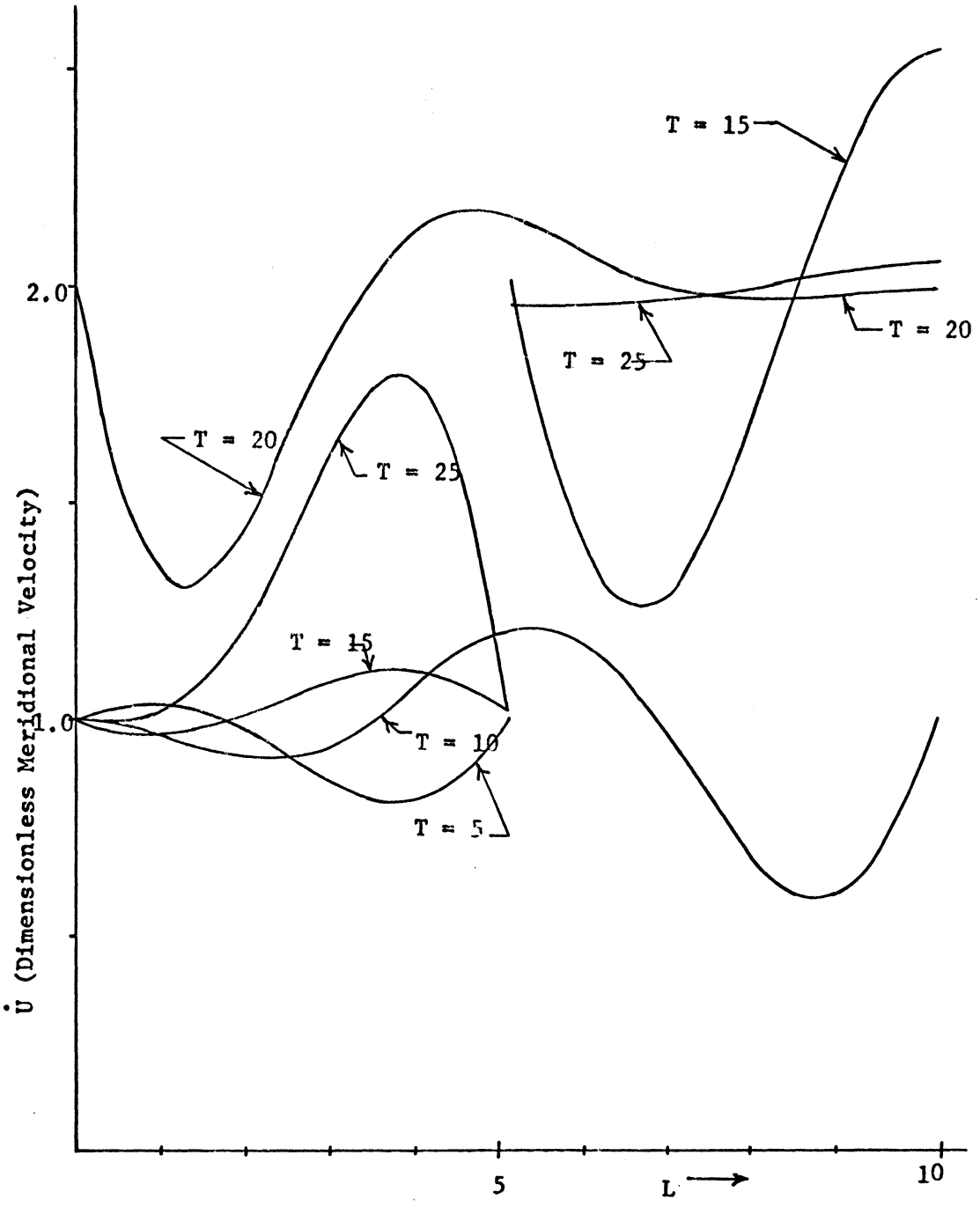


Figure 14. Spatial Distribution of the Nondimensionalized Meridional Velocity at T = 5, 10, 15, 20, 25 in a Finite Cylindrical Membrane (free end at L = 10). $V_o = 1$, $\nu = 1/3$, $dT = 0.025$.

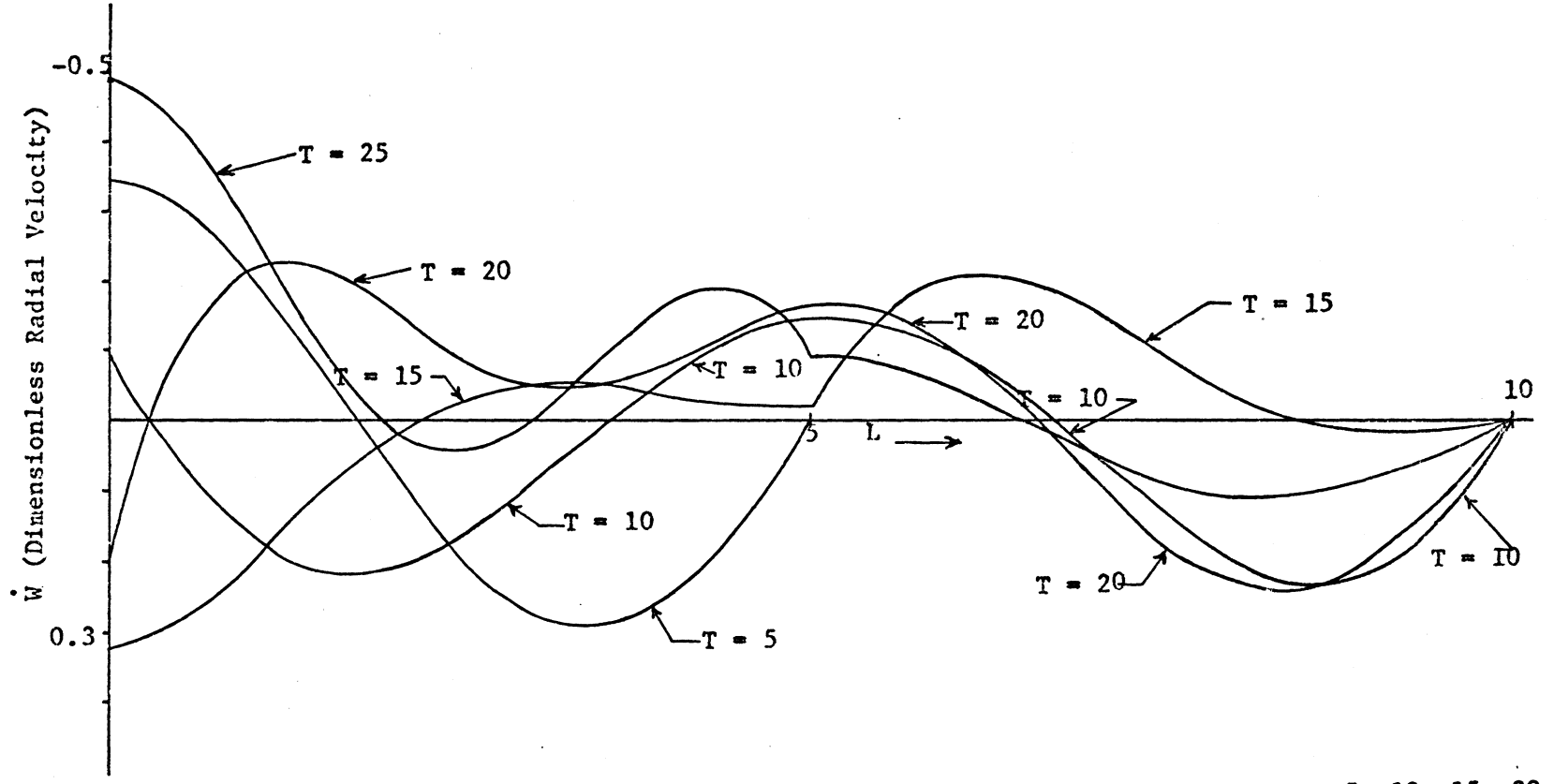


Figure 15. Spatial Distribution of the Nondimensionalized Radial Velocity at T = 5, 10, 15, 20, 25 in a Finite Cylindrical Membrane (free end at L = 10). $V_o = 1$, $\nu = 1/3$, $dT = 0.025$.

membrane by a method-of-images argument.

Figure 16 illustrates the temporal history at the end, X = 0, of the nondimensional meridional and circumferential stresses. The meridional stress represents the force that is required to maintain the velocity of the end of the membrane constant. Both stresses appear to be approximately periodic and in phase and both show an apparent marked increase in temporal frequency with the return of the reflected jump at T = 20. Observing such behavior might prove helpful in an approximate analytical solution.

Semi-infinite Conical Membrane - Figure 17 exhibits the solution for the spatial distribution of the nondimensional meridional stress (SS) in a semi-infinite 15° conical membrane for two different velocity inputs. The solid curve is the result of the velocity being prescribed tangent to the meridional curve at the end X = 0, while the dotted curve is the solution resulting from the axial velocity being prescribed, (see section "Boundary Conditions at the Excitation End" and figure 5). While the curves are similar in both shape and magnitude, the "conical push" problem produces a smoother spatial gradient. Both curves show a slight tendency toward developing a precursor with the tangential velocity input exhibiting this tendency earlier than the axial velocity input. The conical geometry requires that the magnitude of the jump decreases as it propagates outward along the meridian which seems to prevent the signal spike from forming. The solution for the axial velocity input at T = 3.8625 coincides with the results given by King [11] at his corresponding time.

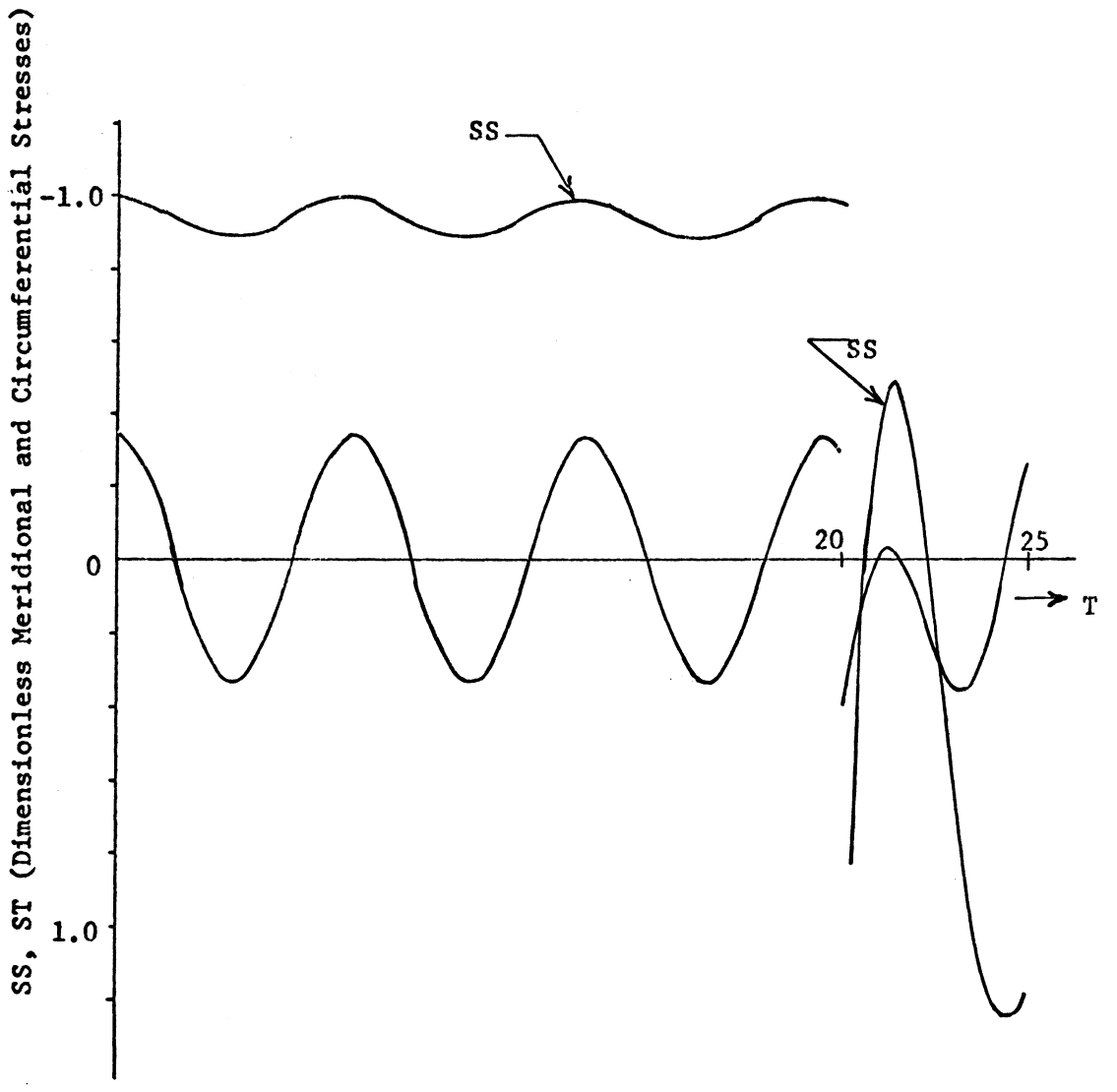


Figure 16. Temporal History of the Nondimensionalized Meridional and Circumferential Stresses at the end, x = 0, in a Finite Cylindrical Membrane (free end at L = 10). $V_o$ = 1, $\nu$ = 1/3, dT = 0.025.

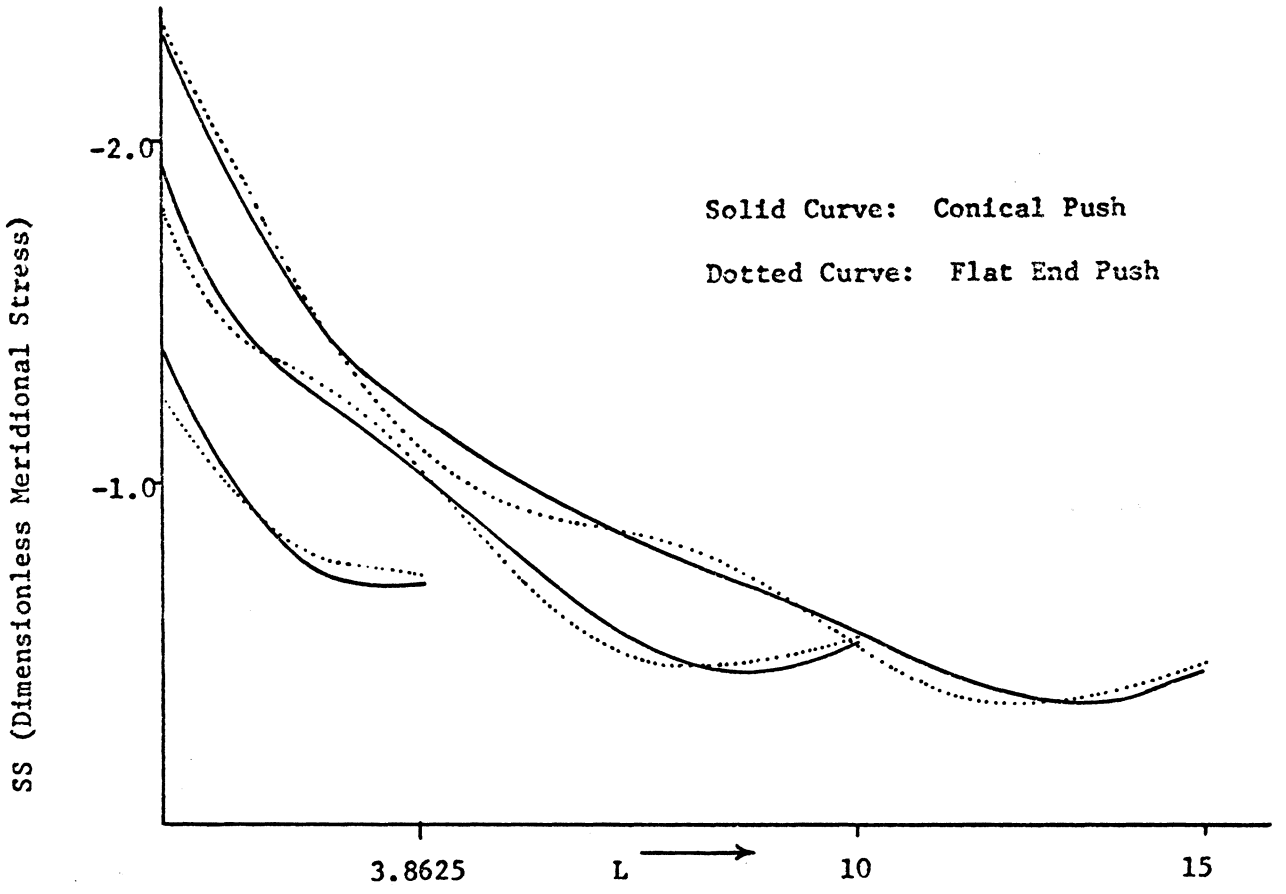


Figure 17. Comparison of Spatial Distribution of the Nondimensionalized Meridional Stresses in a Semi-infinite 15° Conical Membrane at T = 3.8625, 10, 15 resulting from Flat and Tangential Velocity Inputs at x = 0. $V_o$ = 1, $\nu$ = 0.3, dT = 0.0125.

Figure 18 shows the spatial distribution of the nondimensional circumferential stress, (ST), in a semi-infinite 15° conical membrane subjected to a tangential velocity input at the times corresponding to those of figure 17. Although not shown, the circumferential stress for the axial velocity input deviates very little from the result given here.

Finite Conical Membrane - Figures 19 and 20 show the spatial distributions of the nondimensional meridional (SS) and circumferential stresses, (ST), respectively, at T = 15, 20, and 25 in a finite 15° conical membrane. The input excitation is the prescribed tangential velocity of magnitude unity and the free end is at L = 10. It should be noted that the circumferential stress, (ST), does not vanish at the free end of the conical membrane as it did for the cylinder. Figures 21 and 22 show the time history of SS and ST, respectively, at the excited end, L = 0, of this membrane. The meridional stress for the conical membrane shows oscillations superimposed on a steadily increasing value of SS up until the appearance of the reflected jump at T = 20, whereas the stress on the end of the cylindrical membrane (figure 16) remains relatively constant. Since the rate at which more mass is experiencing a momentum change is increasing in the conical membrane, it seems reasonable to expect that the force required to maintain a constant velocity of this end to increase.

Finite Parabolic Membrane - Figures 23, 24, and 25 illustrate some of the results for a finite parabolic membrane of revolution. The input is the prescribed tangential velocity of magnitude unity and the free

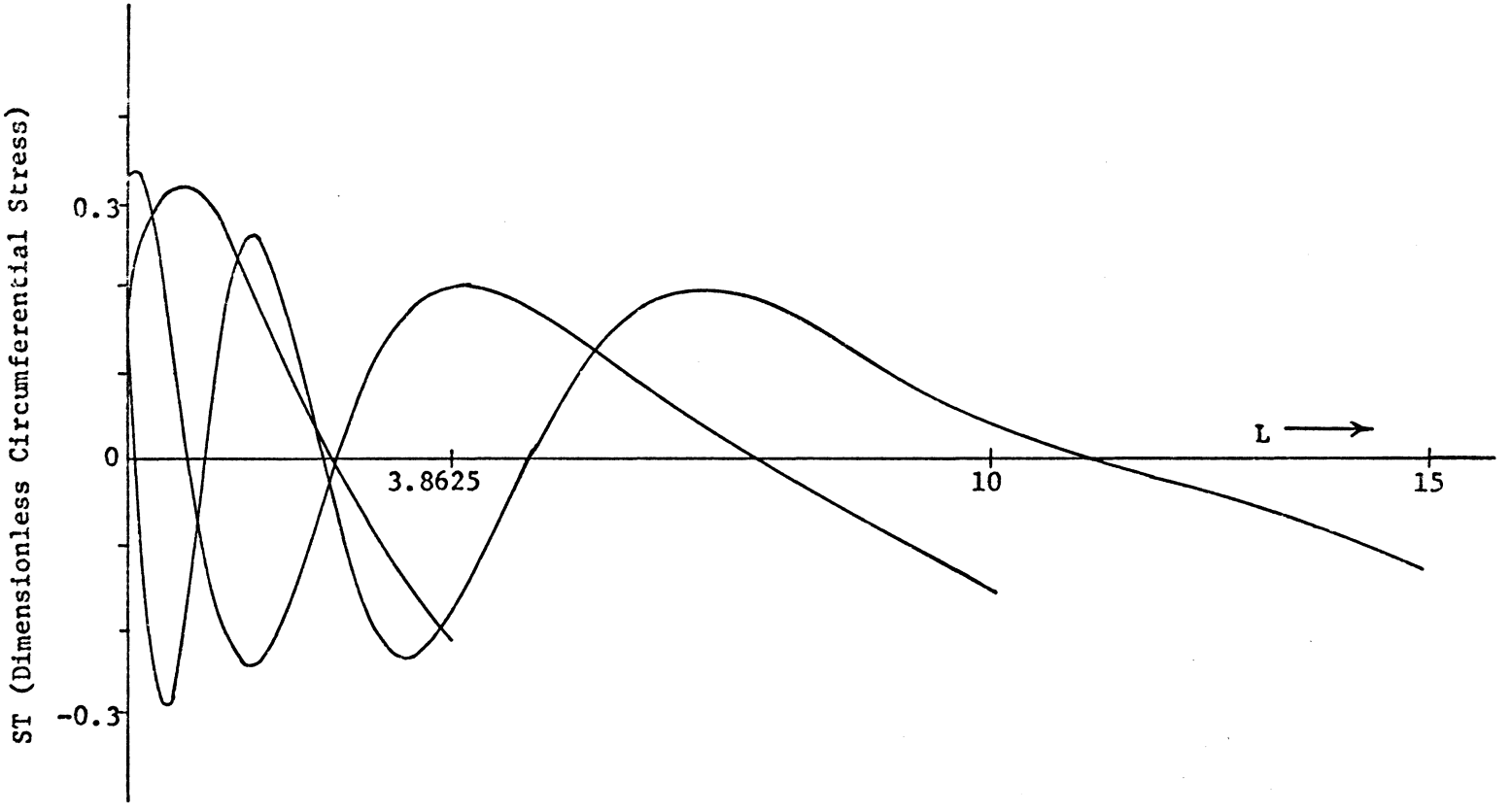


Figure 18. Spatial Distribution of the Nondimensionalized Circumferential Stress in a Semi-infinite 15° Conical Membrane at T = 3.8625, 10, 15. Velocity input Tangent t o Meridian. $V_o = 1$, $\nu = 0.3$, dT = 0.0125.

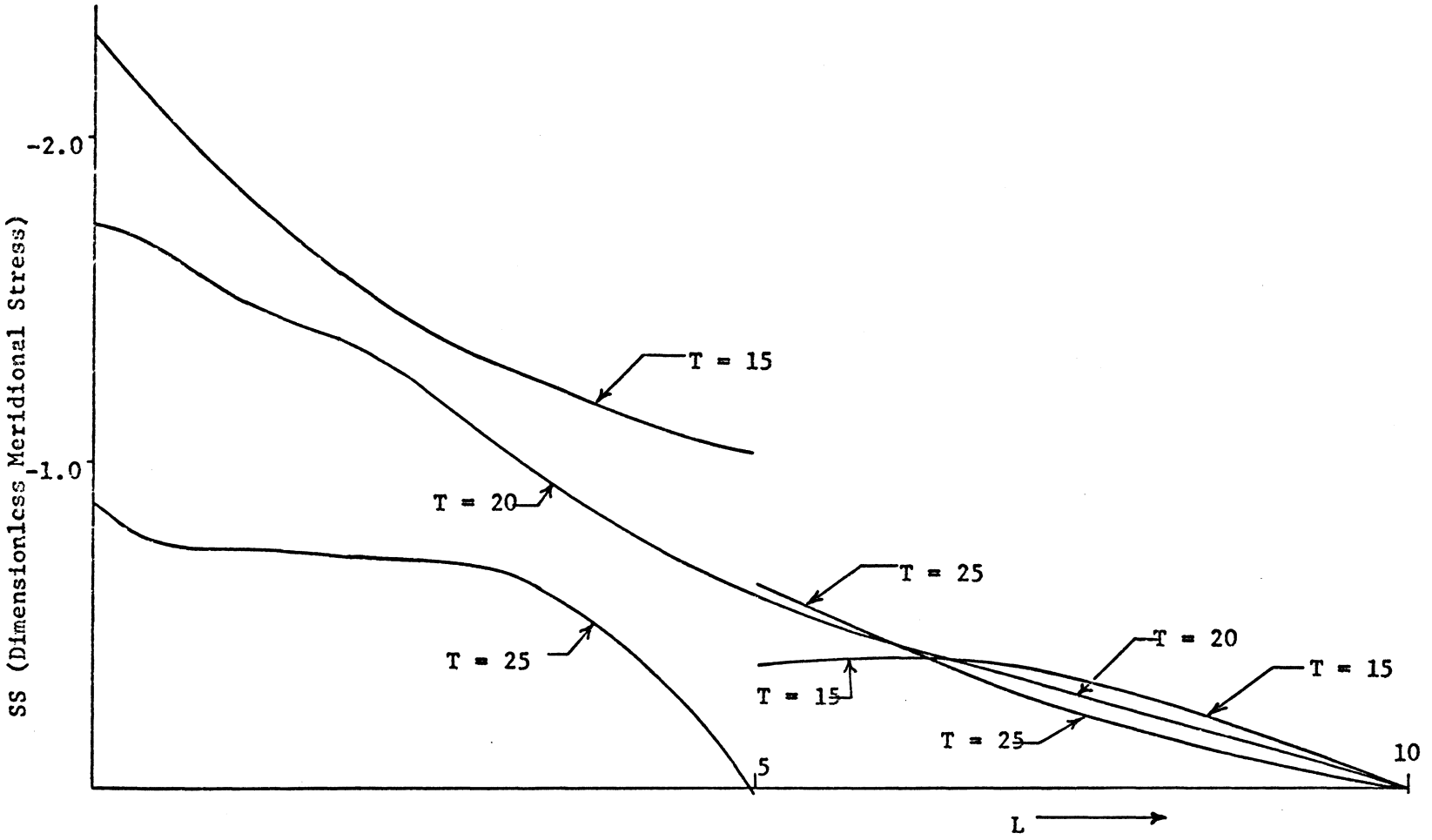


Figure 19. Spatial Distribution of the Nondimensionalized Meridional Stress at T = 15, 20, 25 in a Finite 15° Conical Membrane (free end at L = 10). $V_o = 1$, $\nu = 0.3$, $dT = 0.0125$.

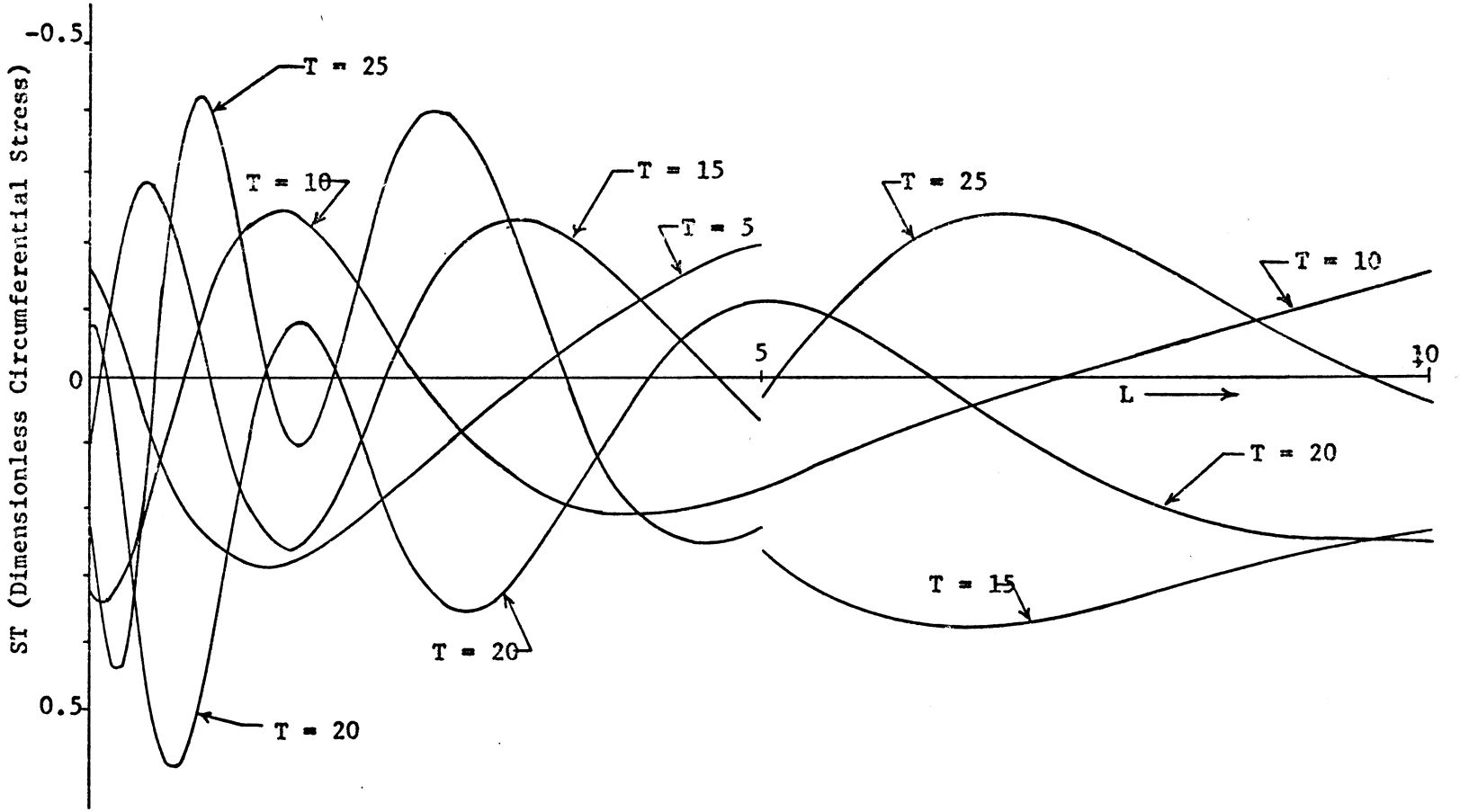


Figure 20. Spatial Distribution of the Nondimensionalized Circumferential Stress at T = 5, 10, 15, 20, 25 in a Finite 15° Conical Membrane (free-end at L = 10. $V_o$ = 1, $\nu$ = 0.3, dT = 0.0125.

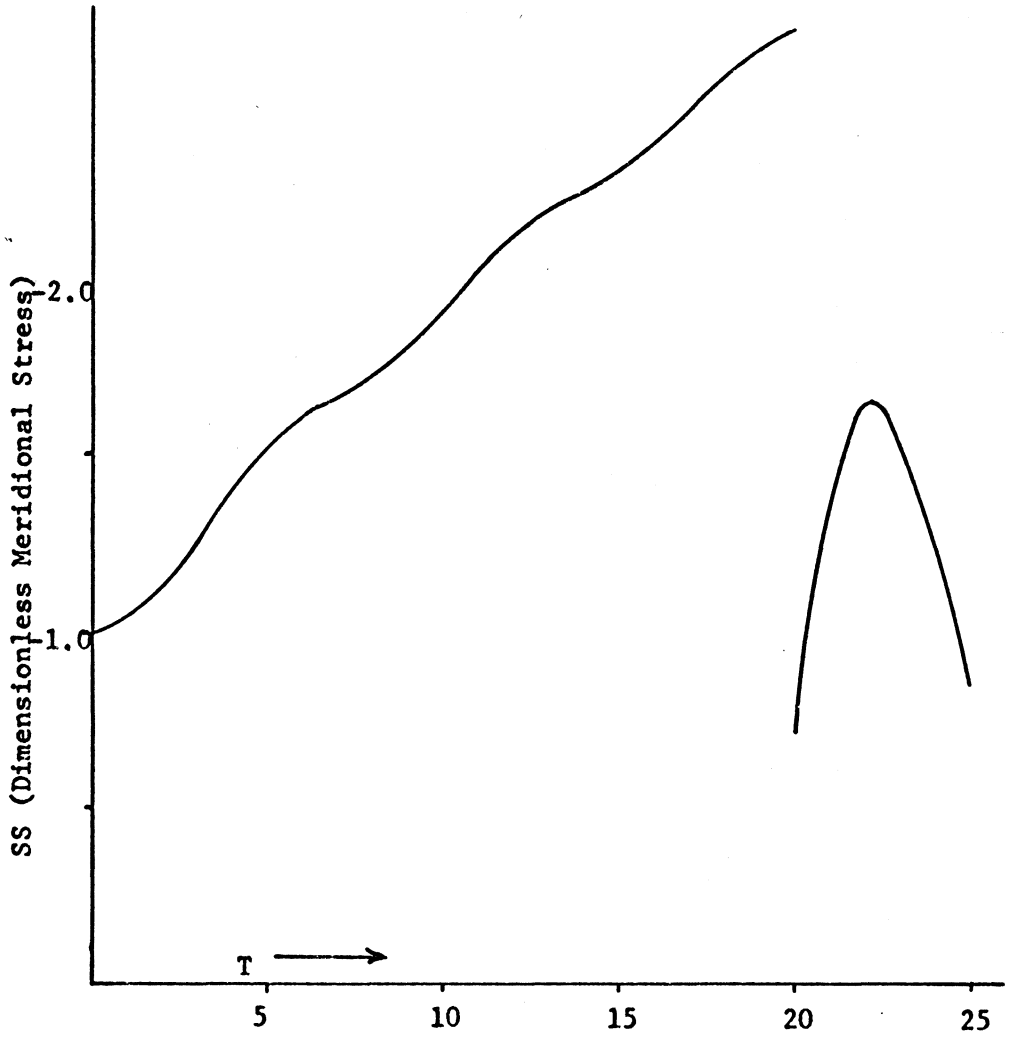


Figure 21. Temporal History of the Nondimensionalized Meridional Stress at the End, x = 0, in a finite 15° conical Membrane (free-end at L = 10) $V_o$ = 1, ν = 0.3, dT = 0.0125.

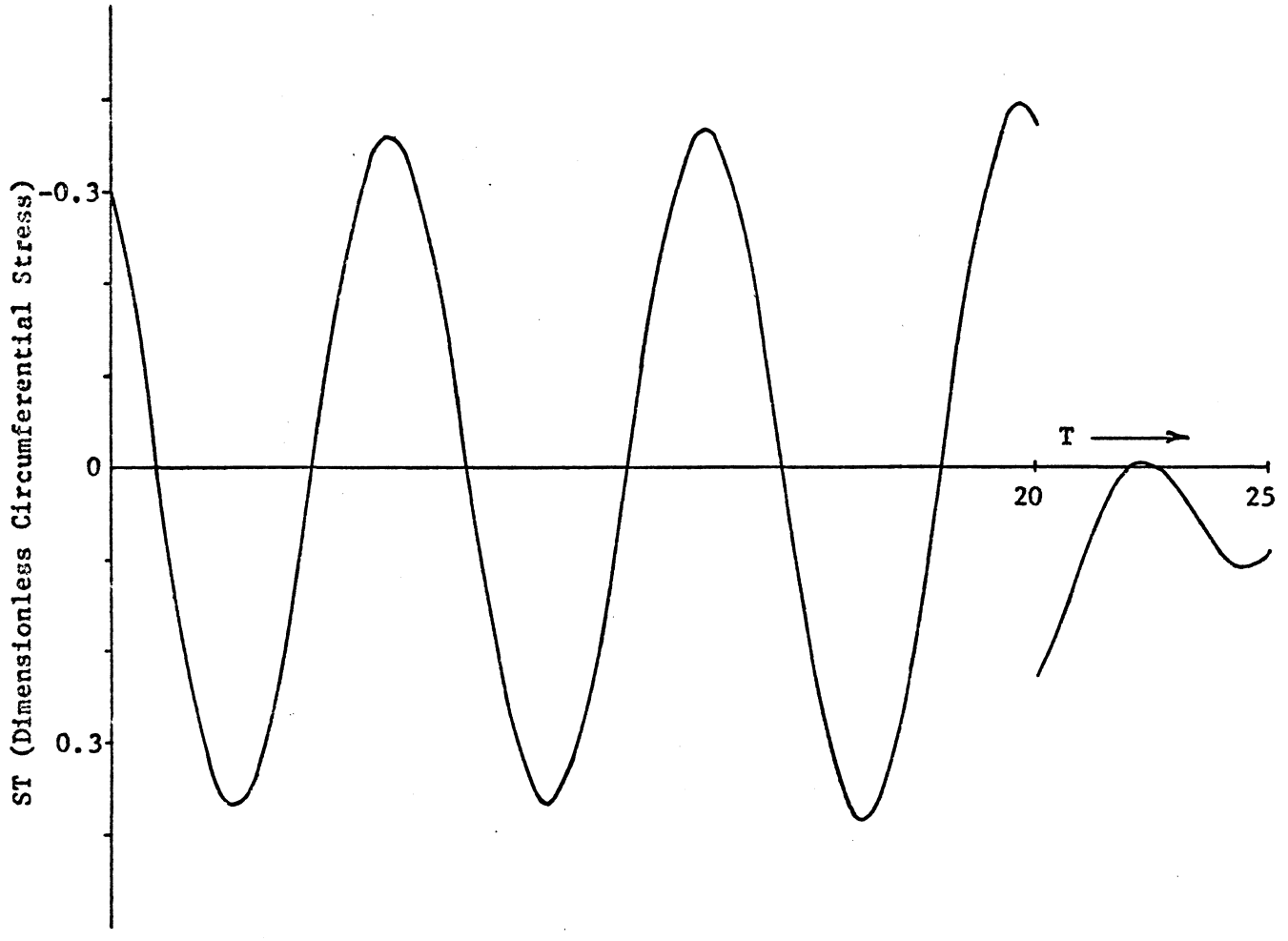


Figure 22. Temporal History of the Nondimensionalized Circumferential Stress at the end, x = L in a Finite 15° Conical Membrane (free-end at L = 10). $V_o$ = 1, ν = 0.3, dT = 0.0125.

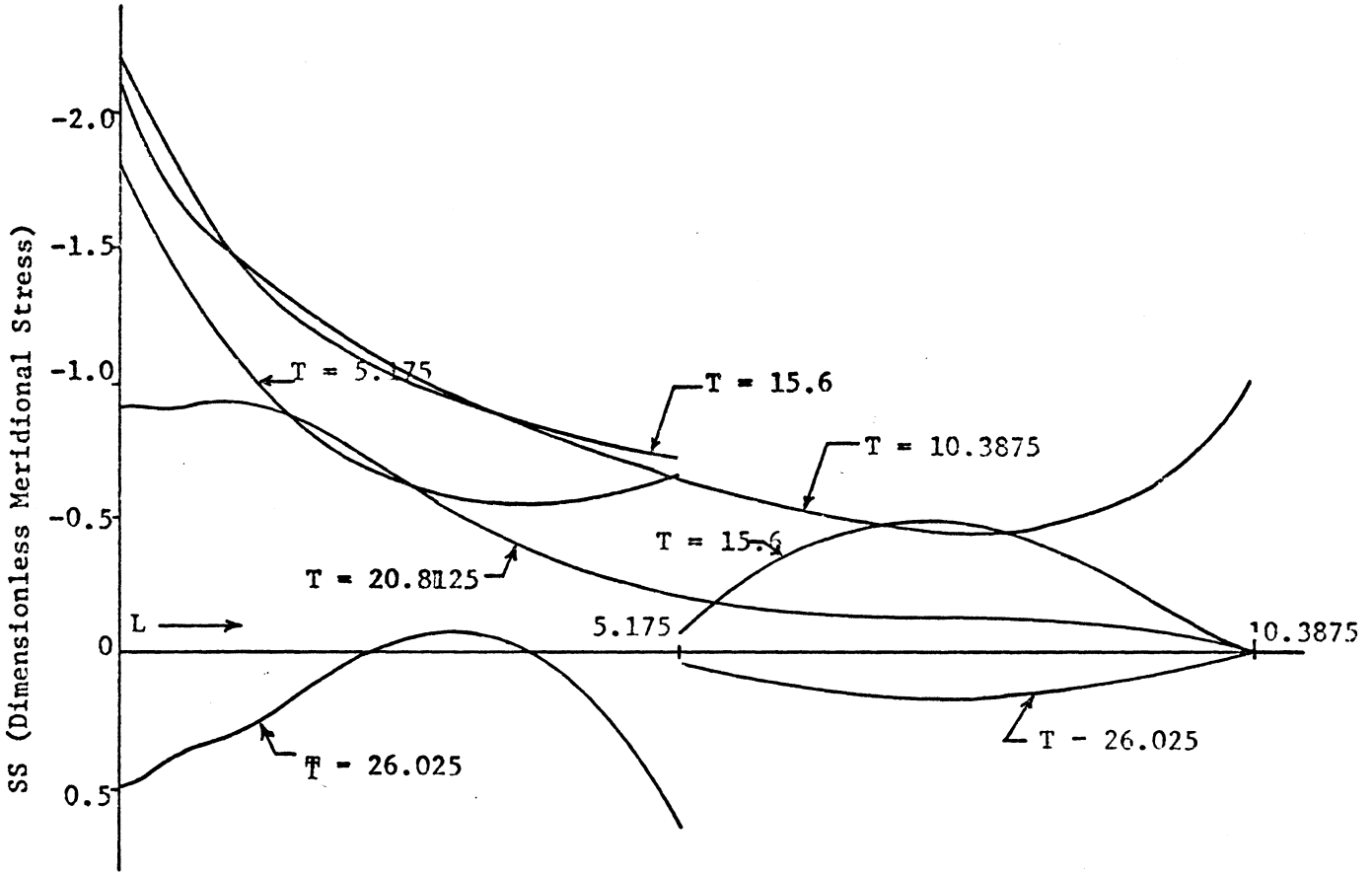


Figure 23. Spatial Distribution of the Nondimensionalized Meridional Stress at T = 5.175, 10.3875, 15.6, 20.8125, 26.025 in a Parabolic Membrane (free-end at L = 10). $V_o$ = 1, $\nu$ = 1/3, dT = 0.0125.

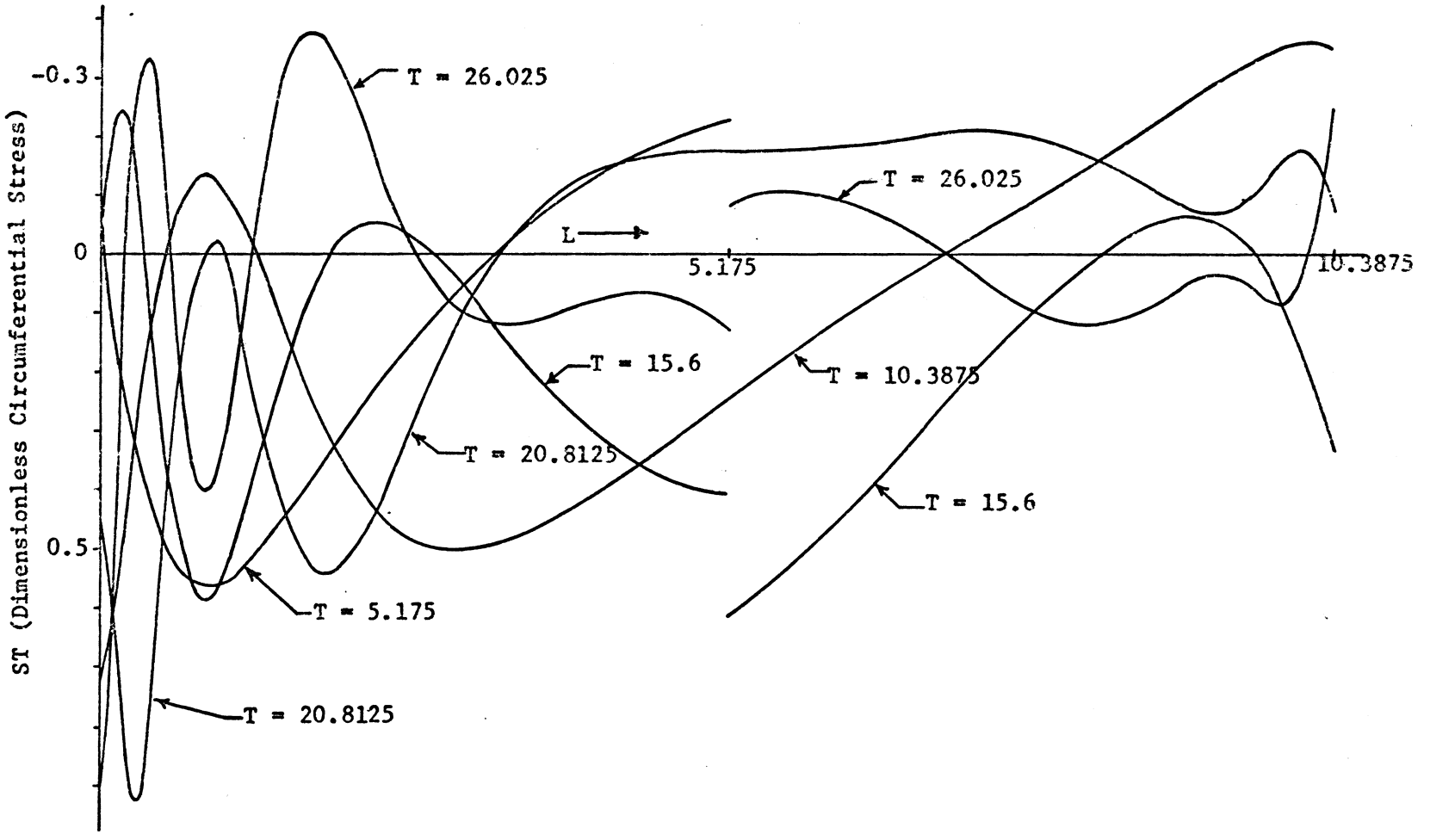


Figure 24. Spatial Distribution of the Nondimensionalized Circumferential Stress at T = 5.175, 10.3875, 15.6, 20.8125, 26.025 in a Parabolic Membrane (free-end at L = 10). $V_o$ = 1, $\nu$ = 1/3, dT = 0.0125.

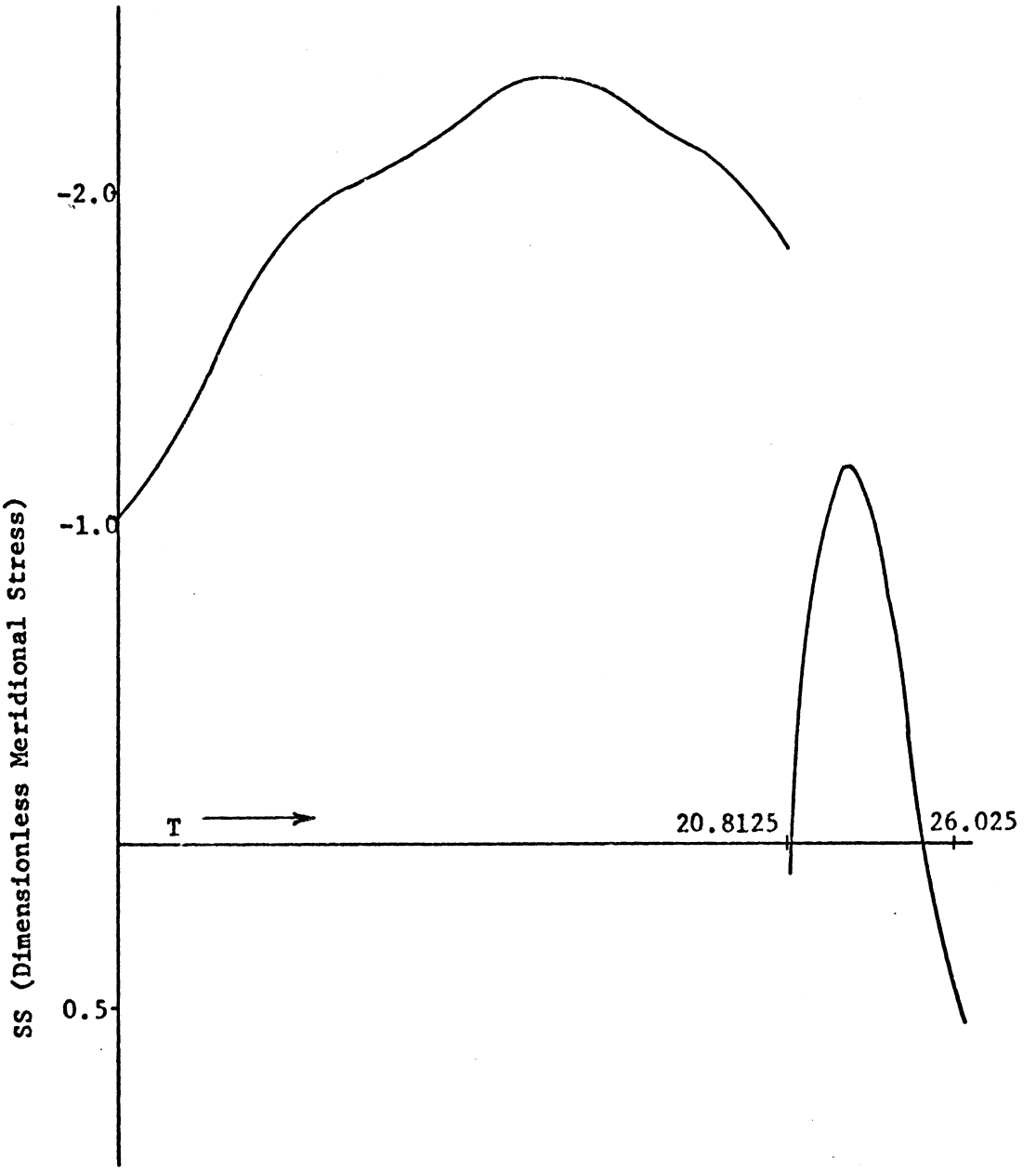


Figure 25. Temporal History of the Nondimensional Meridional Stress at the end, L = 0, of a Parabolic Membrane (free-end at L = 10). $V_o$ = 1, $\nu$ = 1/3, dT = 0.0125.

end is at L = 10.3875, (X = 10). The solutions are consistent with those presented thus far. The effect of the variable slope is to first decrease the magnitude of the jumps to a minimum at the midsection, then to increase them to their initial values at the free end. It may also be noted that, just as in the conical membrane, the circumferential stress does not vanish at the free end. Also, the temporal history of SS at the end L = 0 is geometrically consistent with those of the cylindrical and conical membranes.

Thin Shell Results - Figures 26, 27, and 28 illustrate some of the spatial results for the thin semi-infinite cylindrical shell at T = 1 and 2. Comparison of the spatial distribution of the nondimensional meridional stress, (FX), resultant in figure 26 with those of the moment, (M), and shear, (Q), stress resultants in figures 27 and 28, respectively, indicates that a size difference of about three orders of magnitude exists between membrane and nonmembrane quantities. This difference appears reasonable since axial impact would not excite much bending or shear.

It is interesting to note that the statical relationship between the moment and shear is very clearly exhibited in figures 27 and 28, where zero slopes in moment and zero magnitude shear correspond. Also recall from the preliminary discussion in Chapter 4 that the equations allow jumps to be excited which travel with a slower wavespeed, $C_s$. Although no discontinuities in the shear are excited, the inferred location of any such wavefronts is indicated on figure 28. The disturbances in shear rapidly damp out beyond the location of the slower

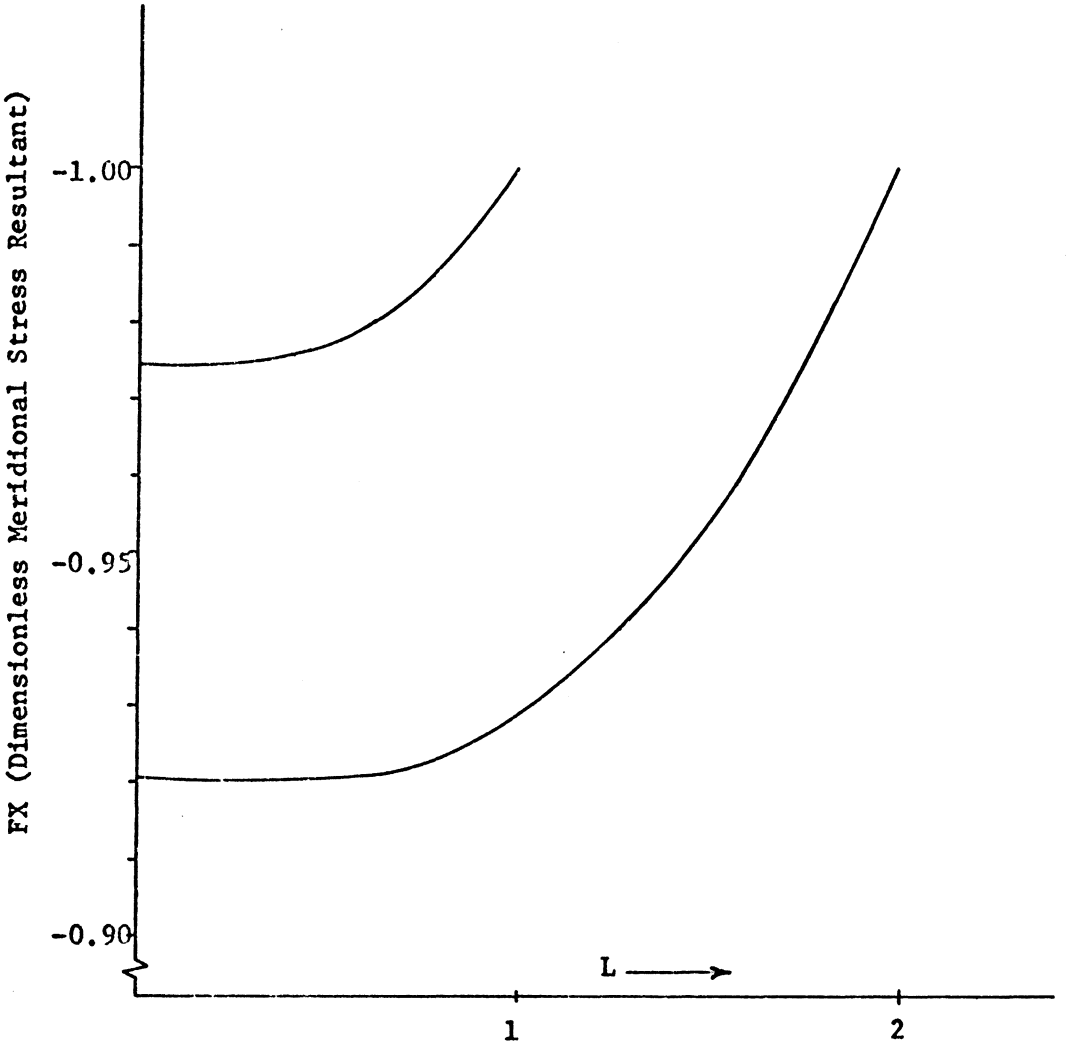


Figure 26. Spatial Distribution of the Nondimensionalized Meridional Stress Resultant in a Semi-infinite Thin Cylindrical Shell at T = 1, 2, resulting from Frictionless Axial Impact. $h/R = 0.1$, $V_o = 1$, $\nu = 1/3$, $k^2 = 0.87$, $dT = 0.005$.

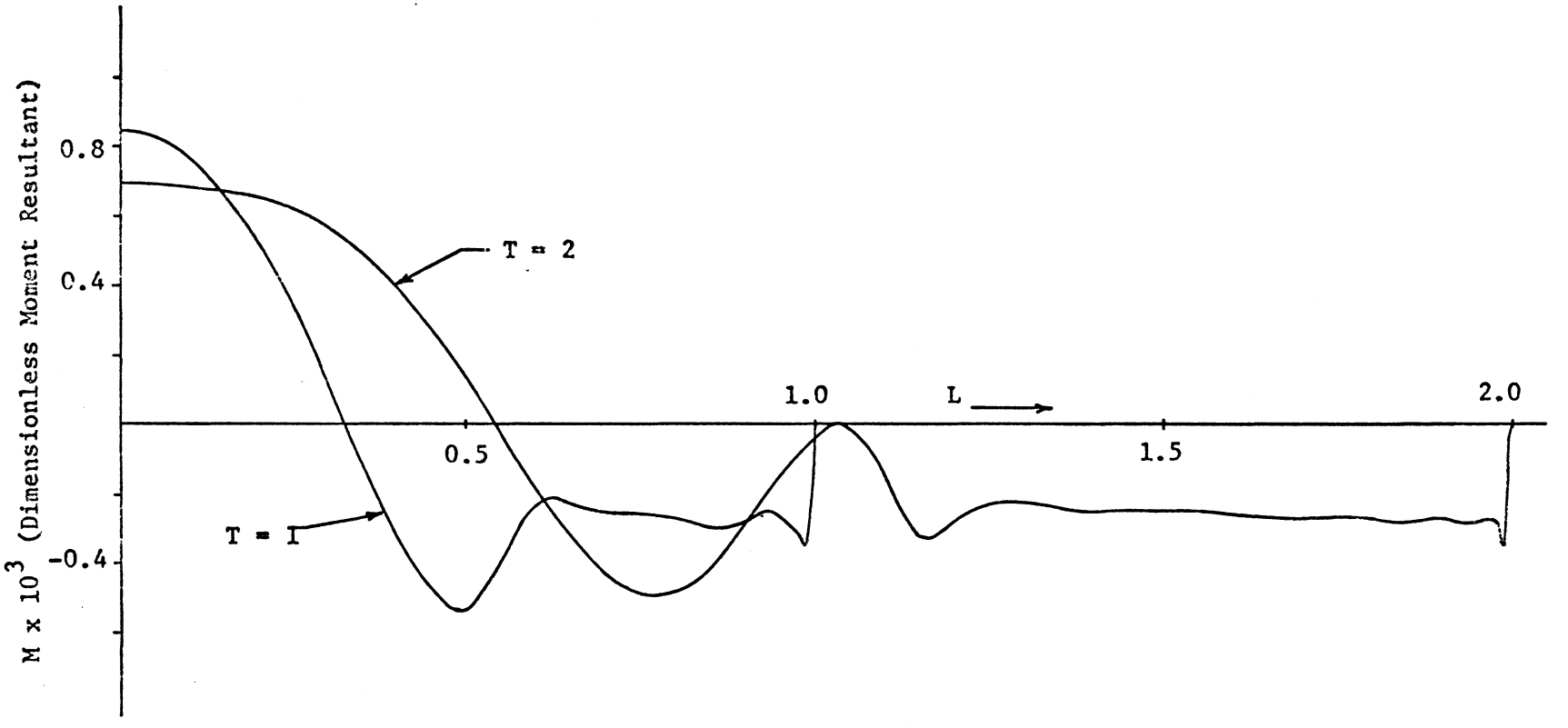


Figure 27. Spatial Distribution of the Nondimensionalized Moment Resultant in a Semi-infinite Thin Cylindrical Shell at T = 1, 2 resulting from Frictionless Axial Impact. h/R = 0.1, $V_o$ = 1, $\nu$ = 1/3, $k^2$ = 0.87, dT = 0.005.

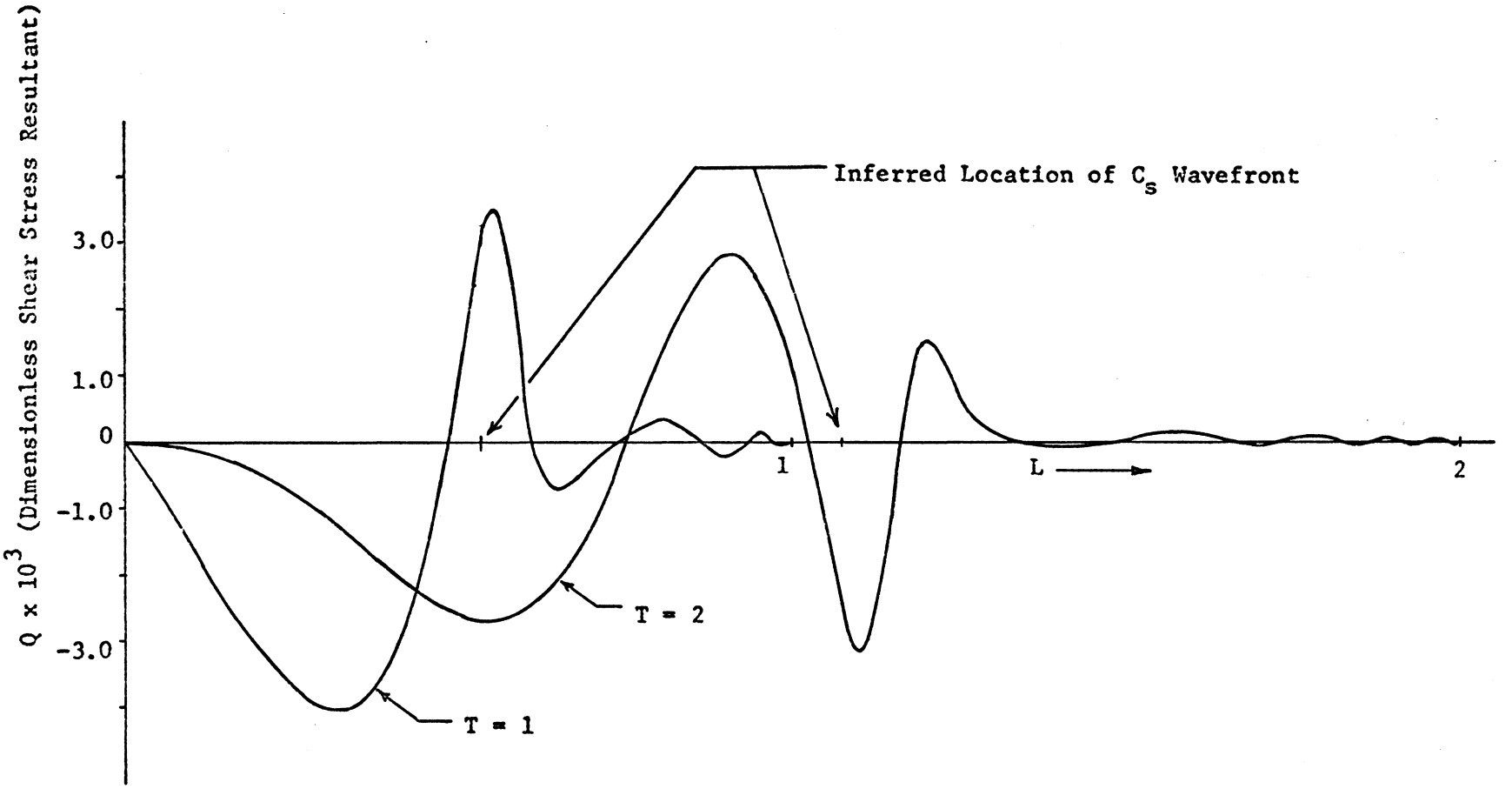


Figure 28. Spatial Distribution of the Nondimensionalized Shear Stress Resultant in a Semi-infinite Thin Cylindrical Shell at T = 1, 2, resulting from Frictionless Axial Impact. h/R = 0.1, $V_o$ = 1, $\nu$ = 1/3. $k^2$ = 0.87, dT = 0.005.

wavefront indicating that the information concerning the slower wave-speed is implicitly contained in the computational procedure. These results compare well with those given in reference [10].

Figures 29 and 30 illustrate the spatial distribution at T = 5, 10, and 15 for the meridional, (FX) and circumferential, (FT), stress resultants in a finite, (L = 10), cylindrical shell. Comparison of figures 29 and 30 with the corresponding membrane results of figures 12 and 13 for the nondimensional meridional and circumferential stresses show that the influence of the shear and rotary inertia is negligible for the meridional type of excitation condition. The meridional stress resultant, (FX), and the meridional stress, (SS), are the same to two significant figures. The magnitude of the circumferential stress resultant, (FT), in figure 30, is approximately the same as that of the circumferential stress, (ST), in figure 13, but the comparison shows that there is a small series of oscillations introduced in the thin shell result. This small oscillation is apparently due to the rotation of the centroidal surface whose influence can be seen from step 16 of equations 4.7.

The spatial distribution of the angular rotation of the centroidal surface, (SI), is plotted at T = 5, 10, and 15 for this shell in figure 31. The maximum value of about 0.3 radians appears reasonable in view of the nondimensional impact velocity of $V_o = \frac{v_o}{C_p} = 1$. The extremely high frequency oscillations for T = 15 seen at about L = 5.3 and extending to about L = 5.8 is due to a slight degree of instability arising from error accumulation. The extent of the region of instability is best

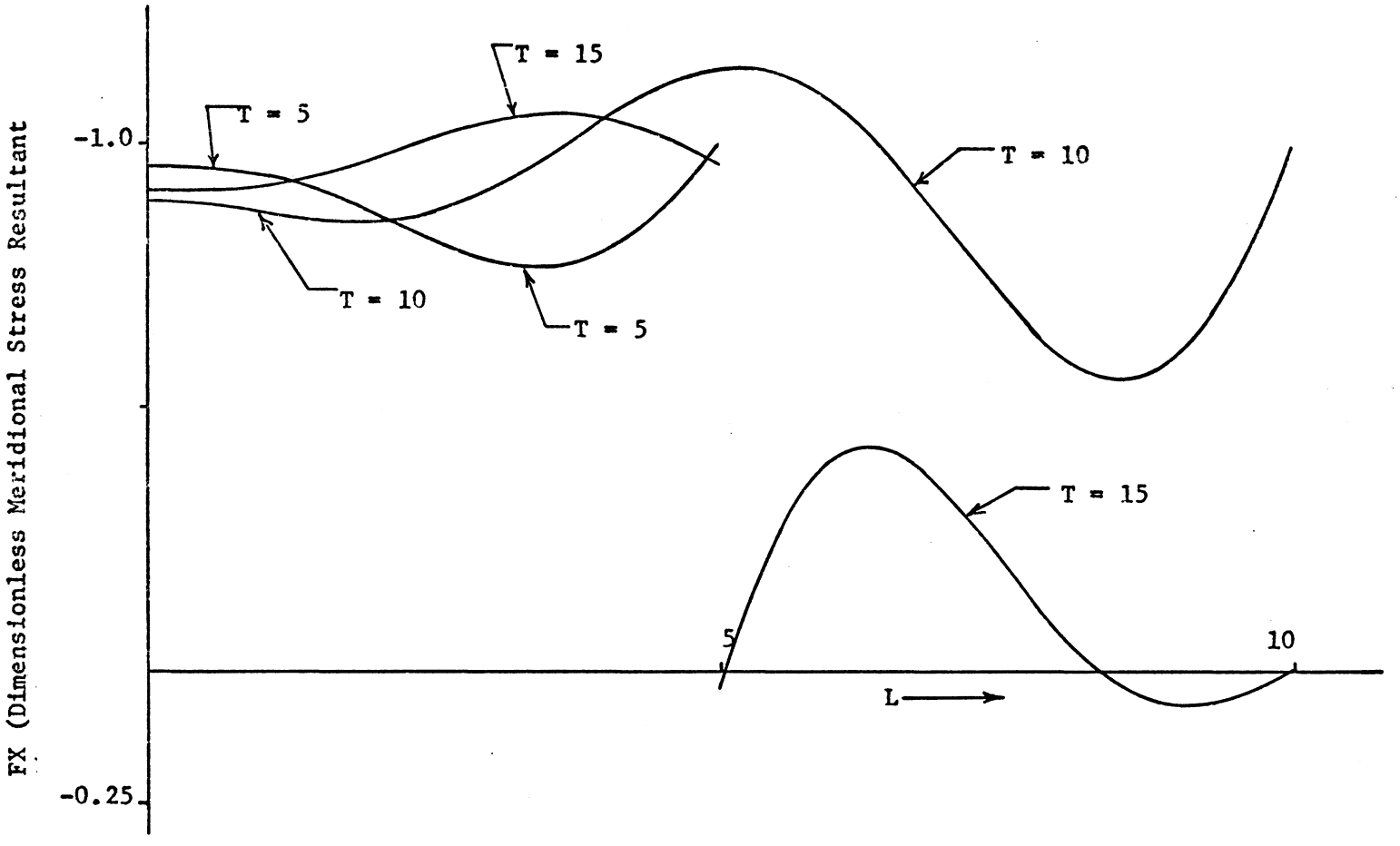


Figure 29. Spatial Distribution of the Nondimensionalized Meridional Stress Resultant in a Finite Thin Cylindrical Shell at T = 5, 10, and 15, resulting from Frictionless Axial Impact, (free end at L = 10). $h/R = 0.1$, $V_o = 1$, $\nu = 1/3$, $k^2 = 0.87$, $dT = 0.005$.

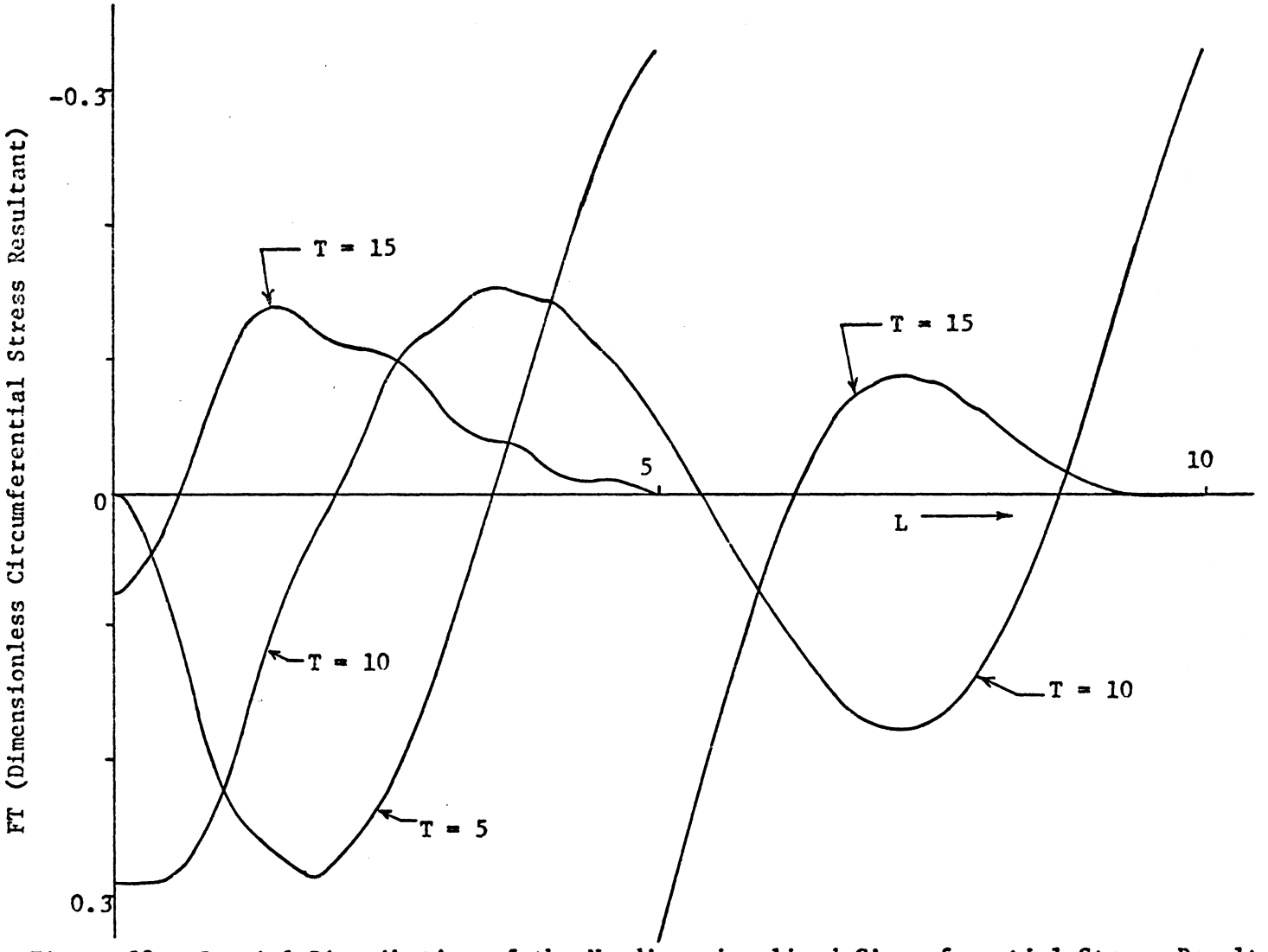


Figure 30. Spatial Distribution of the Nondimensionalized Circumferential Stress Resultant in a Finite Thin Cylindrical Shell at T = 5, 10, and 15, resulting from Frictionless Axial Impact, (free end at L = 10). $h/R = 0.1$, $V_o = 1$, $\nu = 1/3$, $k^2 = 0.87$, $dT = 0.005$.

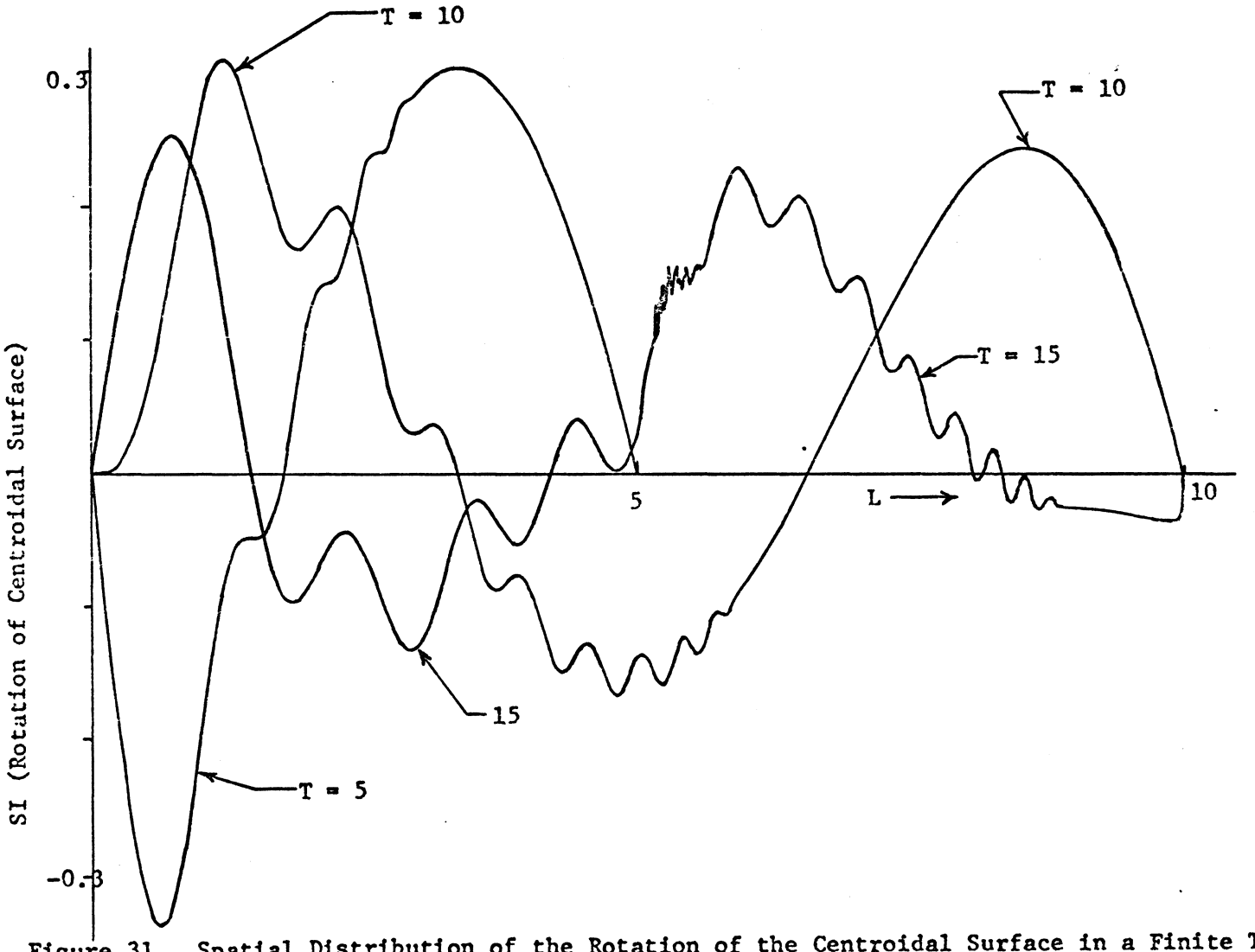


Figure 31. Spatial Distribution of the Rotation of the Centroidal Surface in a Finite Thin Cylindrical Shell at T = 5, 10, and 15, resulting from Frictionless Axial Impact, (free end at L = 10). $h/R = 0.1$, $V_o = 1$, $\nu = 1/3$, $k^2 = 0.87$, $dT = 0.005$.

seen by examining figures 32 through 37 which show the spatial distributions of the nondimensional moment resultant and shear stress resultants at T = 5, 10, and 15. Figures 34 and 37 indicate that the moment and shear have become unstable in the region extending from L = 5 to about L = 6. This region is identified in the computer print-out by growing magnitudes combined with an alternation of sign from element to element. At the time T = 15, these two dependent variables along with SI are the only variables which have become unstable and this instability has not had time to significantly affect the other variables. The evidence for this statement comes from the energy balance check. The initial nondimensional total energy before impact is $\pi\frac{R}{h}LV_o^2 = 314.159$. (The constant $\pi\frac{R}{h}$ has been cancelled from each term in equation 4.11, but it was maintained in the computation of the individual terms.) The total strain energy at the time T = 15 is 178.404 with the total kinetic energy being 135.555. This leaves the energy balanced to within 0.06%. At the time T = 16, the energy is unbalanced by well over 6% and this unbalance is growing rapidly as shown in figure 38.

Figure 38 illustrates a temporal history of the percentage difference between the initial total kinetic energy of the shell and the sum of the computed kinetic and strain energies at time T for two step sizes, dT = 0.01 and 0.005. The cause of the instability is clearly from truncation error as indicated by the fact that the curve for dT = 0.005 shows that the solution is stable out to T = 15, whereas, for dT = 0.01, it is stable only out to T = 9. The sharpness with which the break in the curves develop demonstrates that the energy balance

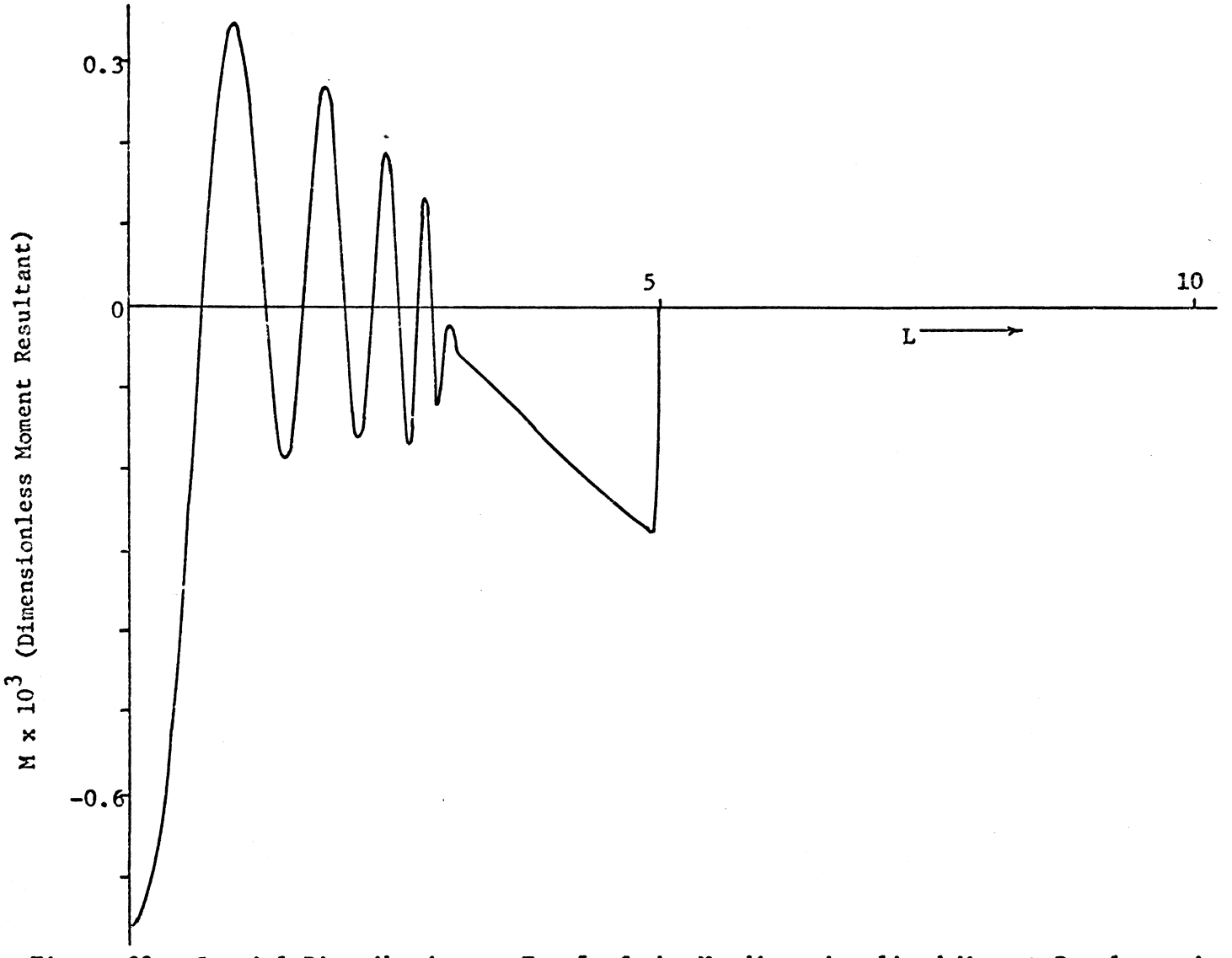


Figure 32. Spatial Distribution at T = 5 of the Nondimensionalized Moment Resultant in a Finite Thin Cylindrical Shell resulting from Frictionless Axial Impact, (free end at L = 10). $h/R = 0.1$, $V_o = 1$, $\nu = 1/3$, $k^2 = 0.87$, $dT = 0.005$.

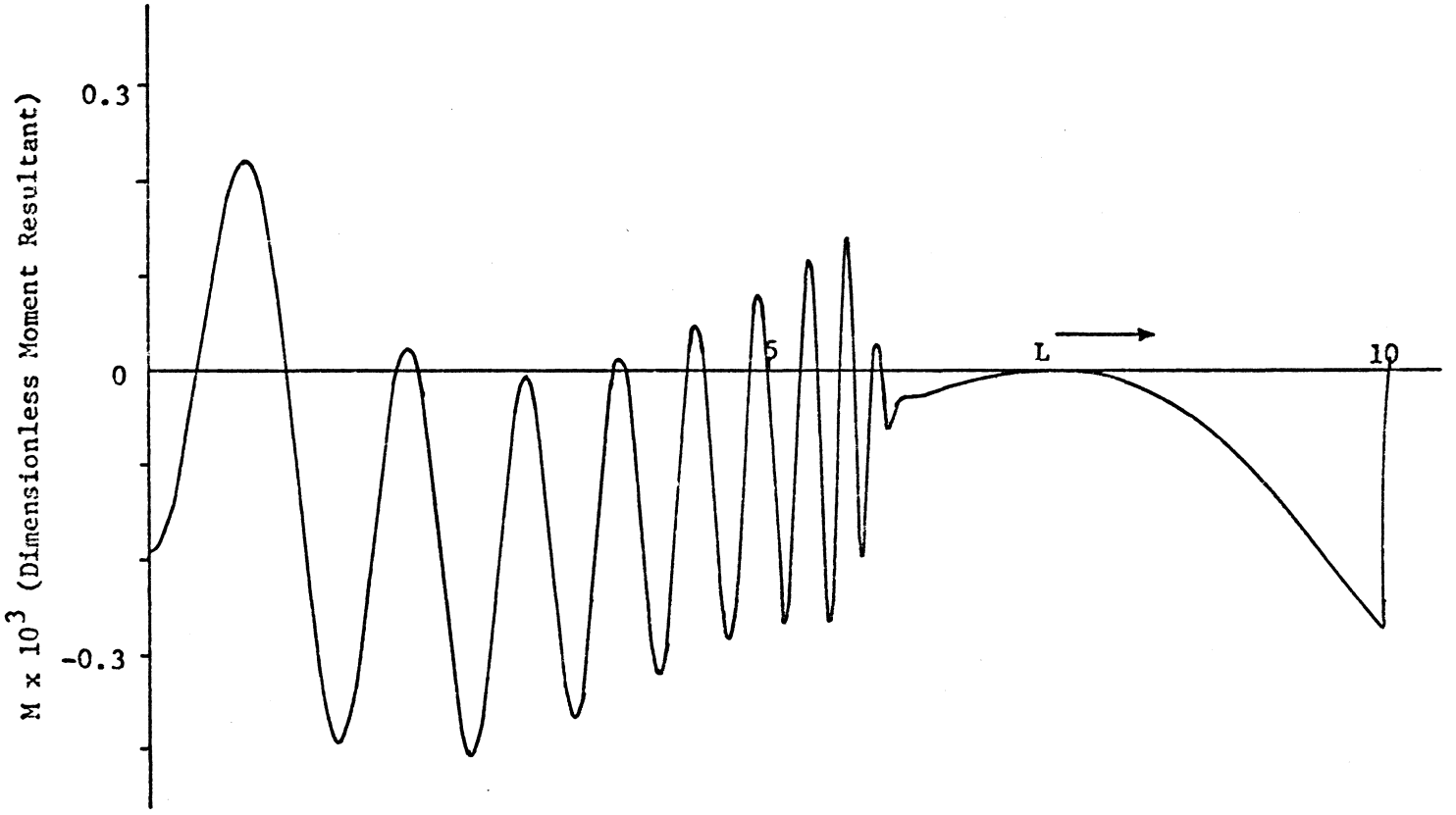


Figure 33. Spatial Distribution at T = 10 of the Nondimensionalized Moment Resultant in a Finite Thin Cylindrical Shell resulting from Frictionless Axial Impact, (free end at L = 10). h/R = 0.1, $V_o$ = 1, $\nu$ = 1/3, $k^2$ = 0.87, dT = 0.005.

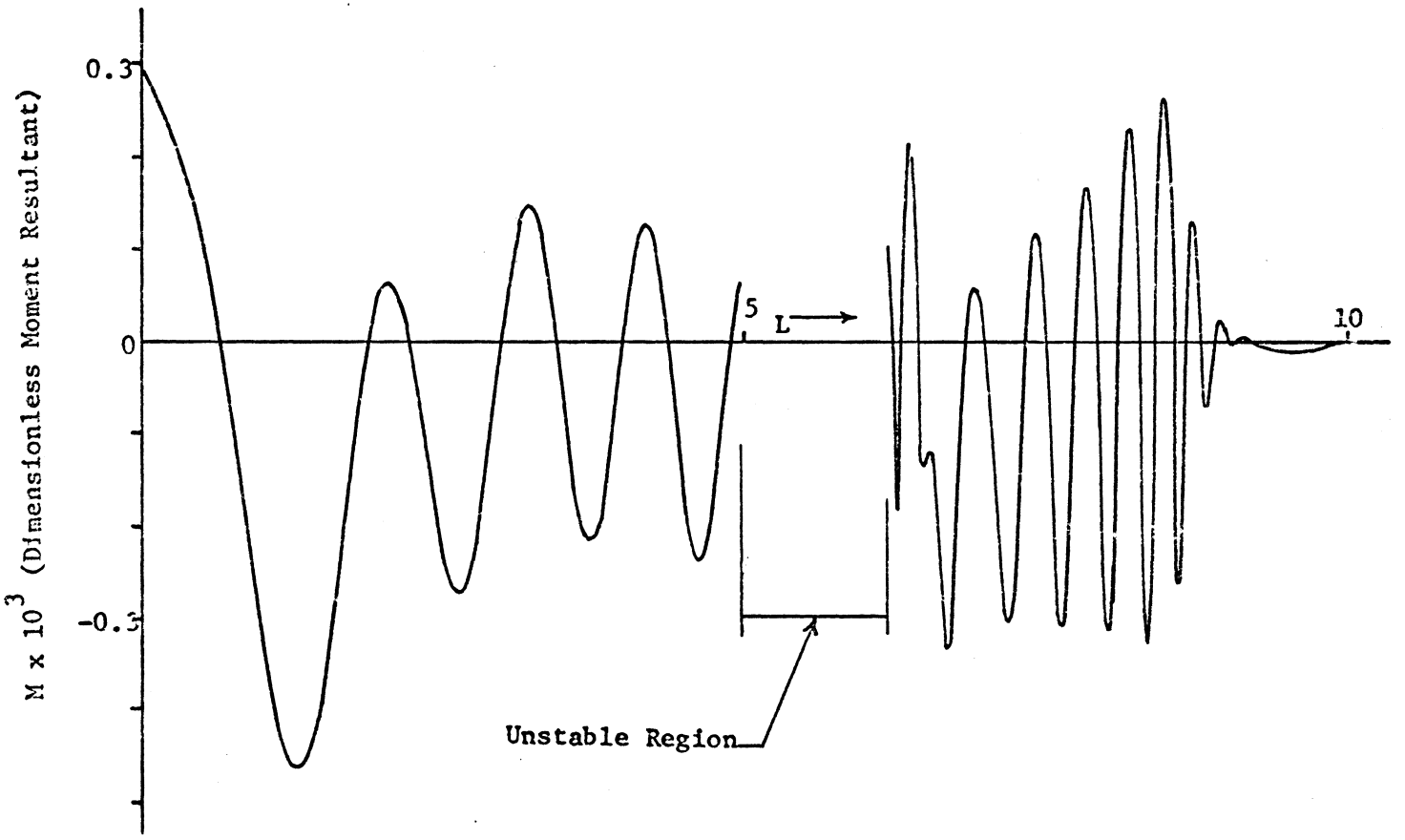


Figure 34. Spatial Distribution at T = 15 of the Nondimensionalized Moment Resultant in a Finite Thin Cylindrical Shell resulting from Frictionless Axial Impact, (free end at L = 10). $h/R = 0.1$, $V_o = 1$, $\nu = 1/3$, $k^2 = 0.87$, $dT = 0.005$.

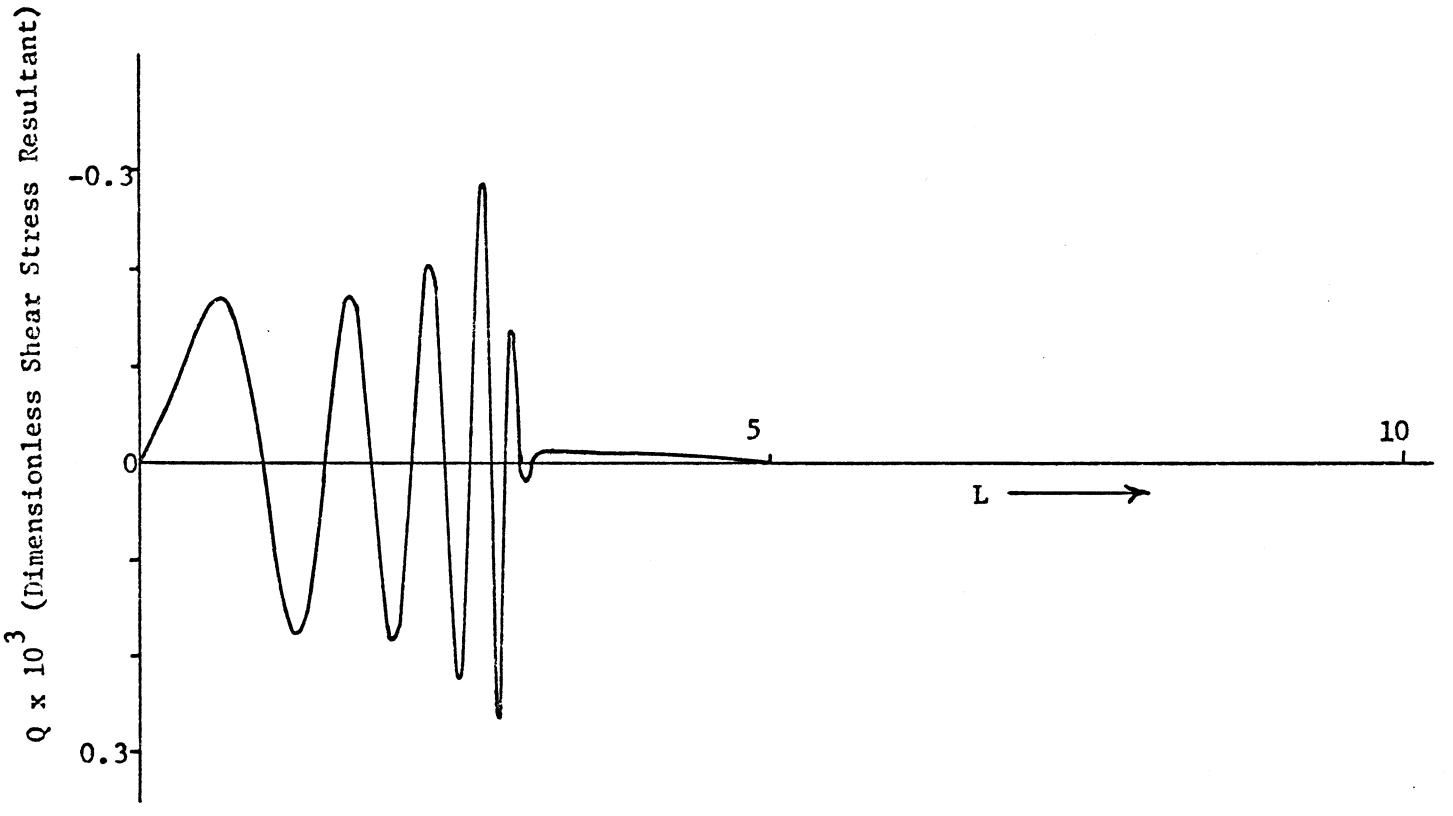


Figure 35. Spatial Distribution at T = 5 of the Nondimensionalized Shear Stress Resultant in a Finite Thin Cylindrical Shell resulting from Frictionless Axial Impact, (free end at L = 10). $h/R = 0.1$, $V_o = 1$, $\nu = 1/3$, $k^2 = 0.87$, $dT = 0.005$.

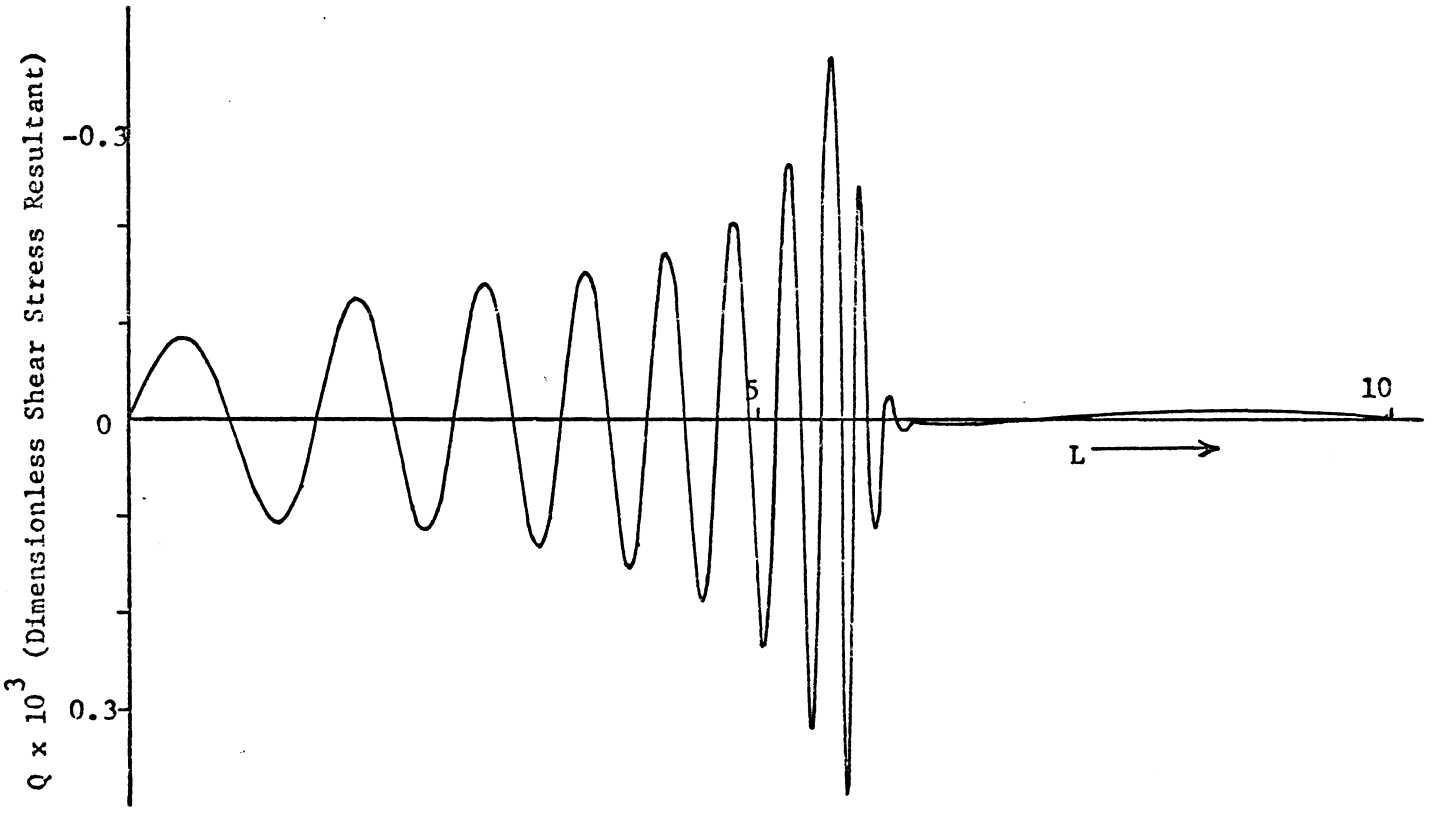


Figure 36. Spatial Distribution at T = 10 of the Nondimensionalized Shear Stress Resultant in a Finite Thin Cylindrical Shell resulting from Frictionless Axial Impact, (free end at L = 10). $h/R = 0.1$, $V_o = 1$, $\nu = 1/3$, $k^2 = 0.87$, $dT = 0.005$.

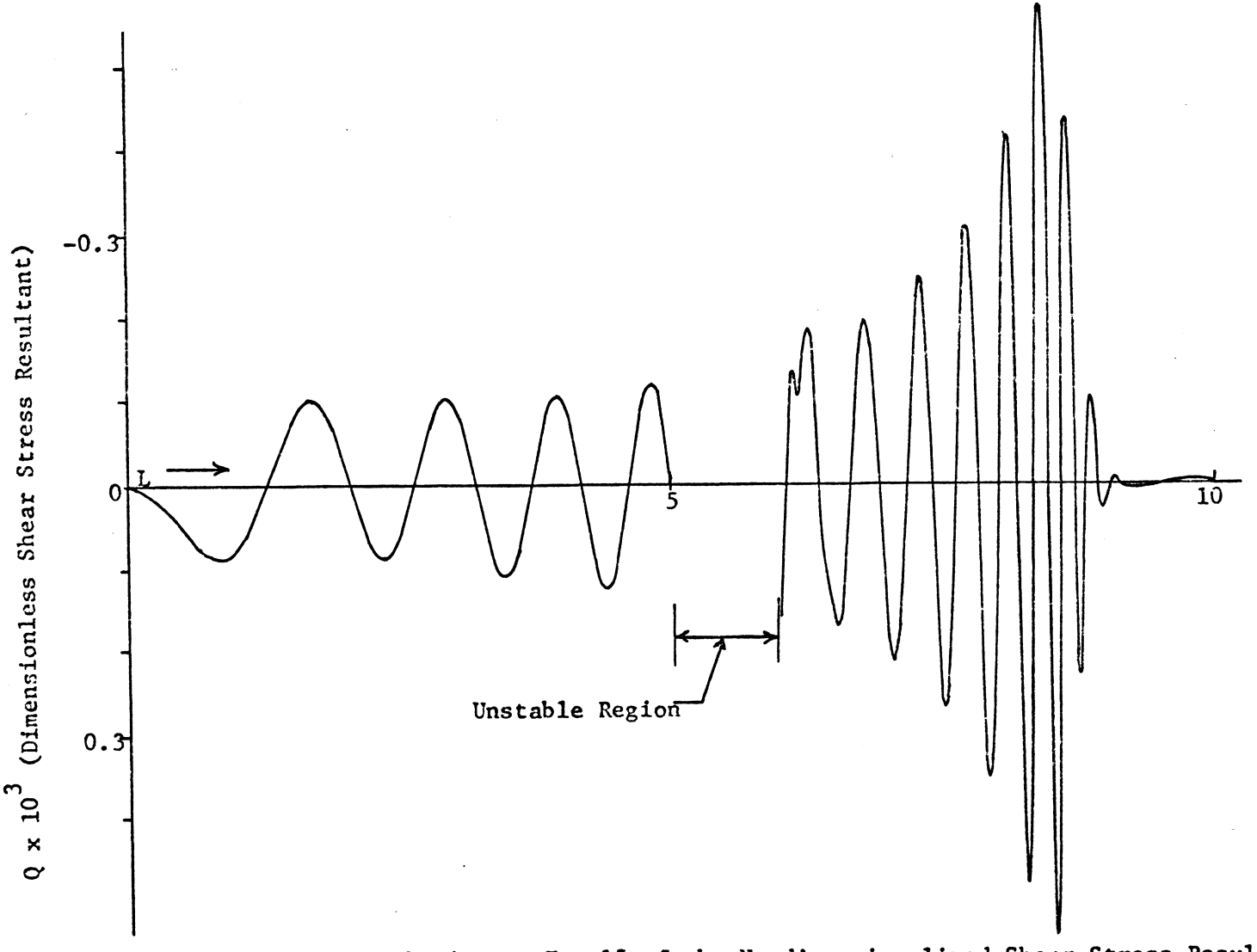


Figure 37. Spatial Distribution at T = 15 of the Nondimensionalized Shear Stress Resultant in a Finite Thin Cylindrical Shell resulting from Frictionless Axial Impact, (free end at L = 10). $h/R = 0.1$, $V_o = 1$, $\nu = 1/3$, $k^2 = 0.87$, $dT = 0.005$.

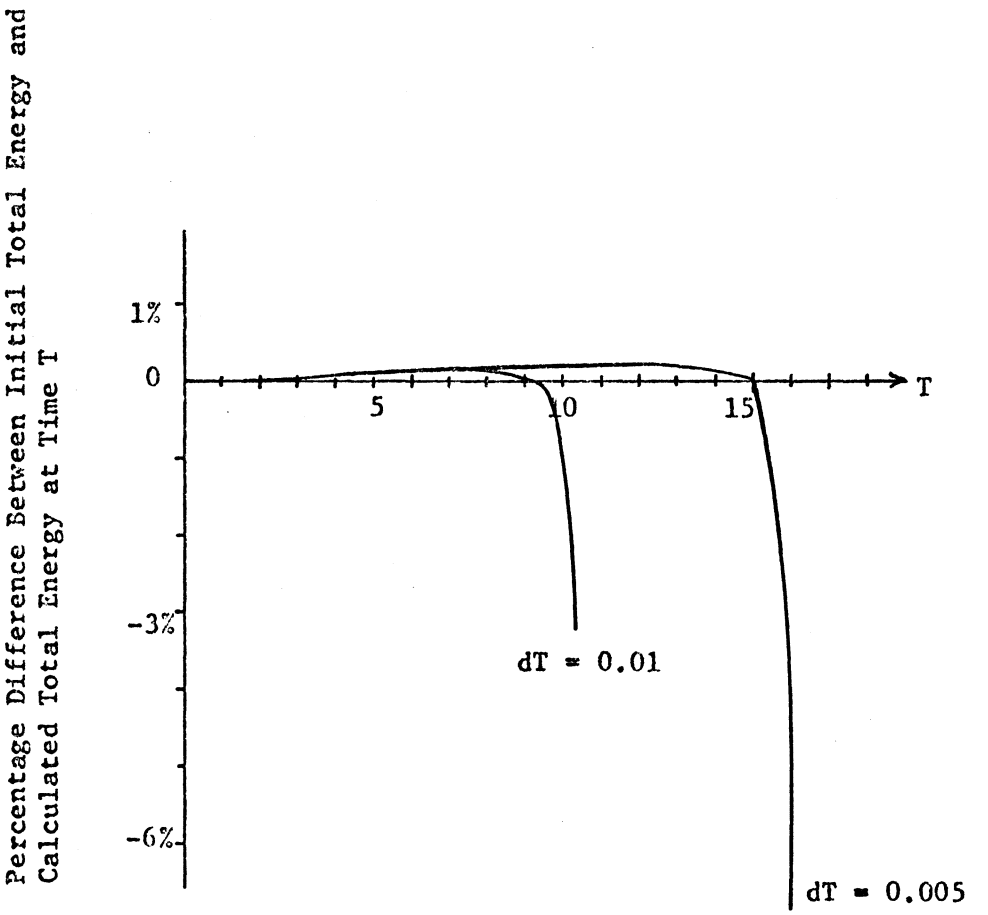


Figure 38. Temporal History of the Energy Balance Check for the Thin Cylindrical Shell.

check is an excellent indicator of the regions of validity for converged results and of overall solution stability.

Figures 32 through 37 clearly indicate the validity of membrane theories for this type of excitation when used with asymptotic methods, since all significant disturbances in shear are well behind the $C_p$ wavefront and the moment in this region is small.

The spatial distribution of the nondimensional meridional velocity, $(\dot{U})$, and displacement, (U), is shown at T = 5, 10, and 15 in figures 39 and 40. The high positive velocities and the rapidly increasing displacements beyond L = 5 at T = 15 show that the free end of the shell has begun to "rebound" from the wall. Note that the jump in the spatial derivative of the meridional displacement is clearly seen at L = 5 for T = 5 and 15.

The spatial distributions of the nondimensional radial velocity, $(\dot{W})$, and displacement, (W), at T = 5, 10, and 15 are given in figures 41 and 42. Comparison of figure 41 with the membrane radial velocity of figure 15 again shows that the effect of the shear and rotary inertia is negligibly small with regard to magnitudes, but that a small series of oscillations is superimposed on the membrane results. Note that the slope of the radial displacement at the end L = 0 is zero as a consequence of not allowing the end to rotate. Figure 43 illustrates the temporal history of the nondimensional radial displacement at the end L = 0 and shows that the "breathing" motion which the end undergoes is approximately periodic.

Figure 44 shows the temporal histories of the nondimensional

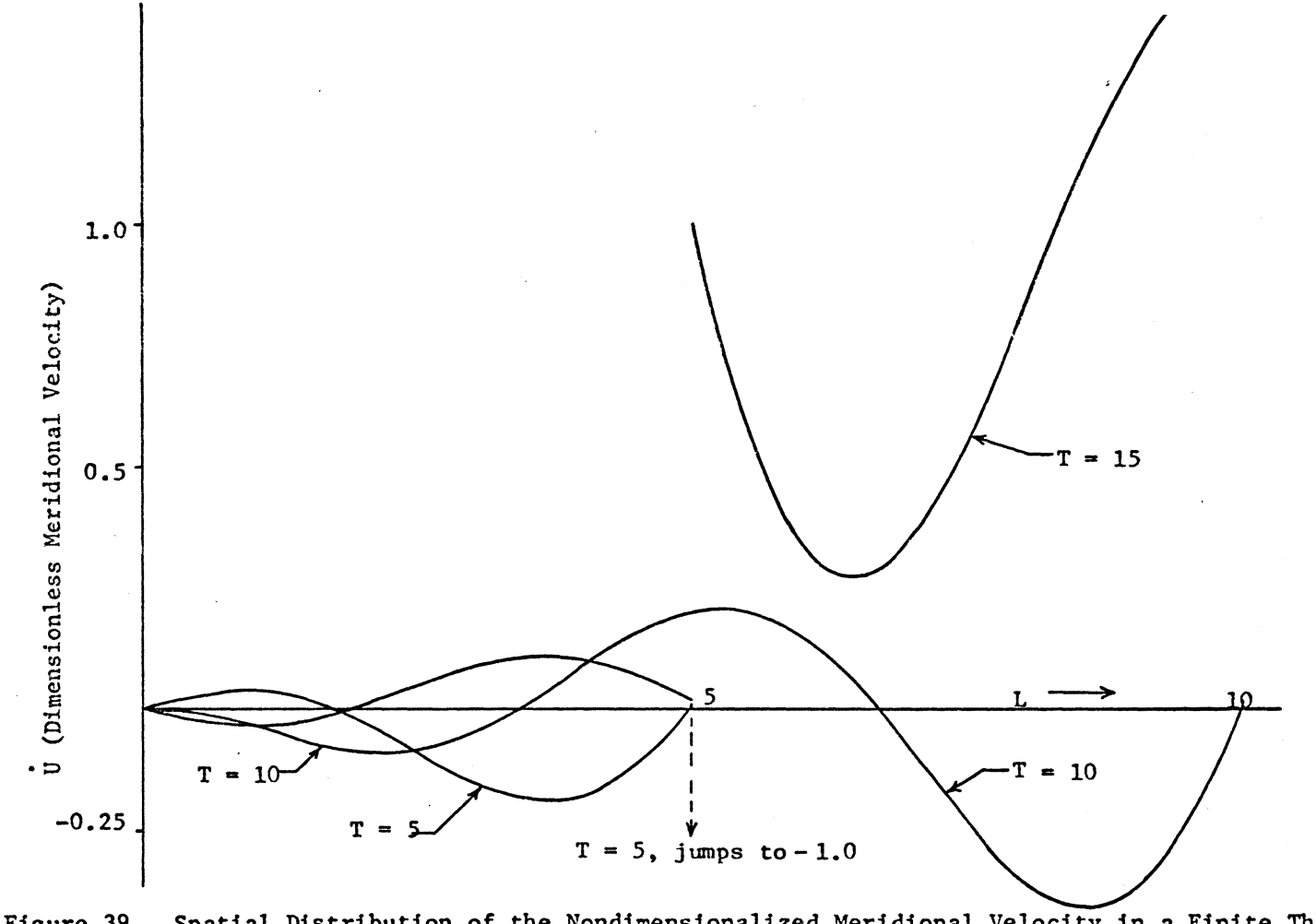


Figure 39. Spatial Distribution of the Nondimensionalized Meridional Velocity in a Finite Thin Cylindrical Shell at T = 5, 10, and 15, resulting from Frictionless Axial Impact, (free end at L = 10). $h/R = 0.1$, $V_o = 1$, $\nu = 1/3$, $k^2 = 0.87$, $dT = 0.005$.

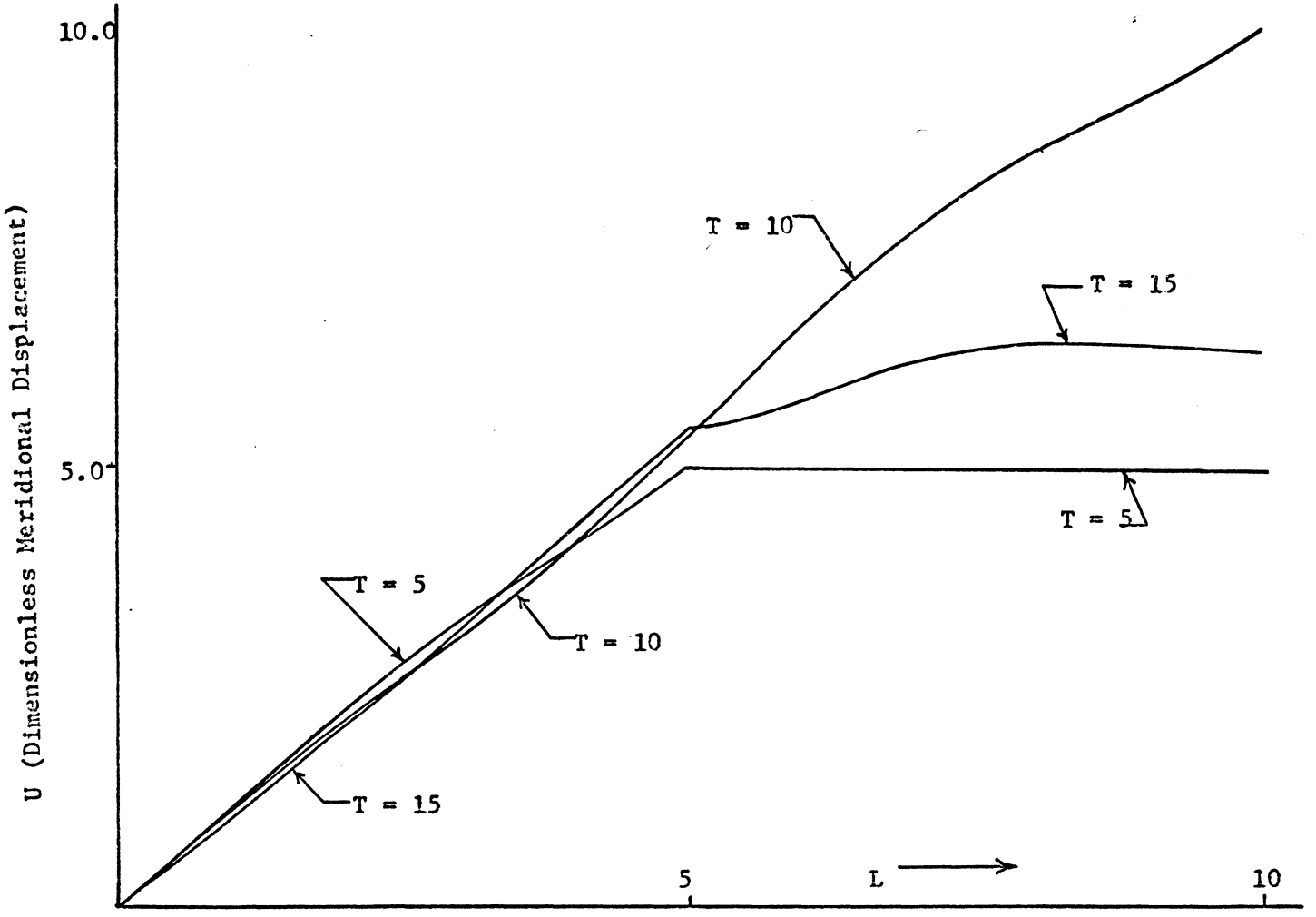


Figure 40. Spatial Distribution of the Nondimensionalized Meridional Displacement in a Finite Thin Cylindrical Shell at T = 5, 10, and 15, resulting from Frictionless Axial Impact, (free end at L = 10). $h/R = 0.1$, $V_o = 1$, $\nu = 1/3$, $k^2 = 0.87$, $dT = 0.005$.

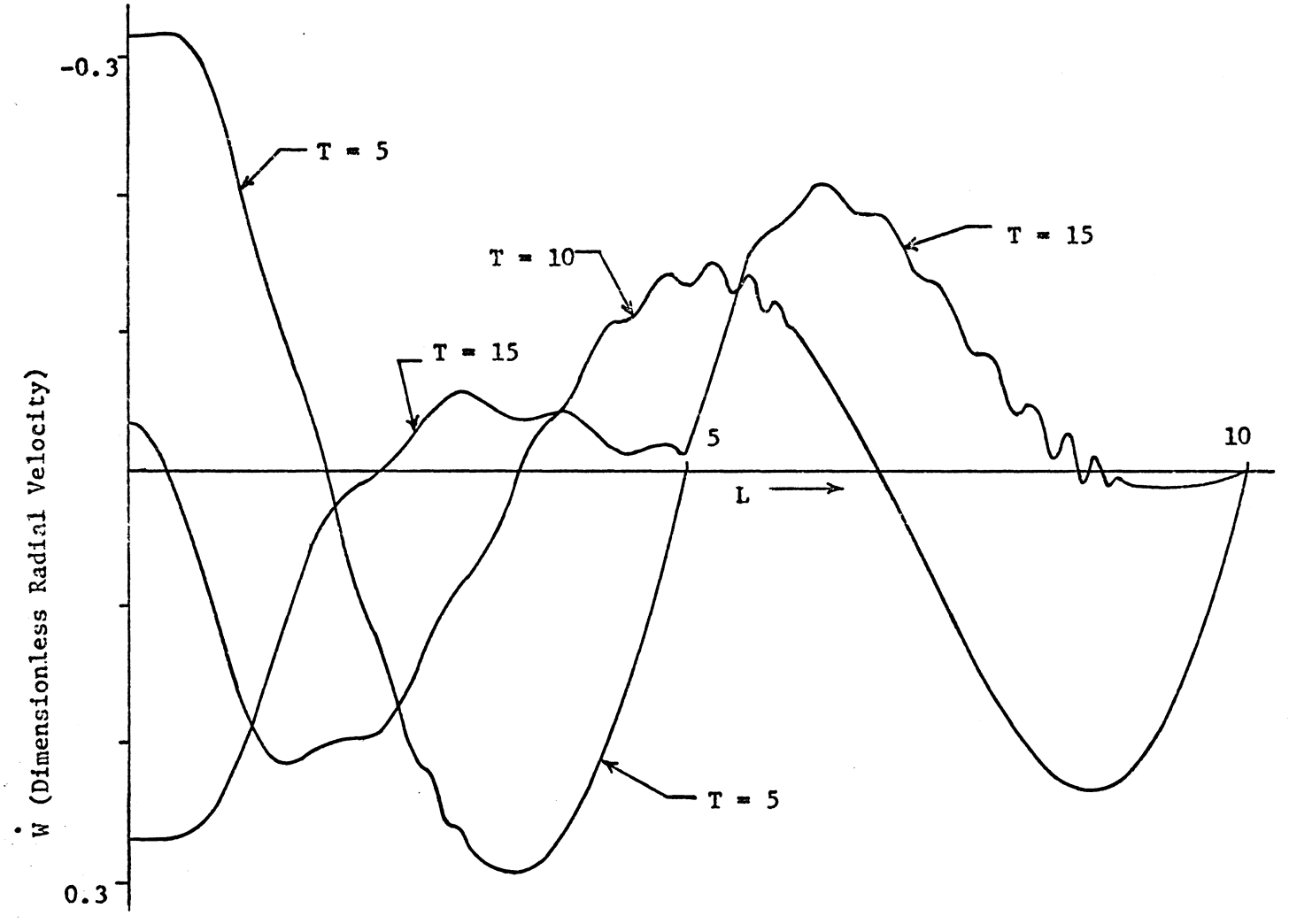


Figure 41. Spatial Distribution of the Nondimensionalized Radial Velocity in a Finite Thin Cylindrical Shell at T = 5, 10, and 15, resulting from Frictionless Axial Impact, free end at L = 10, $h/R = 0.1$, $V_o = 1$, $\nu = 1/3$, $k^2 = 0.87$, $dT = 0.005$.

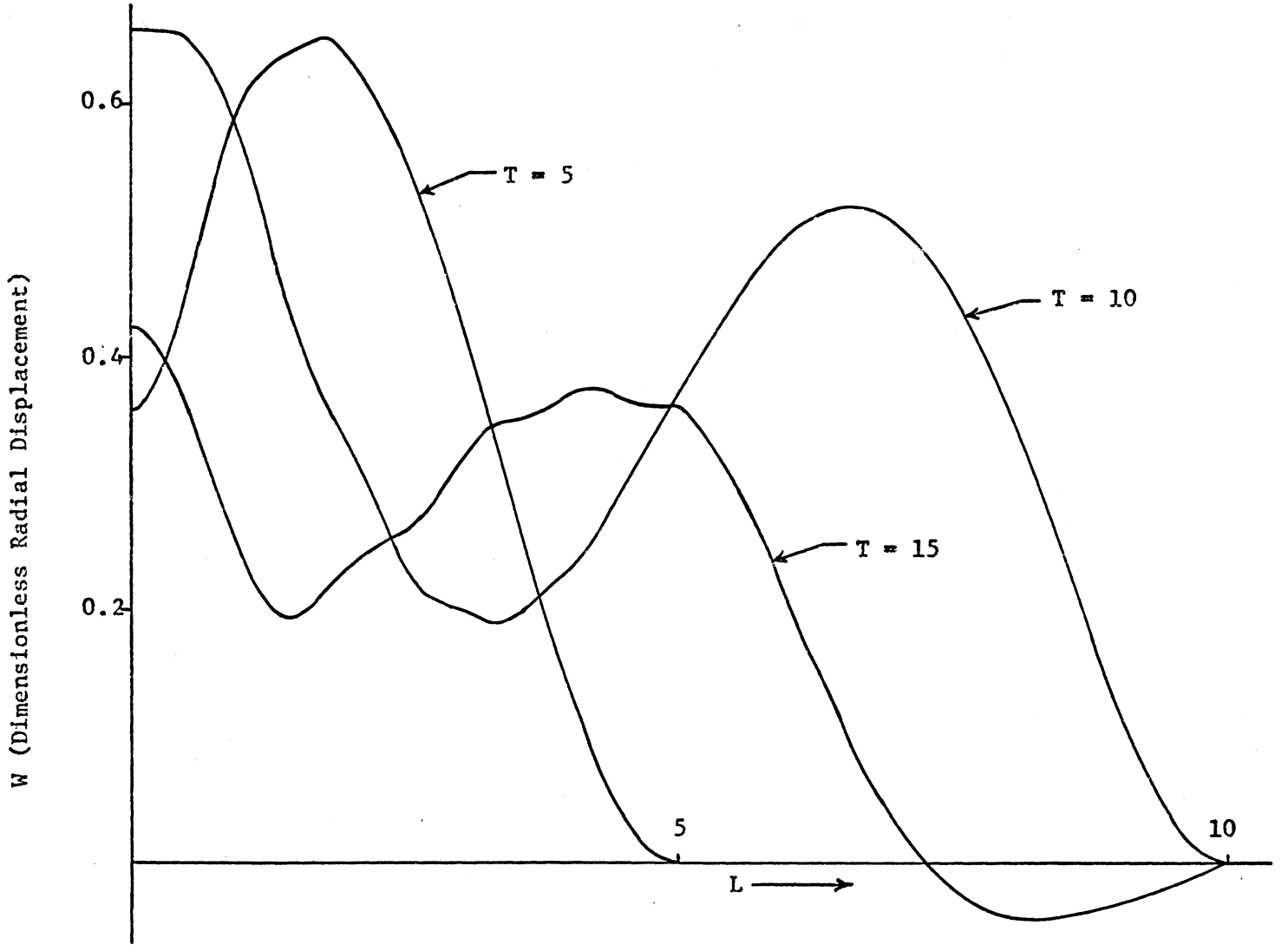


Figure 42. Spatial Distribution of the Nondimensionalized Radial Displacement in a Finite Thin Cylindrical Shell at T = 5, 10, and 15, resulting from Frictionless Axial Impact, (free end at L = 10). $h/R = 0.1$, $V_o = 1$, $\nu = 1/3$, $k^2 = 0.87$, $dT = 0.005$.

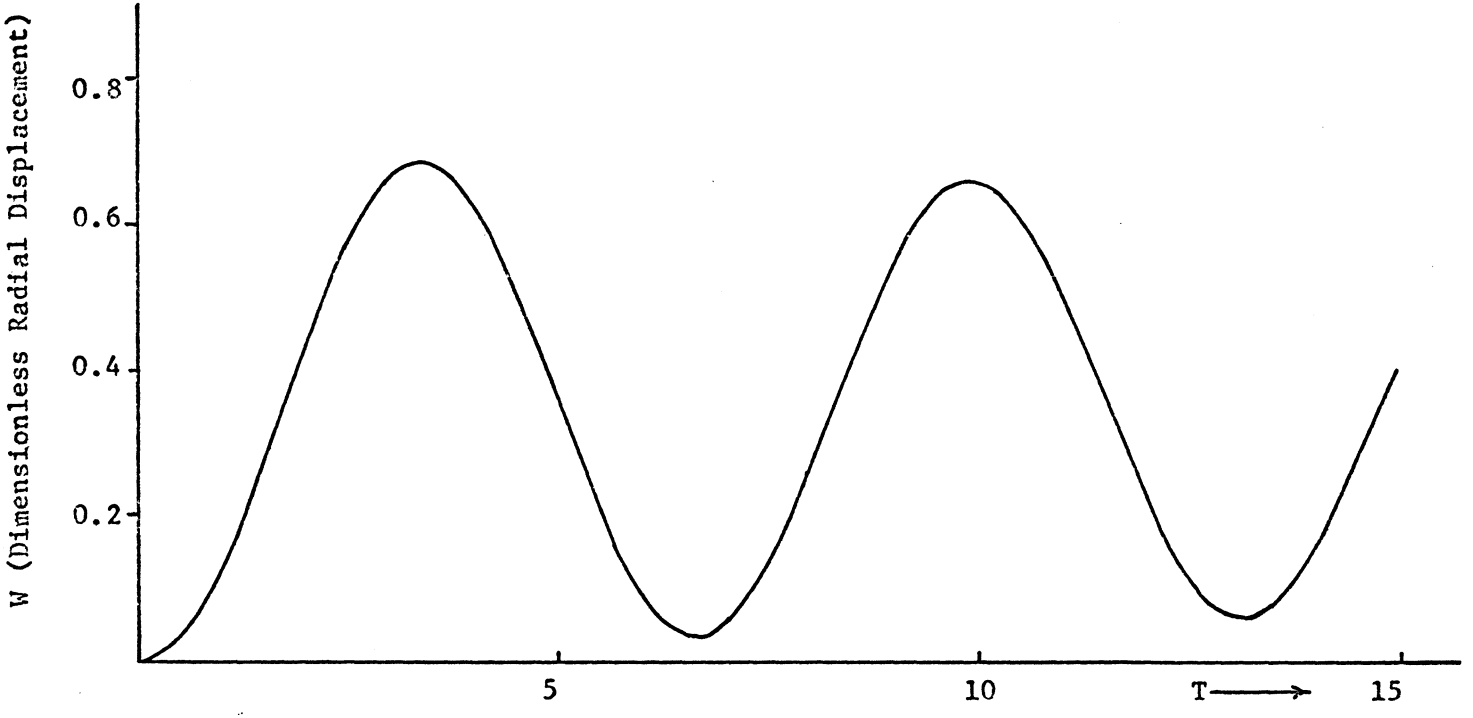


Figure 43. Temporal History of the Nondimensionalized Radial Displacement at the end, L = 0, in a Finite Thin Cylindrical Shell resulting from Frictionless Axial Impact, (free end at L = 10). $h/R = 0.1$, $V_o = 1$, $\nu = 1/3$, $k^2 = 0.87$, $dT = 0.005$.

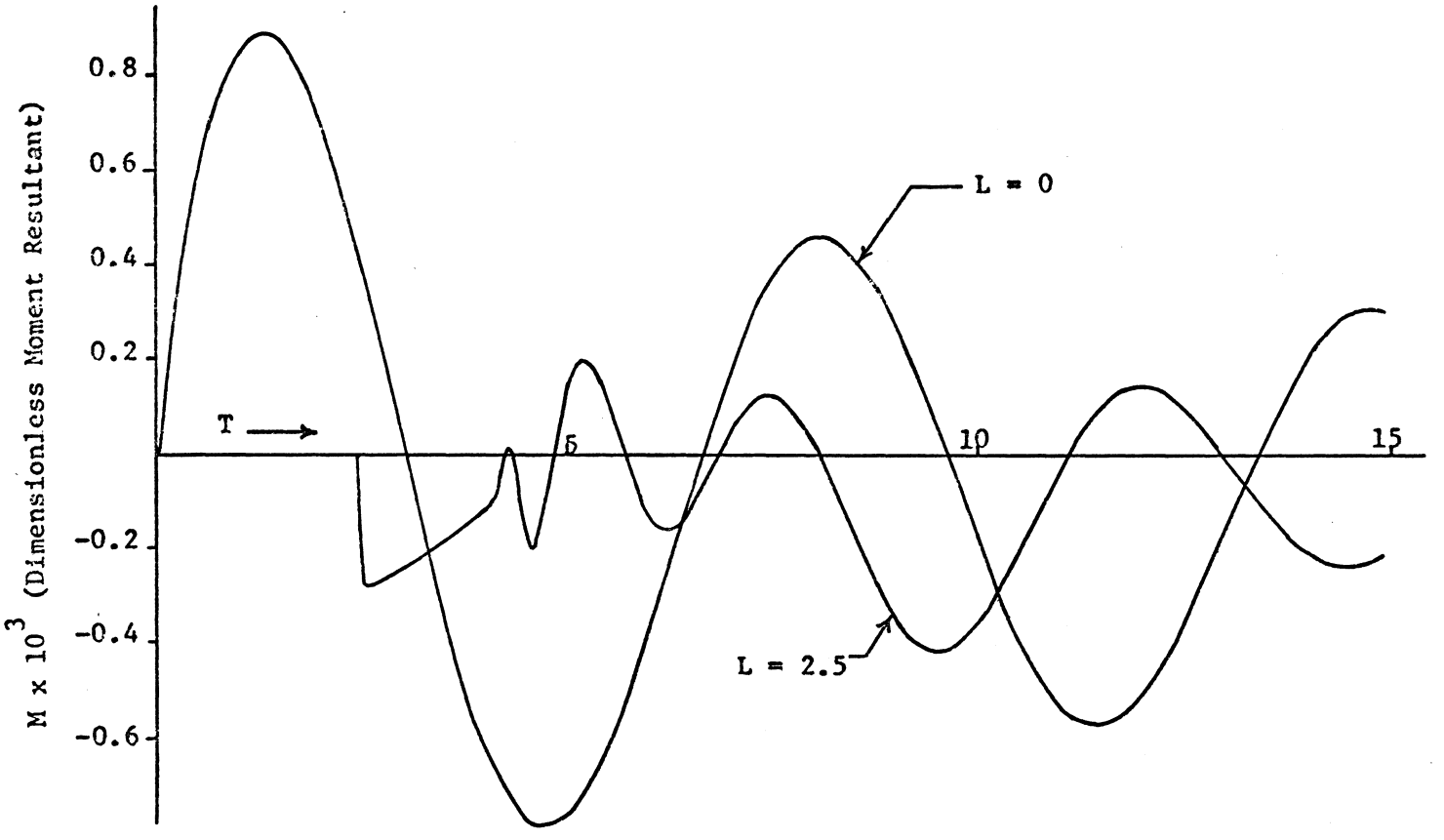


Figure 44. Temporal Histories of the Nondimensionalized Moment Resultant at L = 0 and L = 2.5, in a Finite Thin Cylindrical Shell resulting from Frictionless Axial Impact, (free end at L = 10). $h/R = 0.1$, $V_o = 1$, $\nu = 1/3$, $k^2 = 0.87$, $dT = 0.005$.

moment resultant, (M), at the positions L = 0 and L = 2.5. The figure shows that the moment at L = 0 has magnitudes almost twice as large as those at L = 2.5. This difference represents the additional moment necessary to satisfy the requirement that the meridian remain normal to the wall, SI(0, T) = 0.

## Step Sizes Used and Computational Time

The step sizes which are necessary for adequate convergence vary from 0.025 for the response of the cylindrical membrane to 0.005 for the response of the thin shell. The conical and parabolic membranes solutions both require a step size of 0.0125 for adequate convergence. Of the membrane solutions presented, the parabolic membrane requires the longest computation time of 9.54 minutes to reach T = 25 with dT = 0.0125. The thin shell requires 48 minutes, including the energy balance check, to reach T = 20 with dT = 0.005. The increased number of computational steps and a smaller step size are the main contributions to the additional time required for the cylindrical shell. The energy balance check is performed only before each desired print-out and does not increase the computational time significantly. All computations for the results presented here were performed on an IBM system 360, model 65 computer using double precision arithmetic.

## Concluding Remarks

The dynamical finite element method has been used to solve wave propagation problems which, in theory, could be solved by the method of characteristics. The rules established here for handling free end boundary conditions, and the guidelines regarding the ordering of the computations are original contributions to the method itself. Prior to this thesis, the method has received no clear-cut discussion as to how to proceed to the solution of original problems. The importance of meeting all of the requirements given in the first section of this chapter for establishing that a unique solution has been found cannot be overemphasized. Early in the investigation of the shell, a solution was attempted which forced the wavefront condition to be satisfied without regard to the order in which the calculations were performed. This procedure violated condition 3, page 41 and the results were incorrect. The solution was obtained only after arranging the computational steps in an order which computed the wavefront conditions through the equations themselves.

The inclusion of a check on the energy balance is an elementary computational extension which more than compensates for the additional effort and necessary computational time by the information returned on region of validity and solution stability. This extension should become standard practice when solving problems by this technique.

The technique appears to generally be as efficient for calculation as any other technique. One positive aspect of the technique is the

simplicity of handling reflections. It is believed that the method can easily be extended to handle discontinuities which travel at different speeds and to handle anisotropic structural members. The application of this technique to wave propagation problems in thick shells of revolution should also prove to be a fruitful area of investigation. Preliminary work on the two wavespeed problems indicates that a two element representation of the problem geometry will be necessary, but the basic principles will remain the same.

In conclusion, the original problems solved and the details and guidelines presented concerning the method itself are felt to be useful and original contributions to the literature on wave propagation problems in solids.

## REFERENCES


1. Kolsky, H., Stress Waves in Solids, Dover Publications, 1963.

2. Volterra, E. and Zachmanoglou,E.C., Dynamics of Vibrations, Merrill Books, 1965, pp. 516-610.

3. Davies, R. M., "Stress Waves in Solids," Surveys in Mechanics, Cambridge University Press (1956).

4. Miklowitz, J., "Recent Developments in Elastic Wave Propagation," Applied Mechanics Reviews, vol. 13, 1960, pp. 865-878.

5. Berkowitz, H. M., "Longitudinal Impact of a Semi-Infinite Elastic Cylindrical Shell," Journal of Applied Mechanics, vol. 30, no. 3, Trans. ASME, Vol. 85, Series E, September 1963, pp. 347-354.

6. Testa, R. B. and Bleich, H. H., "Longitudinal Impact of a Semi-Infinite, Cylindrical, Viscoelastic Shell," Journal of Applied Mechanics, Vol. 32, no. 4, Trans. ASME, Vol. 87, Series E, December 1965, pp. 813-820.

7. Berkowitz, H. M. and Bleich, H. H., "Axial Impact of an Elastic Right Conical Membrane Shell," AIAA Journal, Vol. 4, No. 8, August 1966, pp. 1378-1384.

8. Spillers, W. R., "Wave Propagation in a Thin Cylindrical Shell," Journal of Applied Mechanics, Vol. 32, No. 2, Trans. ASME, Vol. 87, Series E, June 1965, pp. 346-350.

9. Herrmann, G. and Mirsky, I., "Three-Dimensional and Shell-Theory Analysis for Axially Symmetric Motions of Cylinders," Journal of Applied Mechanics, December 1956, Vol. 23, No. 4, pp. 563-575.

10. Chou, P. C., "Analysis of a Set of Dynamic Cylindrical Shell Equations for Axisymmetrical Motion by Method of Characteristics," AIAA Journal, Vol. 6, August 1968, pp. 1492-1497.

11. King, W. W., "Axial Impact of an Elastic Conical Membrane," Journal of Applied Mechanics, Vol. 34, No. 2, Trans. ASME, Vol. 89, Series E, June 1967, pp. 496-497.

12. Counts, J. and Akin, J. E., "The Application of Continued Fractions to Wave Propagation Problems in Viscoelastic Rods," DEMVPI Report No. 1-1, Department of Engineering Mechanics, Virginia Polytechnic Institute, August 1968.

13. Akin, J. E. and Counts, J., "Application of Continued Fractions to Wave Propagation in a Semi-Infinite Cylindrical Membrane," Journal of Applied Mechanics, September 1969, Vol. 36, No. 3, Trans. ASME, Vol. 91, Series E, pp. 420-424.

14. Spillers, W. R. and Chapman, J., "A Note on Calculation of Waves in a Cylindrical Shell," Journal of Applied Mechanics, September 1966, Vol. 33, No. 3, Trans. ASME, Vol. 88, Series E, pp. 694-695.

15. Spillers, W. R. and Callegari, A., "Impact of Two Elastic Cylinders: Short-Time Solution," Int. J. Mech. Sci., Pergamon Press, 1969, Vol. 11, pp. 845-851.

16. Davids, N. and Mehta, P., "Computer Analysis Methods in Dynamics," Engineering Research Bulletin B-92, The Pennsylvania State University, May 1965.

17. Koenig, H.A. and Davids, N., "Dynamical Finite Element Analysis for Elastic Waves in Beams and Plates," International Journal of Solids and Structures, Vol. 4, No. 6, June 1968, pp. 643-660.

18. Raney, J. P. and Howlett, J. T., "A Modal Solution for Wave Propagation in Finite Shells of Revolution," Bound volume of technical papers on "Materials and Structural Dynamics, AIAA/ASME 11th Structures, Structural Dynamics, and Materials Conference, April 22-24, 1970, pp. 208-216.

The vita has been removed from the scanned document

# A STUDY OF A DYNAMICAL FINITE ELEMENT ANALYSIS FOR APPLICATION TO AXIAL WAVE PROPAGATION PROBLEMS IN SEMI-INFINITE AND FINITE MEMBRANES AND SHELLS OF REVOLUTION

Joel Gray Bennett

## Abstract

The method known in the literature as dynamical finite element analysis is investigated and applied to wave propagation problems occurring in membranes and thin shells of revolution. Both semi-infinite and finite versions of cylindrical and conical membrane shells are studied and a finite membrane shell having a meridional curve which is parabolic is solved. A thin cylindrical shell is also considered in order to determine the effect of including shear and rotary inertia. The source excitation is generally considered to be the constant velocity motion of one end, but the results for a stress pulse input to one end of a semi-infinite cylindrical membrane shell are also given. The thin cylindrical shell is considered as an initial value problem. The difference in the solutions resulting from prescribing an axial or tangential velocity excitation at the end of a semi-infinite conical membrane shell is presented.

The method itself requires a careful ordering of the calculations and the principles for determining the correct order are discussed. The rules for handling the boundary conditions for finite shells are shown to follow logically from this ordering of the calculations.

An energy balance check on the computations is shown to be an

effective independent check on the correctness and stability of the solution, and a discussion of the conditions used to verify that the numerical results are the solutions is included.

The results for the finite problems are new results and the semi-infinite problems are discussed with respect to previously published results.